

ABSTRACT

Title of Dissertation: TOWARDS BETTER UNDERSTANDING OF AGRICULTURAL DROUGHT: A COMPREHENSIVE ANALYSIS OF AGRICULTURAL DROUGHT RISK, IMPACT AND MONITORING FROM EARTH OBSERVATIONS

Jie Zhang, Doctor of Philosophy, 2017

Dissertation directed by: Professor Christopher Justice, Department of Geographical Sciences

With a changing climate, the frequent occurrence of drought has resulted in unprecedented grain prices and severe market instability, threatening global food security. Earth observation, especially satellite-based observation, has proven its potential for near real-time drought monitoring and early warning. This dissertation undertakes a comprehensive analysis of agriculture-oriented drought risk, impact and monitoring using time-series satellite observation combined with ancillary earth observation data, thus providing a better understanding of agricultural drought.

Agricultural lands exhibit more severe drought regimes during the agricultural growing season. At the global scale, the U.S. Corn Belt, Spain & Eastern Europe, Central Russia, India, North China and Australia, are shown to be the hotspots of agricultural drought risk. For the last three decades, different agricultural drought risk

change patterns are found in different regions with a relatively stable but slight declining drought risk overall for the globe, while Australia exhibits a continuous increase and Brazil exhibits a continuing decrease. Land Surface Temperature (LST) and Evapotranspiration (ET) based indicators show similar capabilities for drought monitoring and have an immediate response after drought; while for Normalized Difference Vegetation Index (NDVI) derived indicators, there shows a lagged and inconsistent drought response. The relationships between NDVI- and LST- derived drought indicators are variable, exhibiting changing functions in both spatial and temporal domains, which provides basis for effectively integrating different data sources for developing a synthetic index. Drought results in varying impacts during the growing season, with generally increasing impacts during the winter wheat main growing season and the most severe drought effects during the grain filling stage around vegetative peaks. As for the Drought Severity Index, better performance is found in rainfed-dominated than irrigation-dominated regions.

This dissertation calls for continuing work to develop an improved impact-oriented agricultural drought indicator by integrating the contributions of different data sources, the dynamics of NDVI-LST interactions as well as the varying drought impacts during the growing season. Improved agricultural drought monitoring and impact assessment, together with agricultural risk analysis, can help prototype an enhanced and integrated agricultural drought monitoring system, thus offering reliable and timely information for drought mitigation, preparedness, response and recovery.

TOWARDS BETTER UNDERSTANDING OF AGRICULTURAL DROUGHT:
A COMPREHENSIVE ANALYSIS OF AGRICULTURAL DROUGHT RISK,
IMPACT AND MONITORING FROM EARTH OBSERVATIONS

by

Jie Zhang

Dissertation submitted to the Faculty of the Graduate School of the
University of Maryland, College Park, in partial fulfillment
of the requirements for the degree of
Doctor of Philosophy
2017

Advisory Committee:
Professor Christopher Justice, Chair
Dr. Eric Vermote
Dr. Inbal Becker-Reshef
Professor Shunlin Liang
Professor Joseph Sullivan

© Copyright by
Jie Zhang
2017

Preface

Chapters 2-5 are journal articles and conference proceedings in which Jie Zhang is the primary and leading author.

Chapter 2 has been submitted as a journal paper to *Agricultural and Forest Meteorology* for review.

- Jie Zhang, Inbal Becker-Reshef, Chris Justice. “Characterizing global agricultural drought regimes and risk using a 30-year data record”, 2017, submitted to *Agricultural and Forest Meteorology*.

Chapter 3 is re-organized from a journal paper in preparation, and three conference proceedings published in *International Geoscience and Remote Sensing Symposium*.

- Jie Zhang, Pietro Elia Campana, Linda See, Ian McCallum, Steffen Fritz, Inbal Becker-Reshef, Chris Justice. “Using remote sensing for agricultural drought monitoring: comparisons and implications”, 2017, in preparation.
- Jie Zhang, Inbal Becker-Reshef. “Drought impact on wheat yield in Oklahoma and Nebraska: a remote sensing perspective”, *IEEE International Geoscience and Remote Sensing Symposium (IGARSS)*, Beijing, China, Jul 10-15, 2016.
- Jie Zhang, Inbal Becker-Reshef, Chris Justice. “Evaluation of the ASCAT surface soil moisture product for agricultural drought monitoring in USA”, *IEEE International Geoscience and Remote Sensing Symposium (IGARSS)*, Milan, Italy, Jul 26-31, 2015.
- Jie Zhang, Inbal Becker-Reshef, Chris Justice. “Evaluating the impacts of drought on crop production from satellite observations: a case study in Kansas”.

IEEE International Geoscience and Remote Sensing Symposium (IGARSS),
Quebec City, Quebec, USA, Jul 13-18, 2014.

Chapter 4 has been published as a journal paper in *Ecological Indicators*.

- Jie Zhang, Qiaozhen Mu, Jianxi Huang. “Assessing the remotely sensed Drought Severity Index for agricultural drought monitoring and impact analysis in North China”, *Ecological Indicators*, 2016, 63: 296-309.

Chapter 5 is in preparation as a journal paper to be submitted in 2017.

- Jie Zhang, Eric Vermote, Shunlin Liang, Inbal Becker-Reshef, Chris Justice. “Exploring the dynamics of vegetation growth and surface temperature interactions for improved agricultural drought monitoring from remote sensing”, 2017, in preparation.

During my PhD, I also participated in other research work which is very relevant to the dissertation topic but not included in this dissertation. The following only lists the journal paper in which I am the leading author.

- Jie Zhang, Pietro Elia Campana, Tian Yao, Yang Zhang, Anders Lundblad, Forrest Melton, Jinyue Yan. “The water-food-energy nexus optimization approach to combat agricultural drought: a case study in the United States”, *Applied Energy*, 2017, <https://doi.org/10.1016/j.apenergy.2017.07.036>.

Dedication

To my family

For their unconditional love and support.

Acknowledgements

This dissertation could not have been finished without all the support I have received all the way during my PhD. I would like to take this opportunity to say thank you to so many people who have helped and supported me during this journey.

First and foremost, I would like to express my sincere gratitude to my supervisor, Prof. Chris Justice for providing me the opportunity to join his research group at the University of Maryland (UMD) and for his constant encouragement, guidance and full support during my entire PhD studies. It has been a great honor to be one of his PhD students and work with the talented researchers in his group.

Many thanks also goes to my committee members, Dr. Eric Vermote, Dr. Inbal Becker-Reshef, Prof. Shunlin Liang, and Prof. Joseph Sullivan, for their continuous guidance and valuable suggestions in my research work and their time in serving on my dissertation committee.

I want to also thank my UMD colleagues and friends, Catherine Nakalembe, Sumalika Biswas, Feng Zhao, Danxia Song, Yi Peng, Huiran Jin, Wenli Huang, Yu Mo, and many more, for the discussions and mental support. My time at UMD was made enjoyable with all your friendship.

I am especially grateful to my former advisor during my Master's study, Prof. Jianjun Wu, from Beijing Normal University (BNU). He and his research group at BNU have always been a great support during my PhD studies even after I graduated from BNU.

I would also like to thank very much my Young Scientists Summer Program (YSSP) supervisors from IIASA, Dr. Linda See, Dr. Steffen Fritz and Dr. Ian McCallum, for their continuous supervision and support during my stay at IIASA in the summer of 2014.

Lastly, I would like to thank my family for all their unconditional love and support. My parents have always encouraged me to pursue my dreams ever since young. As my role model, my elder sister is the person who inspires me to pursue my PhD abroad, provides me tons of suggestions whenever I need, and is always there for me whenever I am feeling down. My beloved fiancé is always encouraging and supporting me during this PhD and helped me get through the hard times of this journey. Thank you all.

Table of Contents

Preface.....	ii
Dedication.....	iv
Acknowledgements.....	v
Table of Contents.....	vii
List of Tables.....	x
List of Figures.....	xi
List of Abbreviations.....	xiv
Chapter 1: Introduction.....	1
1.1 Background.....	1
1.2 Previous Research.....	2
1.2.1 Drought Types, Characteristics, Regimes and Agricultural Drought.....	3
1.2.2 Existing Drought Monitoring Systems.....	5
1.2.3 Current Approaches to Analyzing Drought Risk.....	6
1.2.4 Current Approaches to Monitoring Drought Using Remote Sensing.....	6
1.2.5 Current Approaches to Assessing Drought Impact on Agriculture.....	10
1.2.6 Limitations in Current Drought Research.....	10
1.3 Research Objectives.....	11
1.4 Dissertation Outline.....	12
Chapter 2: Characterizing Global Agriculture Drought Regimes and Risk Using a 30-Year Data Record.....	15
2.1 Introduction.....	15
2.2 Data.....	18
2.2.1 A Self-calibrating Palmer Drought Severity Index.....	18
2.2.2 Global Agricultural Croplands.....	19
2.2.3 Agricultural Growing Season Calendar.....	19
2.2.4 Irrigation.....	20
2.2.5 Crop Production Values.....	20
2.3 Methodology.....	20
2.3.1 Depicting Drought from Self-Calibrating PDSI.....	20
2.3.2 Characterizing Drought Regimes.....	21
2.3.3 Developing the Global Agricultural Drought Risk Index (GADRI).....	22
2.4 Results.....	24
2.4.1 Global Agricultural Drought Regimes.....	24
2.4.2 Global Agricultural Drought Risk.....	31
2.4.3 Evolution of Global Agricultural Drought Risk for the Past 3 Decades.....	33
2.5 Discussions.....	37
2.6 Conclusions.....	40
Chapter 3: Investigating the Capabilities of Existing Remotely Sensed Indicators for Agricultural Drought Monitoring and Impact Assessment in Southern U.S. Great Plains.....	42
3.1 Introduction.....	42
3.2 Study Area.....	45
3.3 Data.....	46

3.3.1	Remote Sensing Data.....	46
3.3.2	In situ Soil Moisture Data.....	47
3.3.3	Agricultural Statistics.....	48
3.4	Methodology.....	48
3.4.1	Remotely Sensed Indicators.....	48
3.4.2	In situ Soil Moisture Composite.....	50
3.4.3	Statistical and Lagged Statistical Analysis.....	50
3.4.4	Response Time Decision Rules.....	51
3.4.5	Drought Impact Analysis.....	52
3.5	Results.....	53
3.5.1	Response of Remotely Sensed Indicators to Drought.....	53
3.5.2	Response Time Maximum Likelihood Region for NDVI Derived Drought Indicators.....	55
3.5.3	Response of Remotely Sensed Indicators to Drought for Major Land Cover Types.....	57
3.5.4	Response of Remotely Sensed Indicators to Drought during Winter Wheat Main Growing Season.....	58
3.5.5	ASCAT Surface Soil Moisture Product for Agricultural Drought Monitoring in Southern U.S. Great Plains.....	61
3.5.6	Impacts of Drought on Agriculture in Southern U.S. Great Plains from Satellite Observations.....	66
3.6	Conclusions and Discussions.....	74
Chapter 4:	Assessing the Remotely Sensed Drought Severity Index for Agricultural Drought Monitoring and Impact Analysis in North China.....	78
4.1	Introduction.....	78
4.2	Study Area.....	84
4.3	Data and Preprocessing.....	86
4.3.1	Remote Sensing Data.....	86
4.3.2	Gridded Meteorological/Soil Moisture data.....	86
4.3.3	In situ Station Data.....	87
4.3.4	Agricultural Statistical Data.....	87
4.4	Methodology.....	88
4.4.1	Remotely Sensed Drought Severity Index.....	88
4.4.2	Meteorological/Hydrological/Agricultural Drought Indicators.....	89
4.4.3	Data Temporal Composite and Spatial Aggregation.....	90
4.4.4	Evaluation Criteria.....	90
4.5	Results.....	91
4.5.1	Evaluation of Annual DSI for Drought Monitoring.....	91
4.5.2	Evaluation of the DSI for Drought Monitoring during the Main Winter Wheat Growing Season.....	96
4.5.3	Evaluation of the DSI for Characterizing Agricultural Drought Severity ..	99
4.5.4	Exploring the Impacts of Agricultural Drought on Winter Wheat Yield during the Main Growing Season.....	101
4.6	Conclusions and Discussions.....	108

Chapter 5: Exploring the Dynamics of Vegetation Growth and Surface Temperature Interactions for Improved Agricultural Drought Monitoring from Remote Sensing	112
5.1 Introduction.....	112
5.2 Study Area	114
5.3 Data.....	115
5.3.1 MODIS Surface Reflectance.....	116
5.3.2 MODIS Surface Temperature	116
5.3.3 Crop Mask.....	116
5.4 Methodology	116
5.4.1 Spatial Aggregation	116
5.4.2 Remotely Sensed Indicators.....	117
5.4.3 Lagged Statistical Analysis for Analyzing VCI-TCI Response	117
5.5 Results.....	117
5.5.1 Dynamics of VCI-TCI Relationships at the Beginning of Main Growing Season	118
5.5.2 Dynamics of VCI-TCI Relationships before the Vegetative Peak	121
5.5.3 Dynamics of VCI-TCI Relationships around the Vegetative Peak	124
5.5.4 Dynamics of VCI-TCI Relationships after the Vegetative Peak	127
5.6 Conclusions and Discussions	130
Chapter 6: Conclusions	134
6.1 Summary Findings	134
6.2 Significance of the Research and Implications	138
6.3 Future Research	140
Bibliography	144

List of Tables

Table 2-1: Classification of Drought	21
Table 3-1: Count of Winter Wheat Stations at Different Response Time during Winter Wheat Main Growing Season	59
Table 3-2: Drought Impacts on Winter Wheat Yield during Key Drought Alert Period	68
Table 4-1: Summaries of Agricultural Drought Impacts on Winter Wheat Yield in 5 Provinces.....	105
Table 5-1: Count of Valid Winter Wheat Pixels at Different Response Times for Each Category (DOY65-DOY81).....	121
Table 5-2: Count of Valid Winter Wheat Pixels at Different Response Times for Each Category (DOY89-DOY105).....	124
Table 5-3: Count of Valid Winter Wheat Pixels at Different Response Times for Each Category (DOY113-DOY129).....	127
Table 5-4: Count of Valid Winter Wheat Pixels at Different Response Times for Each Category (DOY137-DOY153).....	130

List of Figures

Figure 1-1: (a) Percentage of Different Natural Disaster Occurrences (b) Percentage of Different Natural Disaster Affected People	1
Figure 1-2: Wheat Monthly Price	2
Figure 1-3: The Natural and Social Dimensions of Drought (Wilhite, 2005)	4
Figure 1-4: Schematic Diagram of the Proposed Research	12
Figure 2-1: Global Average Drought Intensity over Agricultural Lands from 1980 to 2009.....	25
Figure 2-2: Global Drought Frequency over Agricultural Lands from 1980 to 2009	25
Figure 2-3: Relative Difference of Global Average Drought Intensity over Agricultural Lands (Agricultural Growing Season vs. Entire Year).....	26
Figure 2-4: Relative Difference of Global Drought Frequency over Agricultural Lands (Agricultural Growing Season vs. Entire Year).....	27
Figure 2-5: Agricultural Lands Experiencing Increased Drought Intensity and Frequency during Agricultural Growing Season	29
Figure 2-6: Drought Intensity and Frequency Difference over Agricultural Lands (Agricultural Growing Season vs. Entire Year).....	29
Figure 2-7: Time-series of scPDSI for the Past 3 Decades (1980-2009) for 3 Highlighted Sites (a) Northeast China (b) U.S. Corn Belt (c) Northern Sub-Saharan Africa	31
Figure 2-8: Global Agricultural Drought Risk for the Past 3 Decades.....	32
Figure 2-9. Regional Agricultural Drought Risk for the Past 3 Decades	33
Figure 2-10: Global Agricultural Drought Risk Decadal Change (1990's vs. 1980's)	34
Figure 2-11: Global Agricultural Drought Risk Decadal Change (2000's vs. 1990's)	34
Figure 2-12: Agricultural Lands Experiencing Increased Decadal Drought Risk.....	35
Figure 2-13: Agricultural Drought Risk Decadal Change	35
Figure 2-14: 2011-2012 Summer Global Average Drought Intensity	38
Figure 3-1: Chapter 3 Study Area Showing the Winter Wheat Distribution, Major Winter Wheat ASDs and Locations of In situ Soil Moisture Measurements	46
Figure 3-2: Schematic Chart for Determining Response Time (a) Single Peak (b) Single Peak in Maximum Likelihood Region (MLR) (c) Several Peaks in MLR with One Significantly Higher Correlation (d) Several Peaks in MLR with Similar Correlation	52
Figure 3-3: General Response of Drought Indicators to Soil Moisture at Different Time Lags.....	54
Figure 3-4: Accumulated Probability of Different Response Time for NDVI Derived Indicators.....	56
Figure 3-5: Response of Drought Indicator to Soil Moisture at Different Time Lags for Major Land Cover Types	58
Figure 3-6: Time Series of Drought Indicator-Soil Moisture Correlation during the Winter Wheat Main Growing Season.....	60
Figure 3-7: Relationship between ASCAT Ascending and Descending SSM-RSM Correlation	62

Figure 3-8: Histogram of ASCAT Descending SSM-RSM Correlation	62
Figure 3-9: Spatial Pattern of Descending ASCAT SSM-RSM Correlation.....	63
Figure 3-10: Time Series of ASCAT SSM-RSM Correlation.....	64
Figure 3-11: Relationship between ASCAT Ascending and Descending SSM-RSM Correlation for Crop Stations during Growing Season.....	65
Figure 3-12: Time Series of NDVI Anomaly for Kansas Wheat Areas	66
Figure 3-13: Winter Wheat Yield for Kansas.....	66
Figure 3-14: The Correlation Matrix between CANDVI and Winter Wheat Yield for Kansas.....	67
Figure 3-15: Monthly PDSI Time Series for Oklahoma (Top) and Nebraska (Bottom)	69
Figure 3-16: Time Series of State Aggregated NDVI over Winter Wheat Regions in Oklahoma and Nebraska.....	71
Figure 3-17: State-level 8-day Drought Impacts on Winter Wheat Yield during the Main Growing Season in Oklahoma and Nebraska.....	71
Figure 3-18: Time Series of ASD Aggregated NDVI over the Winter Wheat Regions for Oklahoma and Nebraska (2001-2011 Mean)	72
Figure 3-19: ASD-level 8-day Drought Impacts on Winter Wheat Yield during the Main Growing Season in Oklahoma and Nebraska.....	74
Figure 4-1: Chapter 4 Study Area Showing the MODIS Cropland Used in This Study	85
Figure 4-2: Relationships between Annual DSI and PPA in 5 Provinces (a) 5 Provinces (b) Hebei (c) Shanxi (d) Shaanxi (e) Shandong (f) Henan	92
Figure 4-3: Spatial Pattern of the Correlation between Annual DSI and PPA	94
Figure 4-4: Relationships between Annual DSI and RSW in 5 Provinces (a) 5 Provinces (b) Hebei (c) Shanxi (d) Shaanxi (e) Shandong (f) Henan	95
Figure 4-5: The Correlation between 8-day DSI and PPA in 5 Provinces during the Main Winter Wheat Growing Season.....	97
Figure 4-6: The Spatial Patterns of DSI (Left) and PDSI (Right) for April 2009	99
Figure 4-7: Relationships between Annual Cropland DSI and ADS in 5 Provinces (a) 5 Provinces (b) Hebei (c) Shanxi (d) Shaanxi (e) Shandong (f) Henan.....	100
Figure 4-8: Correlation between 8-day Cropland DSI and Winter Wheat Yield during the Main Growing Season in 5 Provinces.....	102
Figure 4-9: The Correlation Matrix between Cropland DSI and Winter Wheat Yield within the Main Growing Season in Shandong Province	104
Figure 4-10: Winter Wheat Yield Loss at Sub-province Level in Shaanxi Province	106
Figure 4-11: Spatial Patterns of 8-day DSI in Shaanxi Province during March-May, 2007.....	107
Figure 5-1: Chapter 5 Study Area Showing Winter Wheat Distribution at 1km Resolution	115
Figure 5-2: Spatial Distribution of VCI-TCI Response Time (Left) and Corresponding Correlation (Right) for DOY65-DOY81	120
Figure 5-3: Spatial Distribution of VCI-TCI Response Time (Left) and Corresponding Correlation (Right) for DOY89-DOY105	123
Figure 5-4: Spatial Distribution of VCI-TCI Response Time (Left) and Corresponding Correlation (Right) for DOY113-DOY129	126

Figure 5-5: Spatial Distribution of VCI-TCI Response Time (Left) and Corresponding Correlation (Right) for DOY137-DOY153 129

Figure 6-1: Conceptual Diagram of the Integrated Agricultural Drought Alert System 139

List of Abbreviations

Advanced Scatterometer (ASCAT)

Advanced Very High Resolution Radiometer (AVHRR)

Agricultural Statistics District (ASD)

Anomaly NDVI (ANDVI)

Anomaly Vegetation Index (AVI)

Apparent Thermal Inertia (ATI)

Average Drought Intensity (ADI)

Climate Model Grid (CMG)

Climatic Research Unit (CRU)

Cropland Data Layer (CDL)

Crop Water Stress Index (CWSI)

Cumulative Anomaly NDVI (CANDVI)

Drought Frequency (DF)

Drought Severity Index (DSI)

European Drought Observatory (EDO)

Evaporative Stress Index (ESI)

Evapotranspiration (ET)

Evapotranspiration Condition Index (ECI)

Food and Agriculture Organization of the United Nations (FAO)

Fraction of Absorbed Photosynthetically Active Radiation (fAPAR)

Global Agricultural Drought Risk Index (GADRI)

Global Agriculture Monitoring (GLAM)

Global Agro-Ecological Zones (GAEZ)

Global Inventory Monitoring and Modeling System (GIMMS)

Global Map of Irrigation Areas (GMIA)

Gravity Recovery and Climate Experiment (GRACE)

Integrated Drought Index (IDI)

Intergovernmental Panel on Climate Change (IPCC)

Land Processes Distributed Active Archive Center (LP DAAC)

Land Surface Temperature (LST)

Long Term Data Record (LTDR)

Maximum Likelihood Region (MLR)

Meteorological Operational (MetOp)

Moderate Resolution Imaging Spectroradiometer (MODIS)

Monthly Vegetation Condition Index (MVCI)

National Agricultural Statistics Service (NASS)

National Center for Atmospheric Research (NCAR)

National Drought Mitigation Center (NDMC)

National Integrated Drought Information System (NIDIS)

National Land Cover Database (NLCD)

Near Infrared (NIR)

Normalized Difference Temperature Index (NDTI)

Normalized Difference Vegetation Index (NDVI)

Normalized Difference Water Index (NDWI)

Normalized Evapotranspiration Index (NEI)

Normalized Multi-band Drought Index (NMDI)

Normalized Temperature Index (NTI)

Normalized Vegetation Index (NVI)

North American Drought Monitor (NADM)

North American Soil Moisture Database (NASMD)

Numerical Terradynamic Simulation Group (NTSG)

Palmer Drought Severity Index (PDSI)

Percentage of Average Seasonal Greenness (PASG)

Percentage of Precipitation Anomaly (PPA)

Precipitation Condition Index (PCI)

Potential Evapotranspiration (PET)

Relative GADRI (RGADRI)

Relative Soil Moisture (RSM)

Royal Netherlands Meteorological Institute (KNMI)

Self-calibrating PDSI (scPDSI)

Shortwave-infrared (SWIR)

Standardized Evapotranspiration Index (SEI)

Standardized Precipitation Evapotranspiration Index (SPEI)

Standardized Precipitation Index (SPI)

Standardized Temperature Index (STI)

Standardized Vegetation Index (SVI)

Surface Water and Ocean Topography Mission (SWOT)

Surface Soil Moisture (SSM)

Synthesized Drought Index (SDI)
Temperature Condition Index (TCI)
Temperature Vegetation Drought Index (TVDI)
Temperature Vegetation Index (TVI)
Tropical Rainfall Measuring Mission (TRMM)
U.S. Drought Monitor (USDM)
Vegetation Condition Index (VCI)
Vegetation Drought Response Index (VegDRI)
Vegetation Health Index (VHI)
Vegetation Supply Water Index (VSWI)
Vienna University of Technology (TU-WIEN)
Yield Loss Ratio (YLR)

Chapter 1: Introduction

1.1 Background

Drought is a normal and recurring event for all climatic regimes, both dry and humid. Of all natural hazards, drought is the most complex and least understood, affecting a large number of people and resulting in significant economic, social and environmental impacts (Wilhite, 2005). According to the International Disaster Database, the number of drought occurrences makes up only 5% of all natural disasters; however, drought results in about 30% of the total people affected, ranking the top among all natural disasters (Figure 1, <http://www.emdat.be/>).

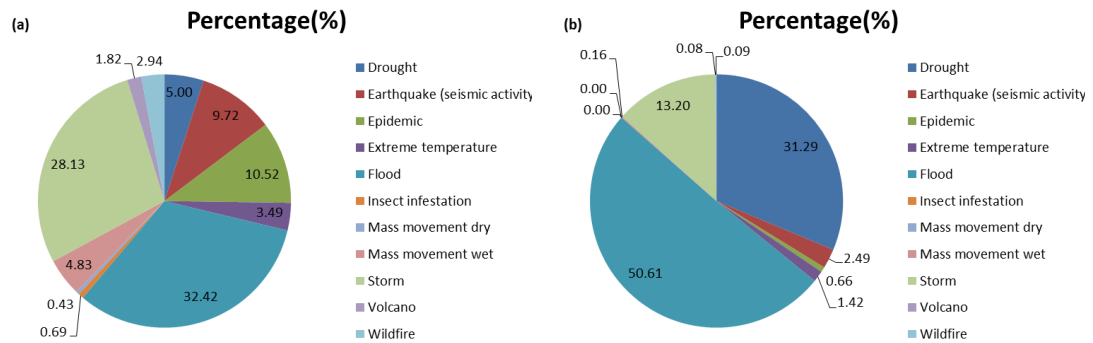


*Figure 1-1: (a) Percentage of Different Natural Disaster Occurrences (b) Percentage of Different Natural Disaster Affected People
(Source: "EM-DAT: The International Disaster Database, <http://www.emdat.be/>)*

Currently, more than half of the world is susceptible to drought with a total loss of about 6-8 billion dollars due to drought each year (Wilhite, 2000). The National Center for Atmospheric Research (NCAR) estimated that the percentage of global terrestrial areas suffering from drought more than doubled from the 1970's to early 2000's, most possibly caused by the rise of global temperature (Dai et. al, 2004). The Intergovernmental Panel on Climate Change (IPCC) pointed out that there is a

gradually increasing trend in future drought risk (IPCC, 2001 & 2007). With the intensification of global warming and the frequent occurrence of extreme events, the issues of global drought and its impacts are becoming more and more pronounced, drawing increasing attention from governments, scientists and the public.

Agriculture is the major sector to be affected by drought. Although agricultural production has been rising in recent years, agricultural drought constitutes the primary causes of crop failure, leading to global food price instability and threatening global food security. Severe droughts in the major agricultural producing countries, such as in the U.S., Russia and Australia, were primary factors for the recent crop price surges (Figure 1-2), calling for close study of global agricultural drought and its impact on crop production.

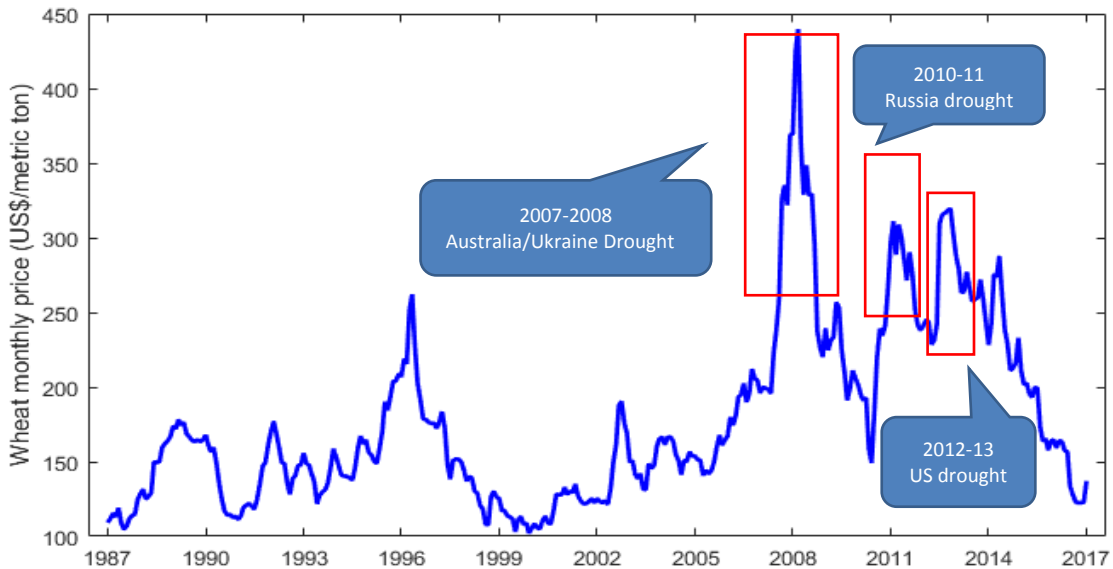


Figure 1-2: Wheat Monthly Price
(Source: INDEXMUNDI, <http://www.indexmundi.com/>)

1.2 Previous Research

Much work has been done on drought, however, the complexity of both drought and agriculture calls for further work on agricultural drought. This section highlights

the complex nature of drought, current research on drought and the challenges it presents for effective agricultural drought monitoring and management.

1.2.1 Drought Types, Characteristics, Regimes and Agricultural Drought

Drought differs from other natural hazards in several ways (Wilhite, 1993 & 2000 & 2005). First, drought is a slow-onset natural hazard (also called a “creeping phenomenon”) and its impacts/effects usually accumulate slowly over a long period (Tannehill, 1947). Thus, it is very difficult to accurately determine the onset and end of drought. Second, there is a lack of a clear, precise and universally accepted definition of drought, which adds to the uncertainty about whether or not drought is occurring, and its degree of severity. Third, compared to other natural disasters, drought doesn’t result in immediate and obvious structural damage and often occurs over a large spatial extent. All these characteristics have hindered the development of accurate, reliable and timely estimates of drought conditions. Drought regimes summarize the temporal and spatial dynamics of drought over time for a given location, and drought monitoring involves the continuous assessment of comprehensive drought regimes. Key elements of comprehensive drought regimes include intensity, onset/end, duration, spatial extent, severity and frequency. These features are closely related to each other and together help distinguish one drought event from another (Wilhite, 1993 & 2000 & 2005).

Drought is of interest to many disciplines. Each discipline incorporates different natural and socioeconomic factors into its own definition. Generally, drought can be grouped into four types: meteorological drought, agricultural drought, hydrological drought and socioeconomic drought (Wilhite & Glantz, 1985). All types of drought originate from a deficiency of precipitation; however, they place different emphasis on

the natural or human/social aspects of drought (Figure 1-3).

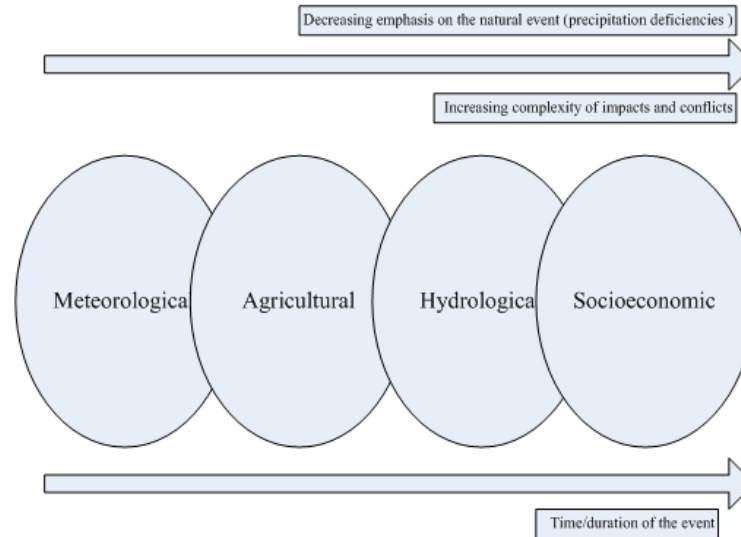


Figure 1-3: The Natural and Social Dimensions of Drought (Wilhite, 2005)

Meteorological drought happens as a consequence of the precipitation shortage over a certain period. Hydrological drought occurs when there is a deficiency in surface or subsurface water, especially in streams, reservoirs, and groundwater levels. Socioeconomic drought occurs when the supply for an economic good cannot meet its demand due to the weather-related deficit in water supply. Agricultural drought relates various characteristics of meteorological (or hydrological) drought to agricultural impacts, focusing more on the availability of soil water for sustaining crop growth and thus the negative crop production impacts (Wilhite, 2000 & 2005). As drought conditions persist over cropped areas during critical growth stages, they can result in destroyed or underdeveloped crops with significant yield loss. Although the final crop production is the result of the interaction among various factors, agricultural drought remains the main driver for reduced crop yield. Agricultural production, especially in poor areas, remains highly dependent on weather conditions. For the past decades, climate change has undoubtedly impacted agricultural production in a significant way.

The agricultural areas with high and very high drought hazard cover about half of global agricultural areas, most of which are located within major crop producing regions (Geng et al., 2015). Despite the varying relationships between the magnitude of crop failure and drought severity across different regions, crop types and growing seasons, drought have resulted in significant crop loss around the world, especially in the major agriculture producing countries, like Midwest U.S. (Mishra & Cherkauer, 2010) and China (Hu et al., 2014; Qin et al., 2014; Wang et al., 2014; Ming et al., 2015). With the exacerbated global warming and irregularity of precipitation in the future, drought and its associated impacts will become even more pronounced. Also, the diversity of an agricultural system adds to the complexity of agricultural drought, due to the composition of various crops with distinct biological characteristics, resulting in different sensitivities to drought. These characteristics have made agricultural drought stand out from other droughts, making it a good candidate for further in-depth study.

1.2.2 Existing Drought Monitoring Systems

With the increased occurrences of droughts all over the world in recent years, it has been clearly recognized that a global-scale drought monitoring, mitigation, and response system would provide important benefits to all nations affected by drought (Heim & Brewer, 2010). Currently, several national Drought Early Warning Systems have been created, including in the U.S. (U.S. Drought Monitor-USDM and National Integrated Drought Information System-NIDIS), Australia, Brazil, Canada, China, and some other countries. The emerging collaboration on global drought monitoring mainly consists of three regional components: the North American Drought Monitor (NADM), the European Drought Observatory (EDO), and Princeton University's African Flood

and Drought Monitor. Besides, there are also a few individual drought monitoring systems with global coverage, such as the Global Drought Information System (<https://www.drought.gov/gdm/>), the Standardized Precipitation Evapotranspiration Index (SPEI, Vicente-Serrano et al., 2010) Global Drought Monitor (<http://spei.csic.es/index.html>), and the Global Integrated Drought Monitoring and Prediction System (<http://drought.eng.uci.edu/>). However, most of these systems are based on meteorological data with very coarse resolution, and not specific to agricultural application, calling for an agricultural-specific and fine-resolution monitoring from the remote sensing perspective.

1.2.3 Current Approaches to Analyzing Drought Risk

Agricultural drought risk describes the probability of the potential negative effects on agriculture (Knutson et al., 1998). Given the significant drought impacts on agricultural production mentioned in Section 1.2.1, a good understanding of global agricultural drought risk can help alert crop analysts to drought-prone areas and the potential impacts, provide useful inputs for agricultural management decision-making and thus effectively help reduce the vulnerability of agricultural ecosystems to drought. Current agricultural drought risk research mainly focuses on regional or national scales, using either drought intensity or frequency for describing drought hazard, thus lacking a consistent, integrated and spatially-explicit agriculture specific drought risk analysis at the global scale. For more detailed description about the work on agricultural drought risk, please refer to Chapter 2 of this dissertation.

1.2.4 Current Approaches to Monitoring Drought Using Remote Sensing

Drought can cause a decline in vegetation vigor which is detectable by satellite.

Satellite observations have also overcome the limitation of station-based meteorological observations to some extent, providing more potential for practical, cost-effective and dynamic large-scale drought monitoring. The use of satellite observations for drought monitoring began in the 1980's using Advanced Very High Resolution Radiometer (AVHRR) data (Justice et al., 1985). Since then, many remotely sensed indicators have been developed, which can be generally divided into indicators based on vegetation conditions, surface temperature, combinations of vegetation conditions and surface temperature, energy balance models, and multi-source data.

- Remotely Sensed Drought Indicators Based on Vegetation Conditions

Vegetation indices are extensively used both in research and in operational systems as the basis for deriving drought indicators. The most commonly used index is Normalized Difference Vegetation Index (NDVI) derived from the Near Infrared (NIR) and red bands. NDVI is an indicator of vegetation photosynthetic capacity and thus vegetation cover, biomass and vigor (Tucker, 1979). Insufficient moisture limits the available water that vegetation can take up and consequently leads to wilting and a reduction in vegetation biomass. Although additional information is needed to distinguish impacts of drought on vegetation from other stress factors, insufficient moisture is frequently the leading cause of reduced photosynthetic capacity when large areas exhibit persistent vegetation stress. Thus, NDVI-based metrics are commonly used as indicators of vegetation stress and drought (Henricksen & Durkin, 1986; Tucker & Choudhury, 1987; Tucker, 1989; Gutman, 1990). Many drought indicators have been developed based on NDVI, such as Anomaly Vegetation Index (AVI) (Chen et al, 1994), Vegetation Condition Index (VCI) (Kogan, 1990; Liu & Kogan, 1996), Standardized

Vegetation Index (SVI) (Peters et al., 2002), Monthly Vegetation Condition Index (MVCI) (McVicar & Jupp, 1998), and the Percent of Average Seasonal Greenness (PASG) (Brown et al., 2008). Another useful indicator of vegetation condition specifically sensitive to leaf water content is the Normalized Difference Water Index (NDWI) (Gao, 1996; Chen et al., 2005; Fensholt & Sandholt, 2003). Calculated from NIR and Shortwave Infrared (SWIR) band, NDWI is sensitive to vegetation water content and some studies have shown that NDWI can detect drought events more readily than NDVI (Gu et al., 2007). Besides, the Normalized Multi-band Drought Index (NMDI) has been proposed as an index for monitoring soil and vegetation moisture (Wang & Qu, 2007), and Rossi et al. (2008) also examined the utility of the fraction of Absorbed Photosynthetically Active Radiation (fAPAR) anomaly for drought detection in Europe.

- Remotely Sensed Drought Indicators Based on Surface Temperature

Land Surface Temperature (LST) can provide vital information on Evapotranspiration (ET) and vegetation water stress (Gutman, 1990) and can be used as an indicator of surface moisture content. For example, Qiao et al. (2003) developed the statistical model between LST derived from the Landsat TM thermal band and soil moisture, which had a correlation coefficient of 0.961. To remove the effect of seasonal temperature variations, Mcvicar & Jupp (1998) developed the Normalized Difference Temperature Index (NDTI) and Kogan (1995a) developed the Temperature Condition Index (TCI) for drought monitoring based on LST.

- Remotely Sensed Drought Indicators Based on Combinations of Vegetation Conditions and Surface Temperature

Several indicators based on combinations of vegetation indices and temperature have been developed such as the Vegetation Health Index (VHI) (Kogan, 1995a), Temperature Vegetation Index (TVI) (McVicar & Jupp, 1998), Vegetation Supply Water Index (VSWI) (McVicar & Jupp, 1998) and Temperature Vegetation Drought Index (TVDI) (Sandholt, 2002).

- Remotely Sensed Drought Indicators Based on Energy Balance

Some drought indices are based on energy balance models. Price (1985) first developed the simplified Apparent Thermal Inertia (ATI) model, in which ATI is calculated from surface albedo and daily temperature variations. This method is suitable for drought monitoring under low vegetation coverage. Jackson (1982) developed the Crop Water Stress Index (CWSI) based on canopy-air temperature differences. Anderson et al. (2007 & 2011) developed the Evaporative Stress Index (ESI) by quantifying anomalies in the ratio of actual to potential ET (PET) and Mu et al. (2013a) developed the Drought Severity Index (DSI) through integrating ET, PET and NDVI.

- Integrated Remotely Sensed Drought Indicator Based on Multi-Source Data

The Vegetation Drought Response Index (VegDRI) was developed as a comprehensive drought indicator, which integrates information from different data sources from satellite observations, climate data to biophysical characteristics using data mining techniques (Tadesse et al., 2005; Brown et al., 2008). VegDRI was developed by National Drought Mitigation Center (NDMC) and currently runs operationally for 48 states in the U.S. Some researchers have adapted this model and applied the improved algorithm for drought monitoring in China (Wu et al., 2013). Liu

& Yang (2001) developed an Integrated Drought Index (IDI) for agricultural drought monitoring in China based on Moderate Resolution Imaging Spectroradiometer (MODIS) data, which incorporates many drought related parameters, including temperature difference, cloud index, NDVI, normalized difference snow index, precipitation anomaly, irrigation eco-region types and previous drought conditions. Also, Du et al. (2012) defined the Synthesized Drought Index (SDI) as the principal component of VCI, TCI and Precipitation Condition Index (PCI) using MODIS and Tropical Rainfall Measuring Mission (TRMM) data.

1.2.5 Current Approaches to Assessing Drought Impact on Agriculture

Drought typically results in the reduction of crop production and the drought impacts on crops are often investigated through crop simulation modelling. Crop growth models simulate the plant behavior under different scenarios, and output the various parameters during crop growth and the final production (Huth et al., 2008; Huang et al., 2015a, 2015b). Most existing crop models can be successfully used for crop simulations at the field scale; however, the large number of input parameters in these models limits its application for crop growth simulations and thus the analysis of crop response to drought at a large scale. For more detailed description of the work on agricultural drought impact assessment, please refer to Chapter 4 of this dissertation.

1.2.6 Limitations in Current Drought Research

According to the IPCC4 report, there has been a trend of increasing droughts during the past decades and future climate projections also point towards continued increasing drought risk. Agricultural drought risk describes the possibility of the potential negative impacts on agriculture. However, as mentioned in Section 1.2.3,

there has been little work to investigate agricultural specific drought risk consistent at the global scale, especially taking into account the agricultural impacts.

As mentioned in Section 1.2.4, many remote sensing based drought indicators have been developed (Chen et al., 1994; Kogan, 1995a, 1995b; Liu & Kogan, 1996; Peters et al., 2002; Anderson et al., 2011). However, most of these indicators are generic and are not specifically developed for agricultural drought. Considering the differences between agriculture and other terrestrial ecosystems, the capability of these remotely sensed indicators for agricultural drought monitoring and the dynamics of the interactions between these indicators require further evaluation, and the production of a spatially and temporally consistent assessment of drought conditions particularly over agricultural lands from an enhanced agricultural drought indicator has yet to be developed.

Also, as mentioned in Section 1.2.5, most current drought impact assessment work is carried out based on the crop modelling with coarse resolution, which calls for a more precise assessment at a finer spatial and temporal resolution from remote sensing and thus provides direct inputs for developing an impact-oriented agricultural drought indicator.

1.3 Research Objectives

This dissertation builds on previous drought research carried out over the past decades to investigate global agricultural drought risk, examine the capabilities of existing remotely sensed indicators for agricultural drought monitoring and impact assessment, and explore the dynamics of different indicators during the growing season, aiming to help inform an improved impact-oriented agricultural drought

indicator. The research mainly utilizes satellite data (MODIS: Reflectance/NDVI/LST/ET, Advanced Scatterometer (ASCAT): soil moisture), ground-based meteorological/hydrological data (precipitation and soil moisture), agricultural statistics, and drought records to address the following research questions:

1. What is the pattern of global agricultural drought risk?
2. What is the capability of existing remotely sensed indicators for agricultural drought monitoring and impact assessment?
3. What is the dynamic of vegetation-temperature interaction during crop growing season and how can it be used for improving agricultural drought monitoring from remote sensing?

1.4 Dissertation Outline

To answer these research questions, the research is divided into the following 4 research tasks (Figure 1-4).

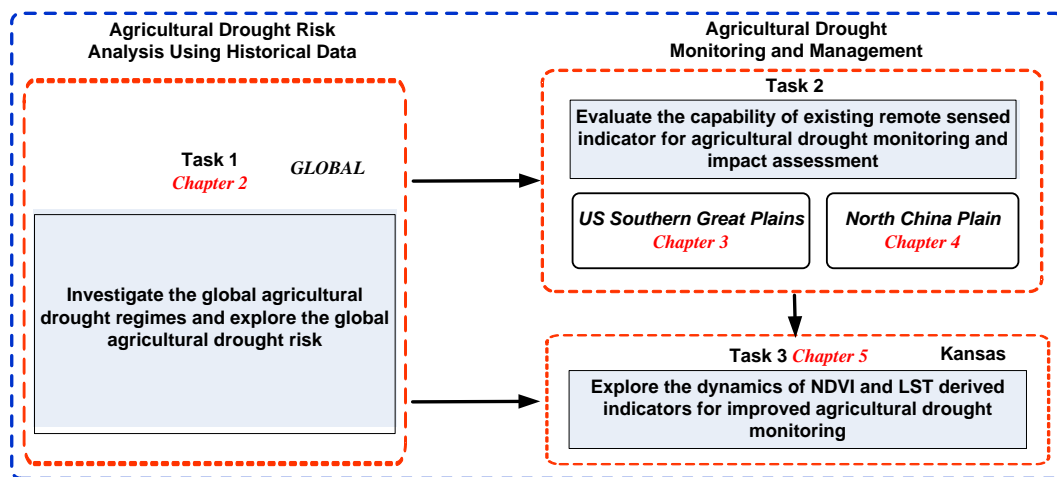


Figure 1-4: Schematic Diagram of the Proposed Research

Chapter 1 is an introductory chapter for describing the research questions carried out in this dissertation, and Chapter 6 is a concluding chapter for summarizing the main

findings and implications in this dissertation. The remaining chapters are summarized as blow:

Chapter 2 characterized global agriculture drought regimes and risk using a 30-year data record. A Global Agricultural Drought Risk Index (GADRI) was firstly developed from the characterization of global agricultural drought regimes, agricultural resilience to drought and agricultural productivity. Agricultural drought risk was then explored at both global and regional scales and global agricultural drought hotspots were identified. The evolution of agricultural drought risk during the past three decades was also investigated.

Chapters 3 & 4 investigated the performance of various remotely sensed indicators specifically for agricultural drought monitoring and the drought impacts on crop yield during winter wheat growing seasons at a finer spatial and temporal resolution from remote sensing. Chapter 3 focused on the U.S. Southern Great Plains (including Kansas, Oklahoma and Nebraska) and Chapter 4 focused on the North China Plain (including Hebei, Henan, Shandong, Shanxi and Shaanxi). These represent two important and also agricultural drought prone crop production regions with different irrigation conditions, field size distributions and crop yields.

In Chapter 3, the capabilities of various remote sensing metrics (e.g. vegetation condition, LST, ET and soil moisture derived metrics), in terms of both responsiveness and effectiveness, were investigated and compared. Also, the impacts of drought and the variability of the impacts across regions were also explored based on the NDVI derived drought indicators.

In Chapter 4, the capability of the MODIS Drought Severity Index (DSI) was evaluated for agricultural drought monitoring and the drought impacts on winter wheat yields were assessed for five provinces in North China. First, the MODIS DSI was compared with precipitation and soil moisture at the province level to examine its capability for characterizing moisture status. Then specifically for agricultural drought monitoring, the MODIS DSI was evaluated against agricultural drought severity at the province level. The impacts of agricultural drought on winter wheat yield during the main growing season were also explored using 8-day MODIS DSI data.

To better understand vegetation-temperature interactions for improved agricultural drought monitoring, Chapter 5 explored the dynamics of NDVI and LST derived drought indicators both spatially in Kansas and temporally at 8-day interval during winter wheat main growing season.

Chapter 2: Characterizing Global Agriculture Drought Regimes and Risk Using a 30-Year Data Record

2.1 Introduction

During the past three decades, several major drought events have been reported in a number of regions, including Russia, Australia, U.S. and southern Europe. According to the National Center for Atmospheric Research (NCAR), the percentage of global terrestrial areas suffering from drought more than doubled from the 1970's to the early 2000's, most possibly caused by the rise of global temperature (Dai et al., 2004). Under a changing climate, droughts have intensified, both locally (Williams et al., 2015) and at the global scale (Dai, 2013). Currently, more than half of the world is susceptible to drought and the world suffers from a total loss of about \$6-8 billion each year due to droughts (Wilhite, 2000). With the increase in global temperature, model predictions suggest increasing droughts in the next 30-90 years (IPCC2001 & 2007; Dai, 2013). Apart from climate change, the increasing water demand due to population growth and economic development has further aggravated drought conditions in many regions, resulting in significant impacts on local population, environment and society and posing severe threats in multiple sectors including agriculture, energy and industry (Mishra & Singh, 2010).

Among those sectors, agriculture is the most impacted and the frequent occurrence of heat waves together with the irregular precipitation has put considerable stress on agricultural productivity at the global scale (Teixeira et al., 2013), requiring a closer investigation of the linkage between climate change and agricultural production

(Mishra & Singh, 2010). Currently, there is a considerable body of research being undertaken to assess the impacts of climate change on agriculture at various scales (Lobell et al., 2007, 2011a, 2011b, 2014; Kucharik & Serbian, 2008; Schlenker & Lobell, 2010; Blanc, 2012; Ming et al., 2015). At the global scale, as of 2002, the warming climate since 1981 has resulted in negative impacts on crop yield, with an annual combined loss of roughly 40 Mt., equivalent to \$5 billion, for wheat, maize and barley (Lobell et al., 2007). A subsequent study by Lobell et al. (2011b) showed that, between 1980 and 2008, heat and precipitation related extreme weather led to a decline in global production of 3.8% for maize and 5.5% for wheat. Despite the crop production rise due to the agronomic improvements, there has been an increased sensitivity of major crops to drought (e.g. corn) associated with a warming climate (Lobell et al., 2014).

Aridity describes a long-term climatic phenomenon of moisture shortage. Different from “aridity”, the term “drought” reflects a prolonged period of abnormal moisture deficiency for a region, which is relatively temporary and can occur in both arid and humid climates (Maliva & Missimer, 2012). Drought regimes describe the temporal and spatial dynamics of drought over time for a given location, and key elements of comprehensive drought regimes include intensity, onset/end, duration, spatial extent, severity and frequency. These features are closely related to each other and together help distinguish one drought event from another (Wilhite, 1993, 2000, 2005), of which drought intensity and frequency are the basis for other drought features and are the emphasis of this paper. Agricultural drought risk describes the probability of the potential adverse effects on agriculture, which is often defined as the interplay between

the hazard of drought and the resilience of agriculture to emerging droughts (Knutson et al., 1998). Caution should be used concerning the definition of “agricultural drought risk”, since this term is sometimes referred to as drought severity or drought probability (e.g., Sun et al., 2012; Blauhut et al., 2015; Potopová et al., 2015), which are different from the definition of “agricultural drought risk” used in this paper. Given the significant impacts of climate change on agricultural production mentioned above, a good understanding of global agricultural drought risk can help alert crop analysts to drought-prone areas and the potential impacts, provide useful inputs for agricultural management decision-making and thus effectively help reduce the vulnerability of agricultural ecosystems to drought. Current agricultural drought risk research mainly focuses on regional or national scales, using either drought intensity or frequency as the indicator of drought hazard, and has been the focus of much work in different regions of the world (Wu & Wilhite, 2004; Wu et al., 2004; Shahid & Behrawan, 2008; Hao et al., 2012 ; He et al., 2013; Xu et al., 2013). These regional studies are useful for analyzing regional agricultural drought risk; however, they often use different data sources and indicators for characterizing drought conditions, focus on one or more local crops, or carry out risk analysis at the administrative-unit level, making it very difficult for precise and consistent spatial comparisons across regions, especially at a global scale. At the global scale, there have only been a few studies on agricultural drought risk. Most recent work at the global scale has been concentrated on investigating drought hazard (Spinoni et al., 2014; Wang et al., 2014; Geng, et al., 2015), and a limited number of global drought risk studies, through the integration of drought hazard and vulnerability, have been undertaken at the national (Li et al., 2009) or sub-national

level (Carrão, et al, 2016). Therefore, there is a lack of a consistent, comprehensive, pixel-based and agriculture-oriented drought risk analysis at the global scale.

The objective of this chapter is to explore global agricultural drought risk, by developing a Global Agricultural Drought Risk Index (GADRI) and identifying global agricultural drought hotspots. First, global agricultural drought regimes, including agricultural drought intensity and frequency, were investigated and global drought regimes were compared during the agricultural growing season and for the entire year. Then, a risk index was developed from the characterization of global agricultural drought regimes, agriculture productivity and agricultural resilience to drought. Based on this index, global agricultural drought risk was investigated for the past three decades, global drought hotspots were identified and the evolution of global agricultural drought risk was examined.

2.2 Data

The datasets used in this study included globally-gridded meteorological data, satellite-based global agricultural land distribution and agricultural growing season calendar, as well as irrigation and crop production value data from the Food and Agriculture Organization of the United Nations (FAO). A detailed description of the datasets is provided below.

2.2.1 A Self-calibrating Palmer Drought Severity Index

An improved version of the original Palmer Drought Severity Index (PDSI), the global self-calibrating PDSI (scPDSI) dataset, generated by the Royal Netherlands Meteorological Institute (KNMI) based on the Climatic Research Unit (CRU) 3.21

dataset was used in this study (Schrier et al., 2013, data available from KNMI Climate Explorer, <https://climexp.knmi.nl>). The data set provides monthly scPDSI for global land areas from 1901 to 2012 at the resolution of 0.5 degree. For this study, the monthly scPDSI data from 1980 to 2010 were used for depicting agricultural drought risk and the data from 2011-2012 were used to characterize recent summer drought conditions.

2.2.2 Global Agricultural Croplands

Several global cropland masks have been developed with different spatial resolutions and accuracies (Pittman et al., 2010; Ramankutty et al., 2008; Thenkabail et al., 2009; Biradar et al., 2009). In this study, the currently “best available” 1km resolution, global hybrid cropland mask produced by IIASA/IFPRI (Fritz et al., 2015, data available from <http://cropland.geo-wiki.org>, 2015 version) was used as the baseline cropland dataset to provide the percentage of cropland within each pixel.

2.2.3 Agricultural Growing Season Calendar

Most commonly used crop calendars are coarse, outdated, subjective and heavily interpolated outside the U.S. (Whitcraft et al., 2015). A new global agricultural growing season dataset, gridded at 0.5 degree, was developed using the 10-year 250m MODIS surface reflectance data for 2001-2010 (Whitcraft et al., 2015). This globally consistent, satellite-derived, spatially explicit agricultural growing season calendar, which depicts the start and end of growing season, was used for this study. Due to very low agricultural land coverage in certain regions (e.g., Amazon, Congo Basin and regions beyond 60°N), no valid growing season values were provided and these regions were masked out in the subsequent analysis.

2.2.4 Irrigation

The most recent FAO "Global Map of Irrigation Areas" (GMIA, version 5) dataset, which shows the percentage of irrigated areas within each grid around 2005 at the resolution of 5 minutes (Siebert et al., 2013), was used for this study. (<http://www.fao.org/nr/water/aquastat/irrigationmap/index10.stm>). Irrigation provides a means to mitigate drought and for the purpose of this study, the presence of irrigation was used to quantify the general resilience to drought.

2.2.5 Crop Production Values

The global crop production value dataset from the FAO Global Agro-Ecological Zones (GAEZ) data portal (<http://gaez.fao.org/Main.html#>), which provides values of crop production per hectare at the resolution of 5 minutes for 2000, was used to generate an indicator of relative agricultural productivity.

2.3 Methodology

2.3.1 Depicting Drought from Self-Calibrating PDSI

The Palmer Drought Severity Index (PDSI) was first developed by Palmer (1965) based on the water supply-and-demand balance model and calculated from the integration of temperature, precipitation and the soil-water holding capacity. Despite its wide use for describing drought conditions since its first appearance (Dai et al., 1998, 2004; Burke et al., 2006; Van der Schrier et al., 2006a, 2006b; Burke & Brown, 2008; Dai, 2011a, 2011b, 2013), PDSI has also received a lot of criticism for inconsistent performance across different climatic regions, which is primarily caused by the fixed empirical parameters derived from the mid-western U.S. during its initial

development (Wells et al., 2004). First introduced by Wells et al. (2004), a self-calibrating PDSI (scPDSI) automatically calibrates the index at any location by replacing empirical constants in the index computation with dynamically calculated values, which makes it more suited than the original PDSI for spatial comparisons and shows considerable advantages for global application. Similar to the PDSI, a classification of drought severity from scPDSI is shown in Table 2-1. The scPDSI was converted to a numeric drought level, which was used in this study for characterizing drought regimes.

Table 2-1: Classification of Drought

scPDSI Value	Drought Intensity	Drought Level
above -1.0	Normal	0
-1.0 to -2.0	Mild Drought	1
-2.0 to -3.0	Moderate Drought	2
-3.0 to -4.0	Severe Drought	3
-4.0 or less	Extreme Drought	4

2.3.2 Characterizing Drought Regimes

To enable characterization of drought regimes, numeric drought levels were first labeled using the scPDSI based on the last column of Table 2-1. For each 0.5 degree grid, the global monthly scPDSI was extracted to calculate both the average drought intensity (ADI) and drought frequency (DF) during the agricultural growing season for the past 30 years and for each decade. For any location where the growing season starts in one year and ends in the following year, the data from 1980-2010 were used, and otherwise the data from 1980-2009 were used. The ADI and DF are defined as below (Equation 2-1):

$$DF = \frac{\sum_{i=1}^4 N_i}{\sum_{i=0}^4 N_i}$$

$$ADI = \frac{\sum_{i=0}^4 i * N_i}{\sum_{i=0}^4 N_i}$$

2-1

Where *DF* equals the probability of drought occurrence during the given time frame, *ADI* is the average drought intensity in the given time frame, *i* is the drought level, and *N_i* is the number of months which suffer from *i*-level drought. For general

drought, the $\sum_{i=0}^4 N_i$ equals all the months during the given time period; for agricultural

drought, $\sum_{i=0}^4 N_i$ equals all the months within the growing season for the given time period. For this study of agricultural drought, emphasis was placed on drought occurrences during the agricultural growing season; also, the drought regimes during the agricultural growing season and the entire year were also compared.

2.3.3 Developing the Global Agricultural Drought Risk Index (GADRI)

Key steps in developing the GADRI involved risk factor selection, rescaling/normalization and risk model selection.

- Risk factor selection

As mentioned before, agricultural drought risk is the outcome of drought hazards and the capability of coping with emerging droughts for the given location. For each grid cell, the drought conditions, the local resilience as well as the agricultural productivity, were considered. The scPDSI was used to describe the drought regimes

(both intensity and frequency); irrigation information was used to describe the general resilience of agricultural lands to drought, with more irrigation indicating a greater resilience and thus lower risk; the cropland area percentage and crop production value per hectare were combined to depict the integrated agricultural productivity for the grid. Together, from the global perspective, drought intensity, frequency, agricultural growing season calendar, crop percentage, crop productivity, and irrigation were combined to define agricultural drought risk.

- Rescaling factors to the same resolution and normalization

For consistent cross comparison, all data layers were scaled to the same 0.5 degree resolution. To this end, cropland percentage, irrigation, and crop production value datasets were first aggregated to 0.5 degree grid. Also, to ensure the compatibility, all factors were normalized to a range of [0, 1] to reduce the dimension using the Equation 2-2:

$$N_Factor = Factor / Max(Factor) \tag{2-2}$$

Where Factor indicates the input factors (*ADI*, *DF*, Irrigation, Cropland Percentage and Crop Production Value), and *N_Factor* indicates the corresponding normalized factors for the input factors. In this study, *Max (ADI)* equals 4, *Max (DF)*, *Max (Irrigation)* & *Max (Cropland Percentage)* equal 1, and *Max (Crop Production Value)* is the maximum crop production value of all grids across the globe.

- Risk model selection

Several risk models have been developed, which can be generally categorized into the sum model (Blaikie et al., 1994) and the more recent product model (Knutson et al.

1998; Wilhite 2000; Hayes et al., 2004). In this study, the product model was used and the grid-based GADRI was developed using Equation 2-3:

$$\begin{aligned}
 GADRI &= DroughtHazards * DroughtResilience * IntergratedAgriculturalProductivity \\
 &= F(CropCalendar, Intensity, Frequency, Irrigation, AgriculturalLand, AgriculturalProductivity) \\
 &= ADI * DF * (1 - C_{Irri}) * C_{Perc} * C_{Prod}
 \end{aligned}$$

2-3

Where *ADI* is the average agricultural drought intensity, *DF* is the agricultural drought occurrence probability during the growing season (see Equation 2-1), *C_{Perc}* is the agricultural land percentage, *C_{Prod}* is the agricultural productivity expressed as the normalized crop production value, and *C_{Irri}* is the irrigation percentage.

2.4 Results

2.4.1 Global Agricultural Drought Regimes

To depict the agricultural drought regimes, the agricultural growing season calendar was incorporated to indicate both the start and the end of growing season for each grid cell and the 0.5-degree monthly scPDSI during the agricultural growing season was used to calculate the per-grid agricultural drought regimes (*ADI* and *DF*) for the past 30 years using Equation 2-1. The spatial patterns of global agricultural drought regimes (*ADI* and *DF*) for agricultural lands are shown in Figure 2-1 and Figure 2-2. It should be noted that only the cropland grid cells with valid growing season calendar data are shown. The global agricultural drought intensity and frequency follow a similar pattern, which demonstrates that regions with more severe droughts also tend to experience more frequent droughts. Both drought intensity and frequency hotspots are found in the Western USA, Western Argentina, Eastern Brazil,

Western Africa, Southern Africa, Spain & Morocco, Eastern Europe, Southern Russia, Northern Mongolia, Northern India, North China, and Eastern & Southwestern Australia.

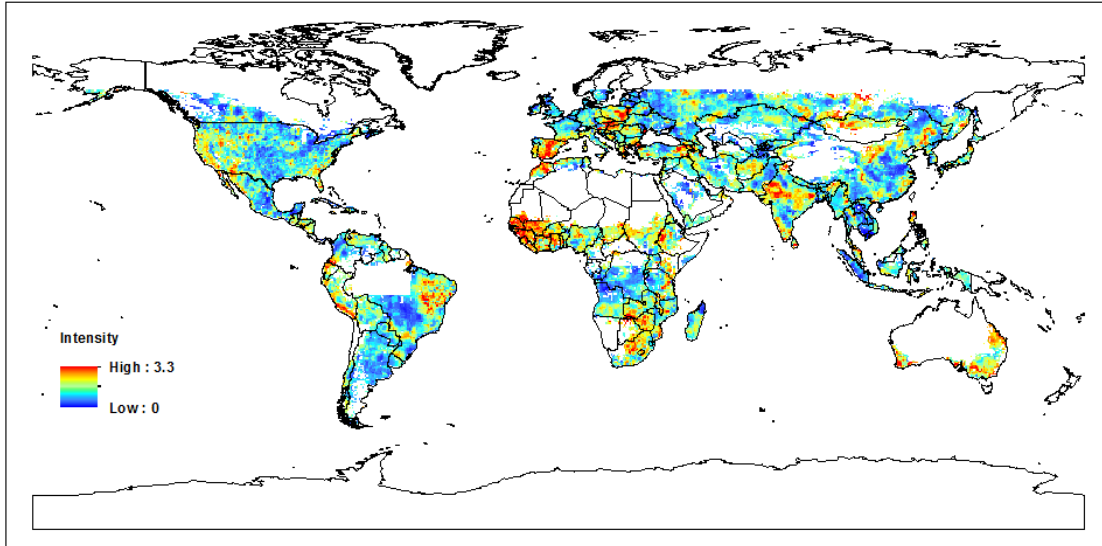


Figure 2-1: Global Average Drought Intensity over Agricultural Lands from 1980 to 2009

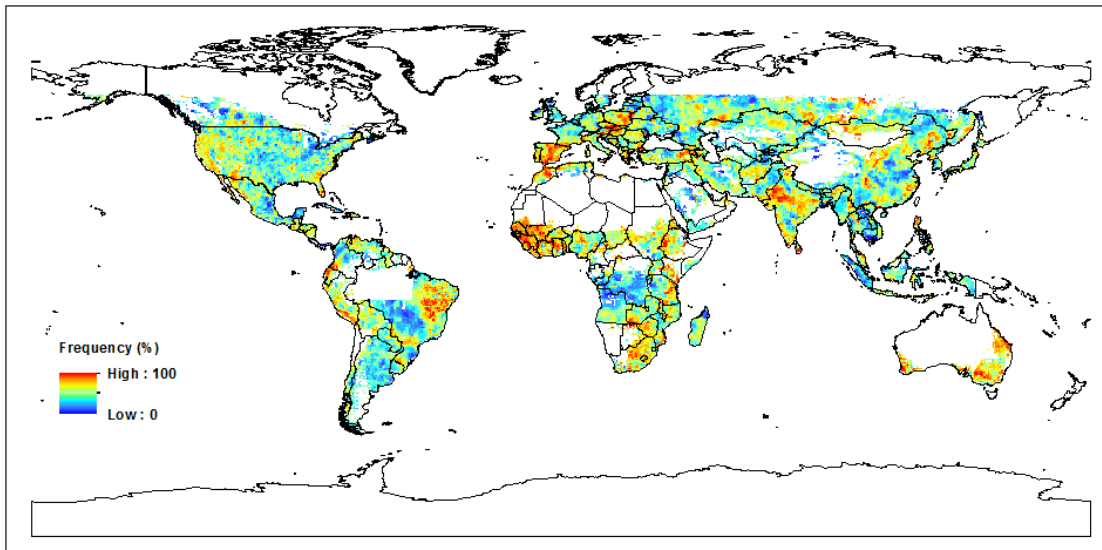


Figure 2-2: Global Drought Frequency over Agricultural Lands from 1980 to 2009

To investigate the difference between drought regimes during the agricultural growing season and for the entire year, monthly scPDSI data from 1981 to 2009 were used to calculate the general drought regimes (ADI and DF) for each grid cell. The

relative differences of drought regimes between the growing season and the entire year were derived (Equation 2-4) and the spatial explicit differences for both drought intensity and frequency are displayed in Figure 2-3 and Figure 2-4.

$$RD = \frac{DR_{GrowingSeason} - DR_{EntireYear}}{DR_{EntireYear}} * 100\% \quad 2-4$$

Where RD , $DR_{GrowingSeason}$ and $DR_{EntireYear}$ respectively represent the relative difference in drought regimes, growing season drought regimes and general drought regimes.

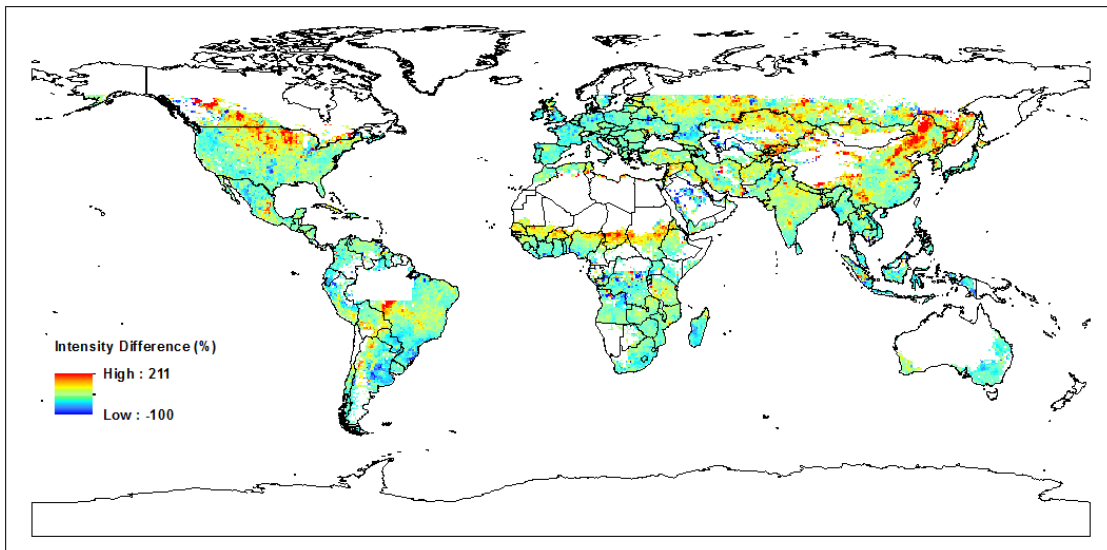


Figure 2-3: Relative Difference of Global Average Drought Intensity over Agricultural Lands (Agricultural Growing Season vs. Entire Year)

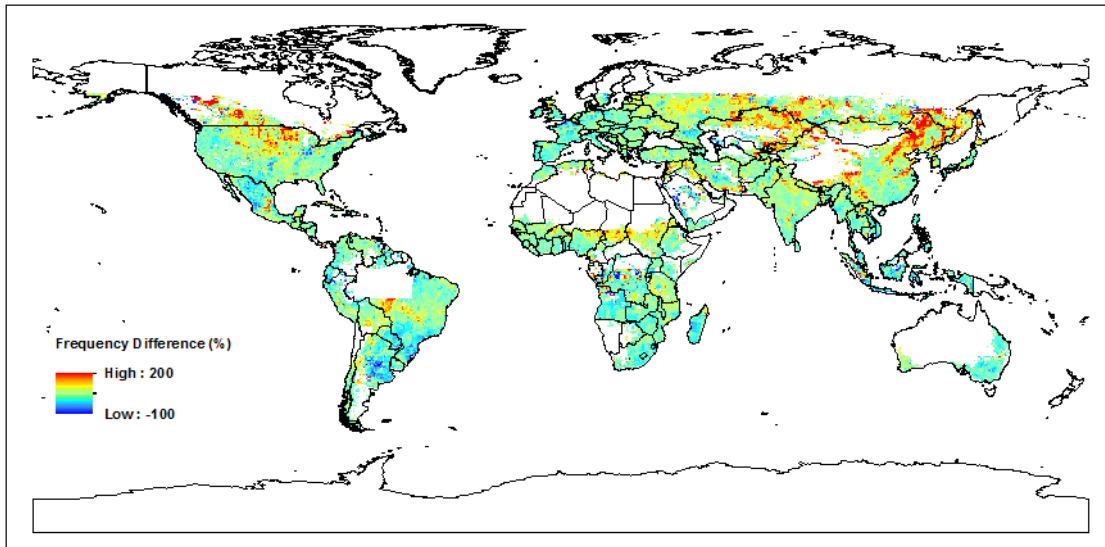


Figure 2-4: Relative Difference of Global Drought Frequency over Agricultural Lands (Agricultural Growing Season vs. Entire Year)

As seen from Figure 2-3 and Figure 2-4, different drought intensity and frequency between the agricultural growing season and the entire year were observed for most regions across the globe. The differences of drought intensity and frequency follow similar patterns, highlighting significantly stronger growing-season drought regimes concentrated in Northeast China, Northern Great Plains of North America, Southern Russia, Kazakhstan, and Northern Sub-Saharan Africa.

To more quantitatively examine the magnitude of drought regime differences after integrating the agricultural growing season calendar, based on Figure 2-3 and Figure 2-4, both the percentage of agricultural areas suffering from increased intensity/frequency (Figure 2-5) and the average intensity/frequency differences (Figure 2-6) at different scales (globe, hemisphere and major agricultural producing countries) are shown. Figure 2-5 shows that more than 70% of the agricultural lands across the globe experienced an increased drought intensity during the agricultural growing season as compared to the entire year, with around 80% in the Northern

Hemisphere and 60% in the Southern Hemisphere. Of the 10 major agricultural producing countries, 9 countries have more than half of the agricultural lands exhibiting an increased drought intensity (except Argentina), with around 60%-80% in Brazil, Ukraine & U.S. and 80-90% in Canada, China, India & Kazakhstan. Similar results were found for drought frequency in Figure 2-5. Most regions (except Australia and Argentina) have the majority of agricultural areas suffering from more frequent droughts during the agricultural growing season, with more than 70% in the Northern Hemisphere as compared to slightly more than 50% in the Southern Hemisphere, and 50-60% in Brazil and more than 70% in all 7 other major agricultural producing countries. Figure 2-6 shows the differences for both drought intensity and frequency for the globe, hemispheres and major agricultural producing countries, with an increased drought intensity at all scales. A higher drought intensity increase during the agricultural growing season was found in the Northern Hemisphere than the Southern Hemisphere, and in Canada, China, Kazakhstan and Russia (around 8-10%) among the 10 major agricultural producing countries. Similarly, most regions and countries (except Australia and Argentina) also showed increased drought frequency during the agriculture growing season, with a higher frequency increase in the Northern Hemisphere than the Southern Hemisphere, and in Kazakhstan, Canada, China and Russia among the 10 agricultural producing countries (around 6-9%). Therefore, after integrating the agricultural growing season calendar, more than half of the agricultural areas in those regions and most countries exhibit an increased drought intensity and frequency (Figure 2-5). They also show an increased drought intensity and frequency (Figure 2-6). These results demonstrate that, despite a similar pattern, agricultural lands

generally have more severe drought conditions and higher probability of drought occurrences during the agricultural growing season as compared to the entire year and global drought regimes (intensity and frequency) are more intensified during the agricultural growing season.

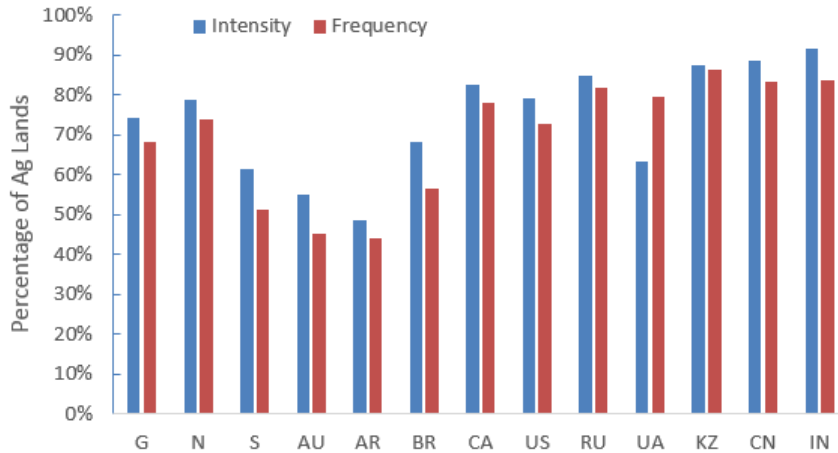


Figure 2-5: Agricultural Lands Experiencing Increased Drought Intensity and Frequency during Agricultural Growing Season

Notes: The x-axis labels indicate the globe (G), Northern (N) and Southern (S) Hemisphere, and 10 major agricultural producing countries: Australia (AU), Argentina (AR), Brazil (BR), Canada (CA), United States (U.S.), Russia (RU), Ukraine (UA), Kazakhstan (KZ), China (CN), and India (IN).

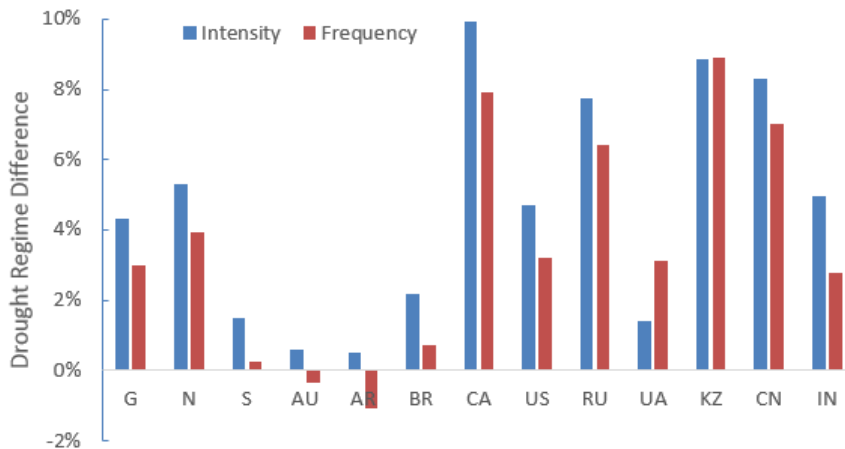


Figure 2-6: Drought Intensity and Frequency Difference over Agricultural Lands (Agricultural Growing Season vs. Entire Year)

Notes: The x-axis labels indicate the globe (G), Northern (N) and Southern (S) Hemisphere, and 10 major agricultural producing countries: Australia (AU), Argentina (AR), Brazil (BR), Canada (CA), United States (U.S.), Russia (RU), Ukraine (UA), Kazakhstan (KZ), China (CN), and India (IN).

These results can be explained by the regional climatology. In most regions, there tend to be more irregular precipitation and heatwave patterns during the agricultural growing season, leading to more severe drought events and more frequent drought occurrence. As highlighted in red in Figure 2-3 and Figure 2-4, Northeast China, Northern Great Plains of North America and Northern Sub-Saharan Africa show significantly stronger drought regimes during the growing season as compared to the entire year, which is related to a larger inter-annual variability of precipitation due to irregular precipitation patterns as well as the more intensive evapotranspiration from higher temperature during the growing season. To more clearly demonstrate this, 3 sites located in those highlighted red regions mentioned above, namely Northeast China (Site 1), U.S. Corn Belt (Site 2) and Northern Sub-Saharan Africa (Site 3), were selected to show drought trajectories during the past 30 years from 1980-2009 (Figure 2-7). As seen from Figure 2-7, despite different drought regimes being observed for those 3 sites (the most severe drought conditions in Site 3, followed by Site 2 and Site 1), more severe and frequent droughts tend to occur consistently during the corresponding growing-season months (May to September for Site 1, May to October for Site 2, and July to November for Site 3).

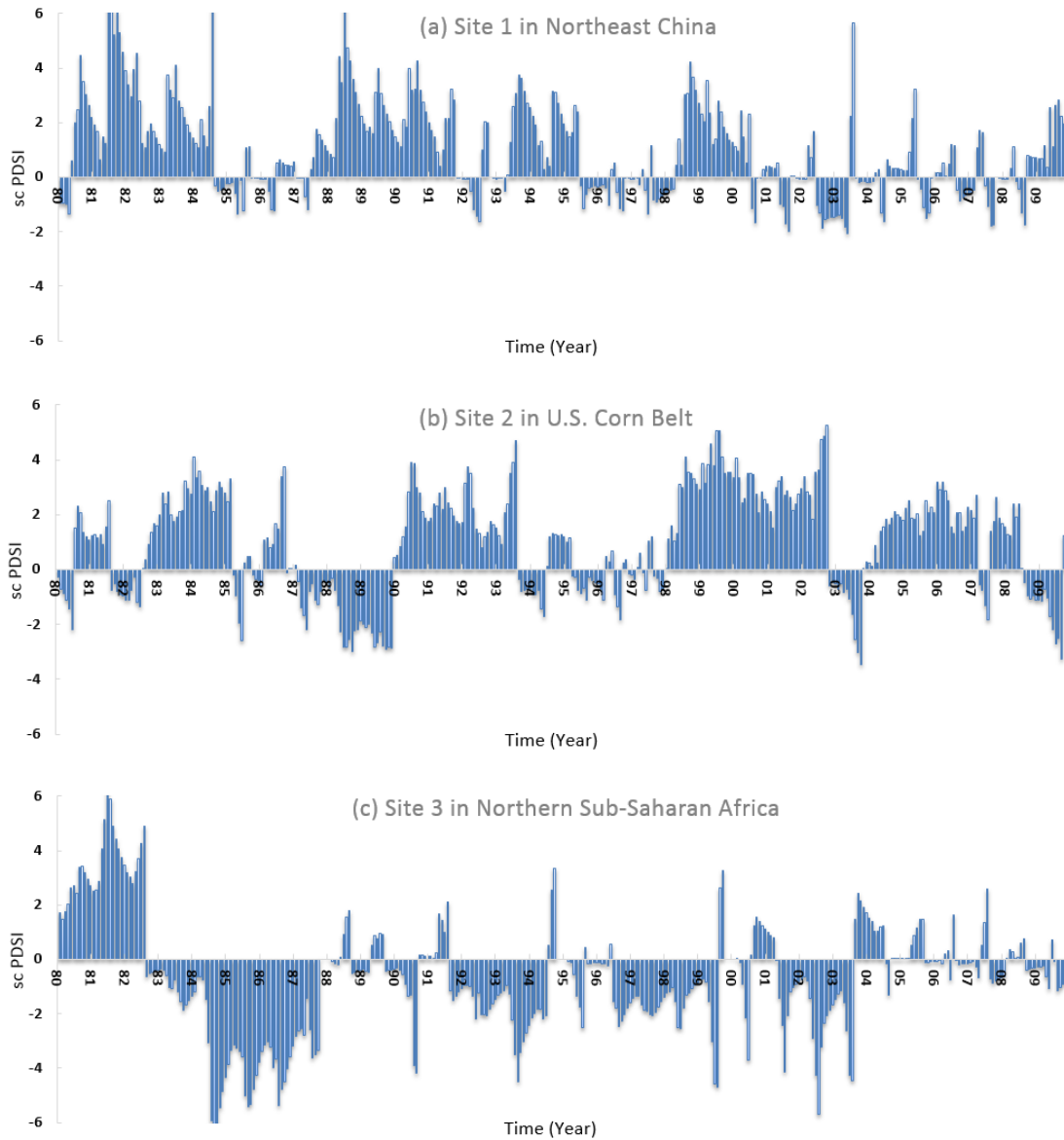


Figure 2-7: Time-series of scPDSI for the Past 3 Decades (1980-2009) for 3 Highlighted Sites (a) Northeast China (b) U.S. Corn Belt (c) Northern Sub-Saharan Africa
 Note: A scPDSI value less than -1 indicates a drought occurrence.

2.4.2 Global Agricultural Drought Risk

Based on the global agricultural drought regimes derived from Section 2.4.1 as well as other inputs from cropland, crop productivity and irrigation, the GADRI was calculated for the past 3 decades from the 1980's to the 2000's for each grid using Equation 2-3. Since the GADRI represents an integrated risk for the entire grid cell,

which involves many normalized factors ranging from 0 to 1, it produces a maximum value of less than 1. To more clearly show the distribution of global agricultural drought risk, the original GADRI was converted into relative GADRI (RGADRI) based on the average GADRI (Equation 2-5). The resulting spatial pattern of global agricultural drought risk is shown in Figure 2-8.

$$RGADRI = \frac{GADRI}{Mean(GADRI)} \quad 2-5$$

Where *Mean (GADRI)* is the average *GADRI* across the agricultural lands of the globe. *RGADRI* is the relative *GADRI*, and areas with a relative *GADRI* value greater than 1 indicate that those regions have a drought risk higher than the global average.

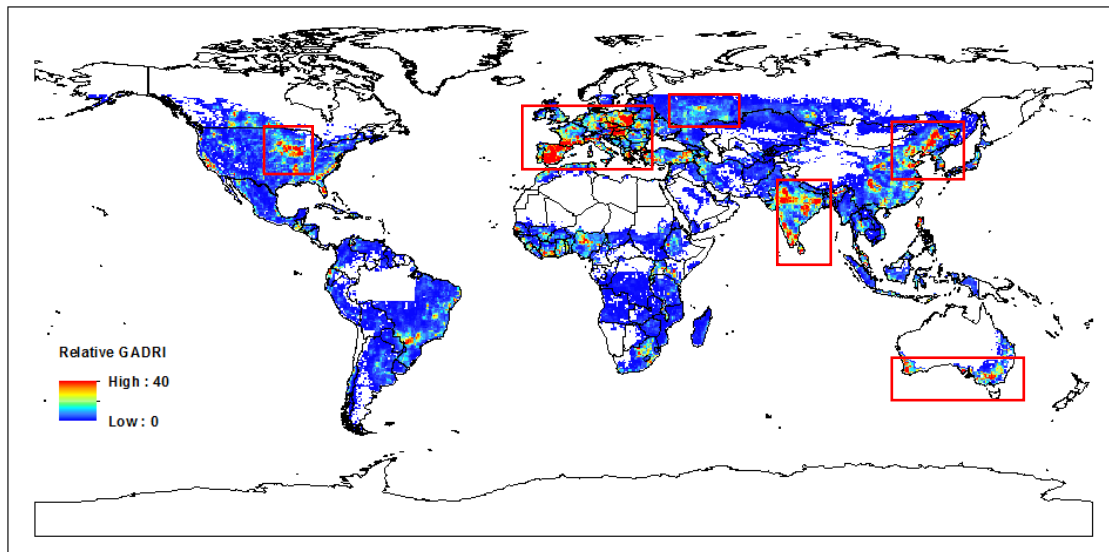


Figure 2-8: Global Agricultural Drought Risk for the Past 3 Decades

From Figure 2-8, several agricultural drought hotspots can be identified, as indicated by the highlighted regions, such as U.S. Corn Belt, Eastern Europe & Spain, Central Russia, India, North & Northeast China, and Australia. Spain stands out with very high agricultural drought risk for the entire country. Similar to Section 2.4.1, to more quantitatively describe the agricultural drought risk, the agricultural drought risk

at the global, hemisphere and major agricultural producing countries were summarized and shown in Figure 2-9. As can be seen from Figure 2-9, the Northern Hemisphere shows a higher average agricultural drought risk as compared to the Southern Hemisphere. Among these 10 major agricultural producing countries, India has the highest agricultural drought risk (RGADRI>2), followed by Australia (RGADRI between 1.5 and 2), Ukraine and China (RGADRI between 1 and 1.5) and the U.S. (RGADRI around 1). It is worth noting that those countries are the major breadbaskets of the world, which play a critical role in the international food market.

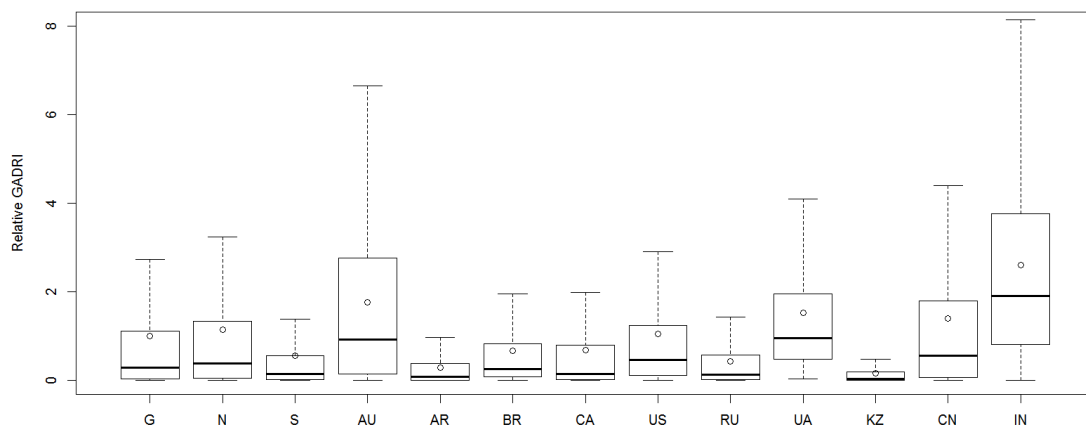


Figure 2-9. Regional Agricultural Drought Risk for the Past 3 Decades

Notes: The x-axis labels indicate the globe (G), Northern (N) and Southern (S) Hemisphere, and 10 major agricultural producing countries: Australia (AU), Argentina (AR), Brazil (BR), Canada (CA), United States (U.S.), Russia (RU), Ukraine (UA), Kazakhstan (KZ), China (CN), and India (IN).

2.4.3 Evolution of Global Agricultural Drought Risk for the Past 3 Decades

To investigate the evolution of global agricultural drought risk for the past 3 decades, the agricultural drought risk for each of the past 3 decades was calculated using the method applied in Section 2.4.1. The decadal relative changes in agricultural drought risk (1990's vs. 1980's, 2000's vs. 1990's and 2000's vs. 1980's) were calculated, and the agricultural drought risk change patterns for both the 1990's vs.1980's (Figure 2-10) and the 2000's vs. 1990's are displayed (Figure 2-11).

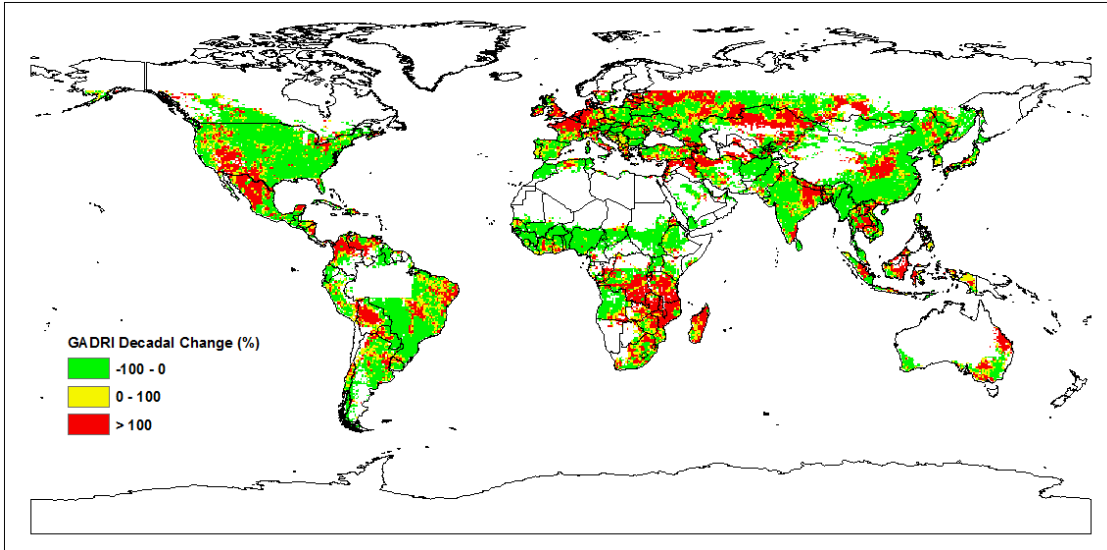


Figure 2-10: Global Agricultural Drought Risk Decadal Change (1990's vs. 1980's)
Note: Agricultural areas in red show that the 1990's had more than twice the drought risk as compared to the 1980's.

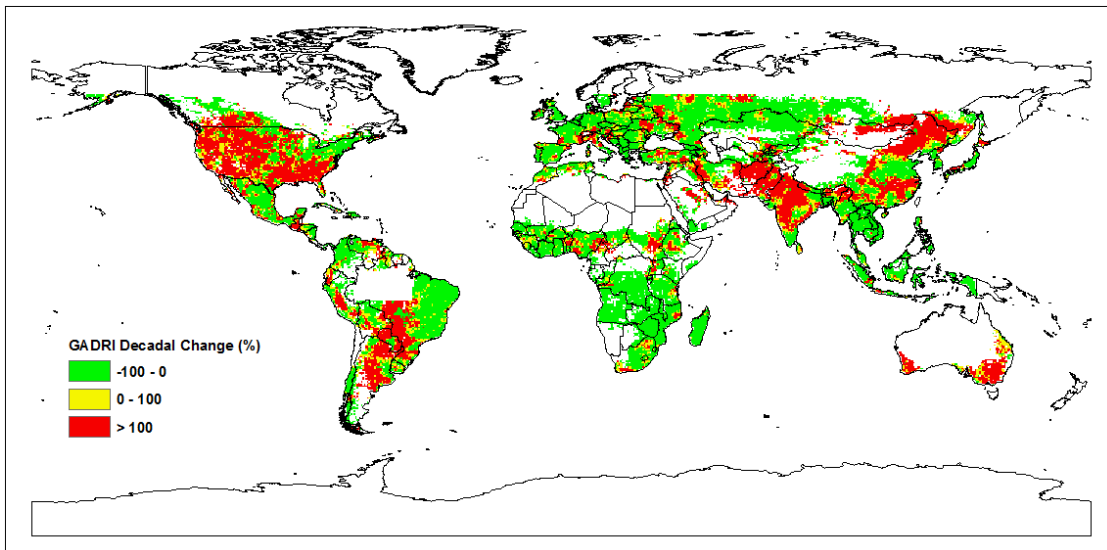


Figure 2-11: Global Agricultural Drought Risk Decadal Change (2000's vs. 1990's)
Note: Agricultural areas in red show that the 2000's had more than twice the drought risk as compared to the 1990's.

Based on the decadal risk change maps, the areas suffering from increased risk for the entire globe, the Northern/Southern Hemispheres as well as the 10 major agricultural producing countries (Figure 2-12), and the average risk changes from the

1980's to 1990's, 1990's to 2000's and 1980's to 2000's (Figure 2-13), were summarized.

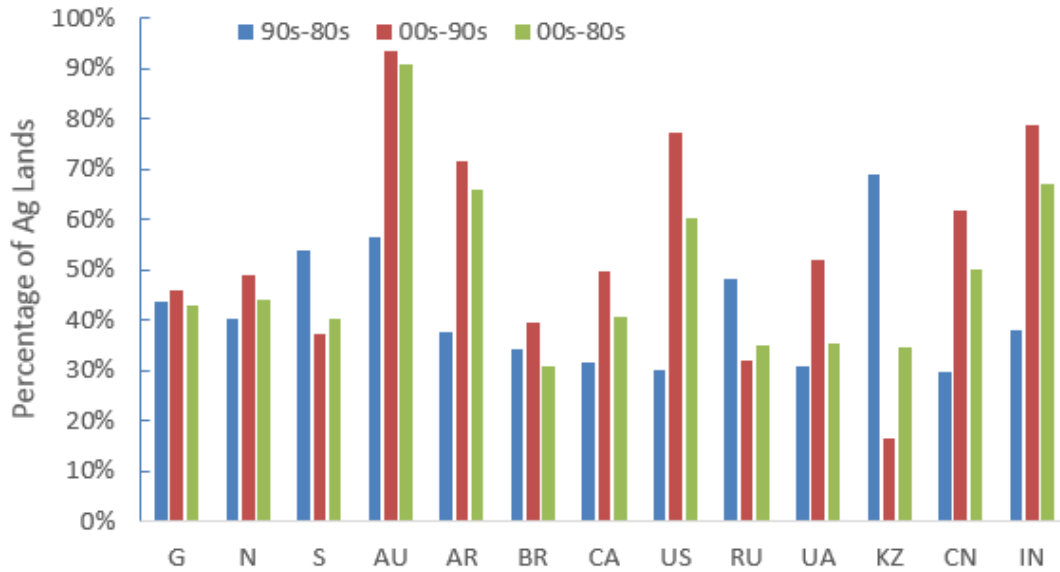


Figure 2-12: Agricultural Lands Experiencing Increased Decadal Drought Risk
Notes: The x-axis labels indicate the globe (G), Northern (N) and Southern (S) Hemisphere, and 10 major agricultural producing countries: Australia (AU), Argentina (AR), Brazil (BR), Canada (CA), United States (U.S.), Russia (RU), Ukraine (UA), Kazakhstan (KZ), China (CN), and India (IN).

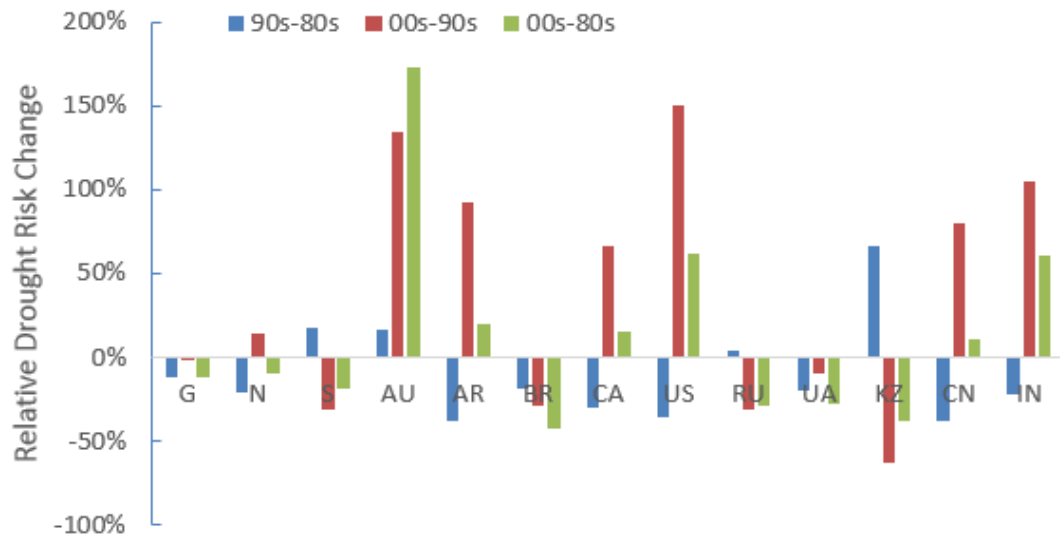


Figure 2-13: Agricultural Drought Risk Decadal Change
Notes: The x-axis labels indicate the globe (G), Northern (N) and Southern (S) Hemisphere, and 10 major agricultural producing countries: Australia (AU), Argentina (AR), Brazil (BR), Canada (CA), United States (U.S.), Russia (RU), Ukraine (UA), Kazakhstan (KZ), China (CN), and India (IN).

The figures show that, from the 1980's to 1990's, more than 40% of agricultural land across the globe experienced an increase in agricultural drought risk (Figure 2-12), with a higher relative increase observed in the Western U.S. and Mexico, Bolivia, Tanzania, Zambia, Mozambique and Southern DR Congo, Western Europe, Northern Kazakhstan, Central Russia, Central China, Northeastern India and Eastern Australia (Figure 2-10). In general, the average drought risk of agricultural lands across the globe and the Northern Hemisphere decreased in the 1990's as compared to the 1980's, while an increased drought risk was observed in the Southern Hemisphere (Figure 2-13). Also, from the 1980's to the 1990's, there is a higher percentage of agricultural areas exhibiting increased drought risk (Figure 2-12) in the Southern Hemisphere as compared to the Northern Hemisphere. A closer comparison of the major agricultural producing countries shows that Australia and Kazakhstan have a higher percentage of agricultural lands experiencing increased agricultural drought risk (Figure 2-12) and a significant agricultural drought risk increase from the 1980's to the 1990's, with Russia showing slightly increased agricultural drought risk and other major agricultural producing countries exhibiting decreased drought risk (Figure 2-13).

From the 1990's to 2000's, about 45% of agricultural lands across the globe experienced increased drought risk, with higher percentage of agricultural lands showing increased drought risk (Figure 2-12) in the Northern Hemisphere. The areas with significant drought risk increase from the 1990's to 2000's are concentrated in U.S., Argentina, Southwestern Brazil, India, Northeast and South China, and Australia (Figure 2-11). Of the 10 major agricultural producing countries, 5 countries have more than half of agricultural areas undergoing increased drought risk, with more than 90%

for Australia, approximately 80% for India and U.S., around 70% for Argentina and 60% for China (Figure 2-12). The entire globe exhibits a similar agricultural drought risk in the 2000s as compared to the 1990s, with an increased risk in the Northern Hemisphere and a decreased risk in the Southern Hemisphere (Figure 2-13). Among the major agricultural producing countries, U.S., Australia, India, Argentina, China, Canada shows increased agricultural drought risk, with more than doubled agricultural drought risk observed in U.S., Australia and India in the 2000s as compared to the 1990s. Despite the different change patterns of agricultural drought risk during the past 3 decades across the globe, we find that Australia and Brazil exhibit continuous increased and decreased drought risk respectively during the past 30 years. Although it is premature to identify these findings as a trend, it calls for further continued monitoring and work on this topic to help identify the long-term trend as more data become available in the future.

2.5 Discussions

By providing a global picture of agricultural drought risk, this research helps to identify the agricultural drought prone regions of the world and those areas which have experienced severe droughts in recent years. Figure 2-14 shows the global drought (ADI calculated from scPDSI) for the 2011-2012 summer. The summer periods were selected to highlight the drought during the growing season most likely to negatively affect crop growth. As seen in Figure 2-14, severe droughts were found in Russia, Ukraine, U.S. Great Plains, Spain and Southwest China during the 2011-2012 summer. Although the study above identified these regions as drought prone, this analysis highlights that on an annual basis there can be simultaneous occurrence of drought in

several major agricultural production areas of the world. The simultaneous drought events in the U.S. and Russia in 2011-2012, resulted in food price increases and had a major impact on the markets, which highlighted the need for increased study and monitoring of drought in agricultural areas in the context of food price volatility and food security (Janetos et al., 2017).

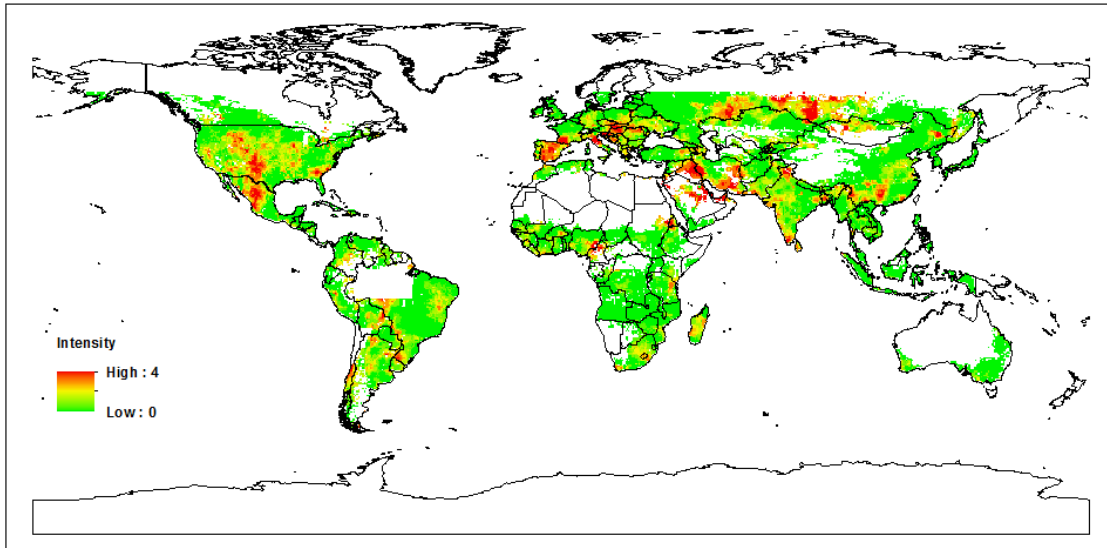


Figure 2-14: 2011-2012 Summer Global Average Drought Intensity

Notes: 2011 December-2012 February was used for Southern Hemisphere, and 2012 June-2012 August was used for Northern Hemisphere.

In this study, the irrigation information was used to characterize the resilience of agricultural ecosystems to drought. The FAO irrigation dataset used was generated around 2005 and is outdated, and an updated irrigation dataset which describes the most recent irrigation status would help to improve the drought risk analysis. Apart from the irrigation areas, the irrigation amount and timing are also important factors for drought risk assessment and therefore the integration of data sources on water storage both underground and surface water, such as those derived from the Gravity Recovery and Climate Experiment (GRACE, data available at <http://grace.jpl.nasa.gov>; Swenson, 2012) and the future Surface Water and Ocean Topography Mission (SWOT,

<https://swot.jpl.nasa.gov/>), could be useful to help improve the drought risk assessment model. Other social/economic factors, such as farmer's accessibility to drought resistant crop varieties and local food trade (import/export) policies, will also impact the resilience of local agriculture to drought and thus agricultural drought risk. While these data may not be readily available globally at the grid scale for now, the incorporation of these factors would enhance the assessment of global agricultural drought risk when those data become available in the future. It should also be noted that, the drought risk index developed in this study describes the integrated drought risk for the entire grid (i.e. 0.5-degree) for application over large regions and for consistent comparison; however, its value is not readily comparable with some other drought risk indices, especially those derived using average conditions for each grid and therefore caution should be used.

As a newly developed satellite-derived dataset, the accuracy of the agricultural growing season calendar is still not established for certain regions and some data gaps exist, thus more extensive accuracy assessment and data gap filling are needed. Considering the varying impacts of drought on different crops, crop-specific growing season calendars as well as crop-specific maps are highly recommended for more precisely describing drought risk. Also, this work is based on drought regime characterization from the 0.5-degree globally gridded monthly scPDSI dataset. With the remote sensing community providing high-quality global satellite data with an increasing data record, this will enable the more precise long-term characterization of global agricultural drought regimes and subsequently the agricultural drought risk at a finer temporal and spatial resolution. For example, the NASA Long Term Data Record

(LTDR, data available from <http://ltdr.nascom.nasa.gov/>; Pedelty et al., 2007), provides an internally consistent, daily-updated, global coverage surface reflectance product since 1981 that could be useful in this regard, especially with the inclusion of a long-term surface temperature record in the future.

2.6 Conclusions

With our changing climate and increased frequency and severity of extreme weather events, drought has gained increased attention in recent years. By developing an agriculture-oriented drought risk index from the best available and globally consistent data, this study provides a unique overview of agriculture specific drought risk consistent at the global scale. The main conclusions of the analysis are as follows:

(1) Different drought regimes over agricultural lands were observed when an agricultural growing season calendar was included. Despite similar spatial patterns, the drought intensity and frequency tend to be higher during the growing season as compared to the entire year, which indicates more severe drought conditions during the agricultural growing season and highlights the desirability of including consistent agricultural growing season data for a more nuanced and accurate large-scale agricultural drought analysis.

(2) The global agricultural drought risk index (GADRI) was developed to quantify the global agricultural drought risk for the past 30 years at the 0.5-degree resolution. The spatially explicit global agricultural drought risk map indicates the U.S. Corn Belt, Eastern Europe, Spain, Central Russia, India, North China and Australia have higher agricultural drought risk and are shown to have been the agricultural drought hotspots. It is worth noting that these are the main agricultural producing regions and include the

major breadbaskets of the World, which can also have direct implications for international markets and food prices.

(3) During the past 3 decades, different change patterns of agricultural drought risk were found for different regions of the globe and the major agricultural producing countries. Agricultural drought risk in Australia has continued to increase during the past 30 years. Further work is warranted to help identify the change trend with a longer data record.

(4) The study highlights the potential for simultaneous drought events in different major agricultural production regions of the world, with implications for global food prices and food security.

With the increased attention to extreme climate events and the impact on agricultural production, there is a continued interest to understand which regions of the globe are most at risk and what are the trends in drought occurrence in agricultural lands. This research can help global crop analysts and decision makers highlight agricultural drought prone areas, thus offering information for drought mitigation, preparedness and response at the global scale.

Chapter 3: Investigating the Capabilities of Existing Remotely Sensed Indicators for Agricultural Drought Monitoring and Impact Assessment in Southern U.S. Great Plains

3.1 Introduction

Originating from a deficiency of precipitation, drought is a recurring event for both dry and humid climatic regimes (Wilhite, 2000 & 2005). As a “creeping” natural disaster, drought has many disciplinary perspectives, resulting in significant impacts in different social sectors. Depending on different emphasis on the natural and socioeconomic factors, drought can be generally grouped into four types: meteorological drought, agricultural drought, hydrological drought and socioeconomic drought (Wilhite & Glantz, 1985).

Agriculture is the primary sector to be affected by drought. Although the final crop production is influenced by various factors during the growing season, drought remains the main driver for reduced crop yield. Compared with other drought types, agricultural drought focuses on the availability of soil water for sustaining crop growth and relates the water deficiency to agricultural impacts (Wilhite, 2000 & 2005). As one dominant factor to influence crop growth and vigor, soil moisture plays an important role for identifying agricultural drought, and understanding the spatial-temporal variability of soil moisture is of key importance for monitoring agricultural drought.

Soil moisture can be measured by either ground based systems or remote sensing. Despite the high frequency of in situ soil moisture observations at different depths, data are only available from a limited number of sites and regional networks. Remote

sensing can provide estimates of soil moisture at a broad scale, and several active (Wagner et al., 1999) and passive (Njoku et al., 2003; Kerr et al., 2010) microwave instruments have been used for retrieving soil moisture. ASCAT is an active microwave instrument operating on-board the Meteorological Operational (MetOp) satellites since 2006, providing a global Surface Soil Moisture (SSM) product derived from the backscatter measurements (Wagner et al., 1999; Naeimi et al., 2009). Due to its operational status and promising long-term prospects, ASCAT SSM products show great potential for numerical weather prediction, hydrological modelling and crop growth monitoring, especially at a global scale (Wagner et al., 2013). However, due to its complexity, the capability of the ASCAT SSM product for regional drought monitoring still needs further evaluation using more extensive measurements.

In addition to the changes in soil moisture status, drought also limits the vegetation growth which can be observed from satellite. Since the appearance of satellite-based drought monitoring in the 1980's using AVHRR data (Justice et al., 1985), many remotely sensed indicators have been developed based on vegetation conditions (Chen et al., 1994; Kogan, 1990; Liu & Kogan, 1996, Peters et al., 2002), surface temperature (McVicar & Jupp, 1998; Kogan, 1995), and energy exchange (Anderson et al., 2007 & 2011). More recently, there has been a growing trend to integrate different data sources for drought monitoring. Several indicators based on the combination of vegetation indices and surface temperature/energy exchange have been developed such as VHI (Kogan, 1995a), TVI (McVicar & Jupp, 1998), VSWI (McVicar & Jupp, 1998) and TVDI (Sandholt, 2002), and DSI (Mu et al., 2013a). These integrated indicators based on LST-NDVI or ET-NDVI relationships have shown to be useful in many drought

monitoring studies. However, due to different responses to drought, the direct integration of vegetation growth condition and LST/ET information might influence the capability of the integrated drought indicators and calls for more detailed sensitivity analysis of the various inputs for drought monitoring. Despite the large number of existing studies on drought monitoring, there has been little emphasis on exploring and comparing the sensitivity of these remotely sensed indicators to drought. Besides, the impacts of drought on crop production, especially at a regional scale, are still poorly understood. Current studies on agricultural drought impacts mainly focus at a small/station scale using crop models (Bryant et al., 1992; Song & Dong, 2006), and there has been little work to investigate these impacts at a spatial and temporal resolution afforded by remote sensing.

The objective of this chapter is to assess the sensitivity of different remotely sensed indicators for agricultural drought monitoring using in situ soil moisture measurements as ground truth, to evaluate the effectiveness of ASCAT SSM for agricultural drought monitoring, and also to explore the impacts of drought on winter wheat yield during the growing season in Southern U.S. Great Plains (Kansas, Oklahoma and Nebraska). For performance evaluation of vegetation condition, LST and ET based indicators, the general response of those indicators to drought was explored for each station, using all available entire year data. The ability of different drought indicators was compared and the performance across different land cover types was analyzed. The capabilities of remotely sensed indicators for agricultural drought monitoring during the main winter wheat growing season (March-June from green-up to harvest) were then examined. For ASCAT, the general ability of ASCAT SSM for describing drought was explored for

each station, the seasonality of ASCAT SSM for characterizing drought was evaluated for different time of year at daily basis, and the capability of ASCAT SSM for charactering agricultural drought during the main winter wheat growing season (March-June) was examined for crop stations. For analysis drought impact on winter wheat, the work was first undertaken for Kansas at the state level, and then extended to Oklahoma and Nebraska at both state and Agricultural Statistics District (ASD) levels to explore the spatial variability. First, vegetation indices and associated metrics (e.g. anomaly/cumulative anomaly derived metrics) were calculated based on MODIS data. Then, the impacts of agricultural drought on winter wheat at different growth stages were explored by examining the statistical relationships between the derived metrics and yields at 8-day interval. Also, the key agricultural drought alert period was identified and the agricultural impacts during the key drought alert period were analyzed.

3.2 Study Area

Three major winter wheat producing states in Great Plains (Kansas, Oklahoma and Nebraska) were selected as the study area (Figure 3-1). These three states make up almost 40% of U.S. domestic winter wheat production and play an important role in wheat markets. The recent droughts in U.S. Great Plains put a continuous stress on local agricultural production and the region covers extensive in situ soil moisture measurements, which make it a hotspot for studying drought.

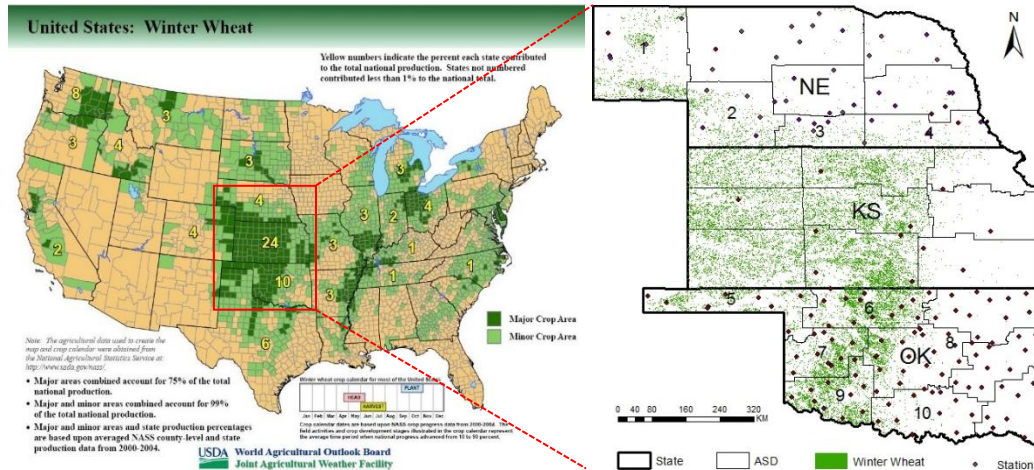


Figure 3-1: Chapter 3 Study Area Showing the Winter Wheat Distribution, Major Winter Wheat ASDs and Locations of In situ Soil Moisture Measurements

3.3 Data

The data used in this research include remote sensing data, in situ soil moisture measurements and agricultural statistics. A more detailed data description is listed as below.

3.3.1 Remote Sensing Data

For performance evaluation of remotely sensed indicators for drought monitoring, the primary remote sensing data used for characterizing drought conditions includes 8-day MODIS NDVI, LST and ET products from 2000-2013. Among these, the 250m MODIS NDVI data were accessed from the Global Agriculture Monitoring (GLAM) system of the University of Maryland (<http://pekko.geog.umd.edu/usda/test/>); the 1km MODIS LST data (MOD11A2) were downloaded from NASA Land Processes Distributed Active Archive Center (LP DAAC, <https://lpdaac.usgs.gov/>) and the 1km MODIS ET/PET data (MOD16) from Numerical Terradynamic Simulation Group (NTSG), University of Montana (<http://www.ntsug.umt.edu/project/mod16>) were used.

For evaluating the soil moisture product for agricultural drought monitoring, the ASCAT SSM product providing daily relative soil moisture in terms of saturation degree between 0 (dry) and 100% (saturated) was used, which was generated by Vienna University of Technology (TU-WIEN, <http://rs.geo.tuwien.ac.at/products/>) using a change detection algorithm first proposed by Wagner et al. (1999) and then improved by Naeimi et al. (2009). For more details about the ASCAT SSM product, please refer to Wagner et al. (2013). In this study, the ASCAT SSM dataset from 2007-2012 was used.

For drought impact analysis, the 8-day MODIS NDVI time-series data for the study area were acquired from Global Inventory Modeling and Mapping Studies (GIMMS) system (<http://gimms.gsfc.nasa.gov/>). The 2010 Cropland Data Layer (CDL) from USDA National Agricultural Statistics Service (NASS) was used (<http://nassgeodata.gmu.edu/CropScape/>) to show the distribution of winter wheat in these three states.

3.3.2 In situ Soil Moisture Data

The in situ soil moisture data were accessed from North American Soil Moisture Database (NASMD, <http://soilmoisture.tamu.edu/>) of Texas A&M University, which is a harmonized and quality-controlled platform that integrates soil moisture observation from several regional networks and is the only consolidated and comprehensive source soil moisture data for North America. The soil moisture at various depths for these stations is available at different periods from 1991 up to 2013. The top layer soil moisture measurements at 5/10cm depths were used (2000-2013 for performance evaluation of MODIS derived drought indicators, and 2007-2012 for

evaluation of ASCAT SSM product). This region has extensive in situ soil moisture networks. As indicated in Figure 3-1, there are a total of 165 stations with valid surface soil moisture measurements at 5/10cm depths since 2007 (124 stations at 5cm and 41 stations at 10cm). For Kansas (11 stations) and Oklahoma (108 stations), all stations have measurements at 5cm, while Nebraska has a combination of measurements at 5cm (5 stations) and 10cm (41 stations). Among all stations, 22 are for cultivated crops according to the land cover description of the National Land Cover Database (NLCD) 2001 classification scheme (<http://www.epa.gov/mrlc/classification.html>), with 2 from Oklahoma at 5cm and 20 from Nebraska at 10cm. The 2010 CDL from USDA NASS was also used to help distinguish the different land covers for all stations.

3.3.3 Agricultural Statistics

The winter wheat yield for 3 states and 10 ASDs in Oklahoma and Nebraska were acquired from the USDA NASS Quick Stats database (<http://quickstats.nass.usda.gov/>).

3.4 Methodology

3.4.1 Remotely Sensed Indicators

The primary remotely sensed indicators used in this study include vegetation condition, LST and ET based indicators calculated from time-series MODIS products (2000-2013).

Vegetation growth conditions are widely used as the basis for deriving drought indicators. As mentioned in Chapter 1, NDVI provides a good estimate of vegetation photosynthetic capacity and biomass (Tucker, 1979). Thus, NDVI-based metrics are

commonly used as indicators of vegetation stress and drought (Henricksen & Durkin, 1986; Tucker & Choudhury, 1987; Tucker, 1989; Gutman, 1990). LST and ET can provide vital information on vegetation water stress (Gutman, 1990; Anderson et al., 2011), which can be used as indicators of surface moisture status and thus drought conditions.

In this study, for each dataset (NDVI, LST, ET/PET), three drought indices (Normalized indicators: Equations 3-1/4/7, Standardized indicators: Equations 3-2/5/8, Condition indicators: Equations 3-3/6/9) were calculated and together nine drought indices were compared in this study.

$$NVI = (NDVI - NDVI_{mean}) / NDVI_{mean} \quad 3-1$$

$$SVI = (NDVI - NDVI_{mean}) / \sigma_{NDVI} \quad 3-2$$

$$VCI = (NDVI - NDVI_{min}) / (NDVI_{max} - NDVI_{min}) \quad 3-3$$

$$NTI = (LST - LST_{mean}) / LST_{mean} \quad 3-4$$

$$STI = (LST - LST_{mean}) / \sigma_{LST} \quad 3-5$$

$$TCI = (LST_{max} - LST) / (LST_{max} - LST_{min}) \quad 3-6$$

$$NEI = (ET / PET - ET / PET_{mean}) / ET / PET_{mean} \quad 3-7$$

$$SEI = (ET / PET - ET / PET_{mean}) / \sigma_{ET/PET} \quad 3-8$$

$$ECI = (ET / PET - ET / PET_{min}) / (ET / PET_{max} - ET / PET_{min}) \quad 3-9$$

Where X , X_{mean} , X_{min} , X_{max} , and σ_x , is respectively the current value, the average, minimum, maximum and standard deviation of multi-year values (X respective indicates $NDVI$, LST and ET/PET).

For each station, the pixel values of NDVI/LST/ET/PET were first extracted for the entire time series and subjected to a data quality check. After the out-of-range data were removed, the drought indicators for each station were calculated based on the time series using Equations 3-1~3-9.

3.4.2 In situ Soil Moisture Composite

The raw ground-based soil moisture data are daily. To match the temporal resolution of MODIS data, the 8-day composite for each station was generated by averaging all valid observations within an 8-day period.

3.4.3 Statistical and Lagged Statistical Analysis

For MODIS derived drought indicators as mentioned in Section 3.4.1, the (lagged) correlation between remotely sensed indicators and soil moisture at different time lags (Equation 3-10) was calculated for each station and compared across different stations to help identify the response time of each indicator to drought. Also, for each 8-day period during the main winter wheat growing season, both the correlation and lagged correlation between remotely sensed indicators and soil moisture (Equation 3-10) were also calculated to indicate their suitability for agricultural drought monitoring during that growing stage. For investigating the performance of ASCAT SSM for agricultural drought monitoring, the correlation (Equation 3-10) was used to explore the agreement between ASCAT SSM pixel values and in situ soil moisture at daily basis. .

$$R = \frac{\sum_{i=1}^n (x_i - \bar{x})(y_i - \bar{y})}{\sqrt{\sum_{i=1}^n (x_i - \bar{x})^2 \sum_{i=1}^n (y_i - \bar{y})^2}} \quad 3-10$$

Where R indicates the (lagged) correlation, x represents the (lagged) drought indicator, y represents in situ soil moisture, and n is the number of sample.

3.4.4 Response Time Decision Rules

The response time was determined from the peak correlation between remotely sensed indicators and soil moisture for different time lags. Ideally, there is only one peak within the 2 month time lag (Figure 3-2a), so it would be easy to pick up the response time at the peak. However, the reality is much more complicated, especially when considering different growth stages of the crop growing season, and there are a lot of cases in which several peaks exist (Figure 3-2b/c/d). For these cases, it is very important and necessary to determine the Response Time Maximum Likelihood Region (MLR) where most of the response occurs, especially when the study area covers a large area across space. Once the MLR has been determined, when there are peaks located both inside and outside MLR, only the peak within MLR is picked (Figure 3-2b); when there is more than one peak in the MLR and these correlation peaks have significant differences, the peak with higher correlation is picked (Figure 3-2c); when there are several peaks within MLR and these peaks have similar correlations, the first peak is selected (Figure 3-2d).

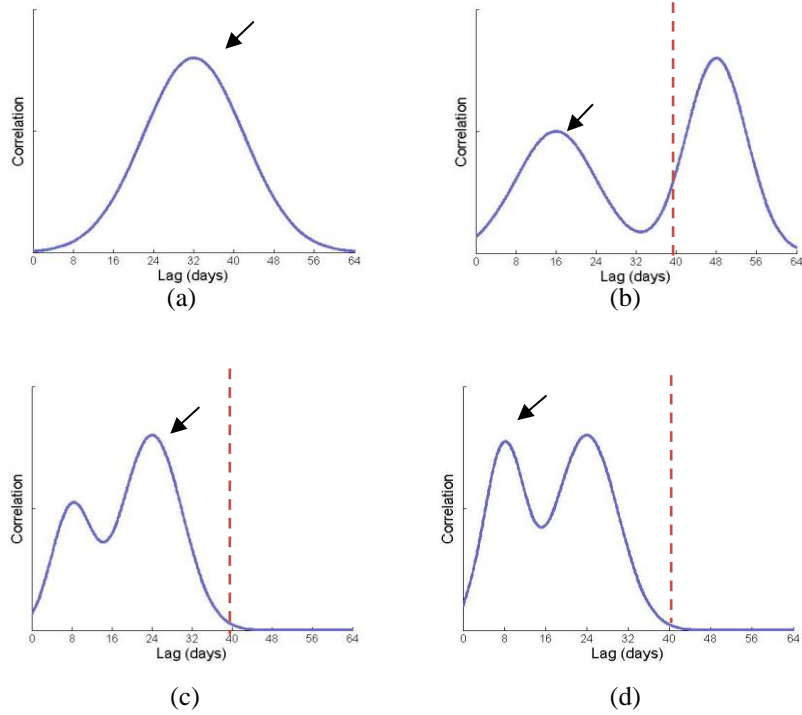


Figure 3-2: Schematic Chart for Determining Response Time (a) Single Peak (b) Single Peak in Maximum Likelihood Region (MLR) (c) Several Peaks in MLR with One Significantly Higher Correlation (d) Several Peaks in MLR with Similar Correlation

3.4.5 Drought Impact Analysis

For the drought impact analysis in this study, both the Anomaly NDVI (ANDVI) and the Cumulative Anomaly NDVI (CANDVI) at different aggregated time periods were used to quantify the drought conditions observed from remote sensing.

$$NDVI = (NIR - R) / (NIR + R) \quad 3-11$$

$$ANDVI = NDVI - NDVI_{mean} \quad 3-12$$

$$CANDVI = \sum_{i=start-date}^{i=end-date} ANDVI_i \quad 3-13$$

Where $NDVI_{mean}$ indicates the long-term $NDVI$ average and is calculated based on the ten-year data from 2001 to 2011; $CANDVI$ represents the accumulation of $ANDVI$ from the start date to the end date. If the end date is the same as the start date, then $CANDVI$ is equivalent to the $ANDVI$ for the specific date.

To make the drought indicators and agricultural statistics comparable at the same spatial scale, the remote sensing derived metrics need to be aggregated to match the scale of agricultural statistics. First, the winter wheat pixels for Kansas were selected using the 2010 NASS CDL and then NDVI was aggregated to the state level using the wheat pixels within the state. Also, to derive the drought indicator for composite periods of $N*8$ ($N=2, 3, \dots$) days, the NDVI for that specific period was the accumulation of all single 8-day periods. Then, the state-level ANDVI and CANDVI for different temporal periods were computed using Equations 3-12 & 3-13 based on the spatial aggregated and temporal composite NDVI. The Pearson's correlation (Equation 3-10) between aggregated CANDVI and yield was calculated for each period of the growing season to explore the agricultural impacts of drought and identify the key drought alert periods for winter wheat.

3.5 Results

The drought indicators (as in Equations 3-1~3-9) from 2000-2013 were first computed for each station at 8-day interval and the overlapping time period with both remote sensing and soil moisture record was selected for each station. Then, the drought indicators were compared with soil moisture at different time lags to examine its sensitivity for characterizing drought conditions.

3.5.1 Response of Remotely Sensed Indicators to Drought

To explore the general sensitivity of remote sensed indicators to drought, using all available data, the correlation between each drought indicator and in situ soil moisture

was calculated at different time lags for each station and the results are displayed in Figure 3-3.

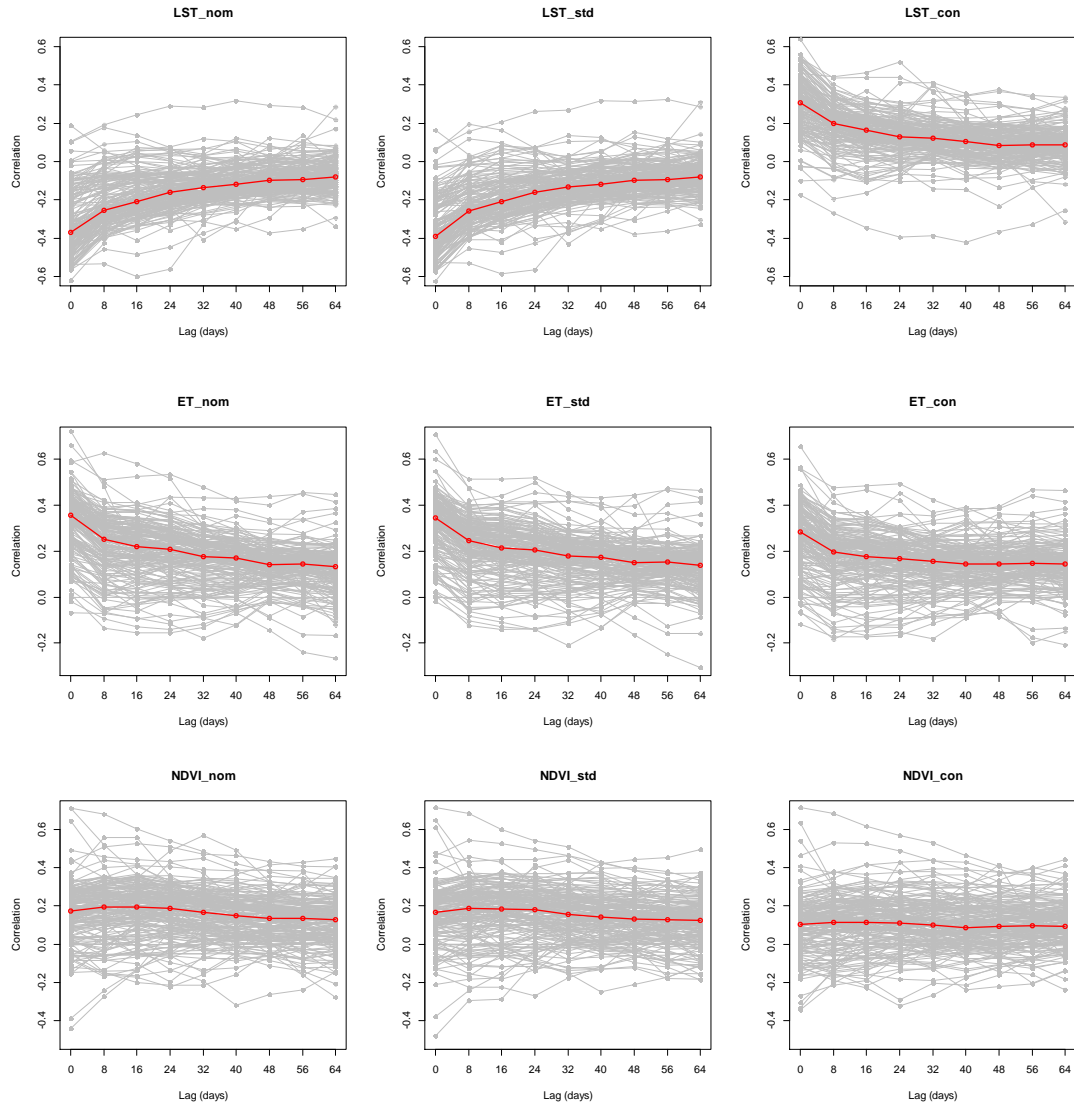


Figure 3-3: General Response of Drought Indicators to Soil Moisture at Different Time Lags
Notes: Each row indicates the results for indicators derived from the same variable, respectively LST, ET and NDVI from the 1st to 3rd row. Each column represents the results for different types of indicators, respectively normalized, standardized and condition indicators from the left to right. The gray lines indicate the results for different stations and the red line is the median for all stations.

As seen from Figure 3-3, for all indicators, there is large variability across different stations. Among these three categories of drought indicators, LST and ET derived indicators show similar performance. As the time lag increases, both LST and ET

indicators have declining correlation with soil moisture, demonstrating that LST and ET are quite sensitive to drought and show immediate response after drought occurrence. While for NDVI related indicators, there is no consistent response to soil moisture. With the increase in time lag, the correlation shows large fluctuations, in which case it is quite important to determine a response time MLR where most of the response time is located (this will be detailed in Section 3.5.2). It can also be found that LST/ET indicators are better correlated with soil moisture than NDVI indicators. Besides, within each category of drought indicators, the three indices have similar performance, of which the normalized and standardized indicators are more similar and show slightly better average correlation than the condition indicators.

3.5.2 Response Time Maximum Likelihood Region for NDVI Derived Drought Indicators

As mentioned in Section 3.5.1, there is no consistent response time for NDVI related indicators across stations. To investigate the general response for large scale applications, the response time MLR needs to be identified. In this section, using all stations both without and with distinguishing different land covers, the number of stations with response time at each time lag will be summarized and normalized into percentage. The accumulated probability of different response time for three NDVI derived indicators is shown in Figure 3-4.

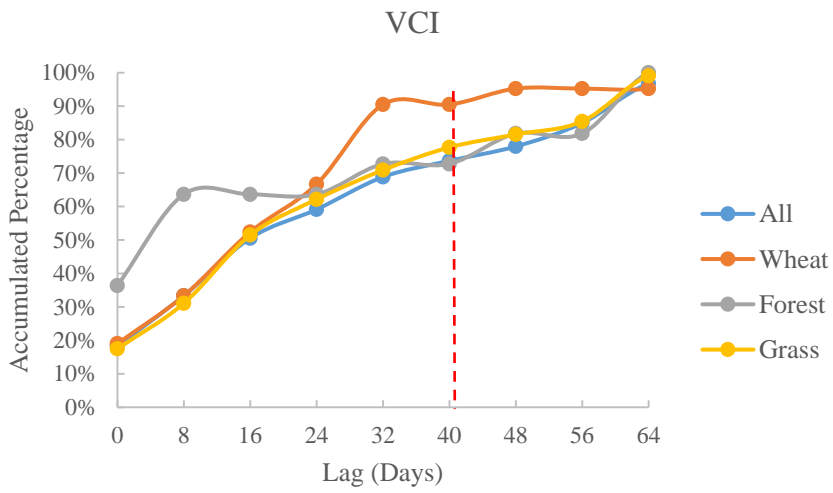
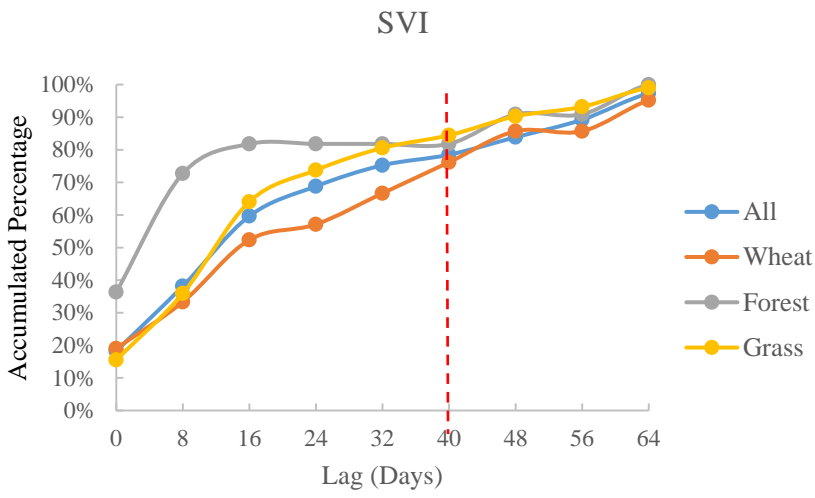
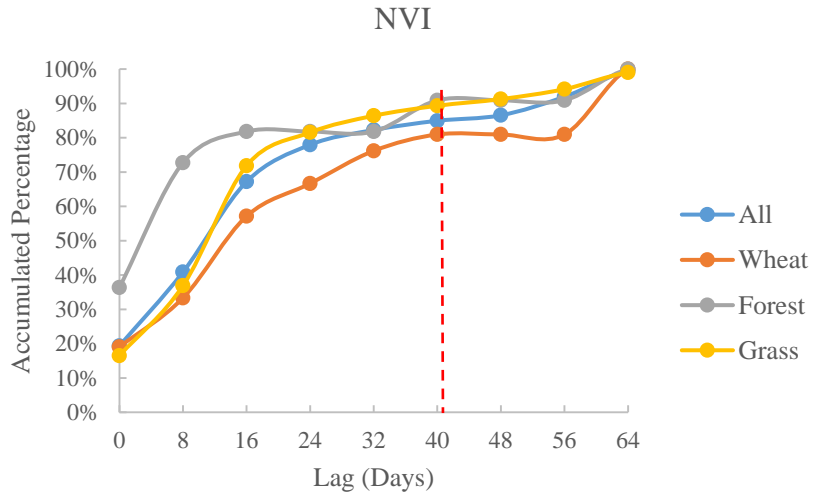
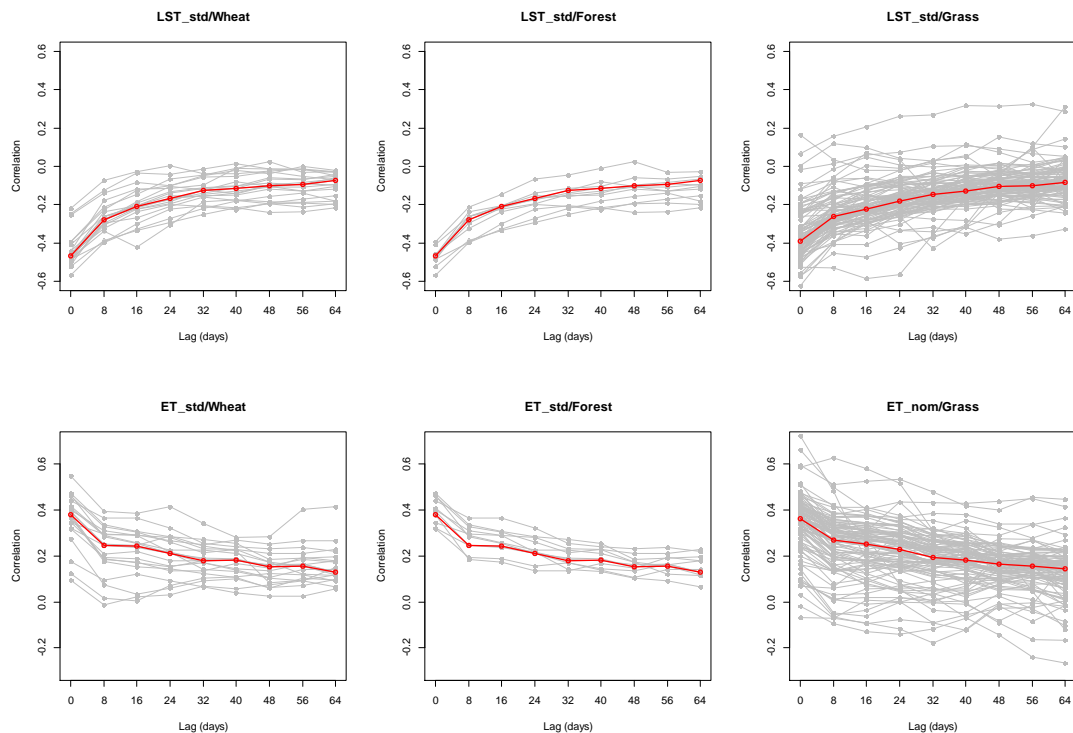


Figure 3-4: Accumulated Probability of Different Response Time for NDVI Derived Indicators

As seen from Figure 3-4, for all NDVI derived indicators, the accumulated probability reaches around 80% within a time lag of 40 days, showing no significant increase afterwards. This indicates that 40-day can be used as an effective threshold to delineate the MLR and the general response of NDVI indicators to drought is within 5 weeks, which will be very useful for helping identify the response time during the winter wheat growing season when several correlation peaks occur.

3.5.3 Response of Remotely Sensed Indicators to Drought for Major Land Cover Types

To further explore the variations of drought indicators' response across different land covers, the results for three major land covers (i.e., winter wheat/forest/grass) are stratified. As mentioned in Section 3.5.1, drought indicators within each category show similar performances, and for simplicity, only the results for standardized indicators are displayed in Figure 3-5.



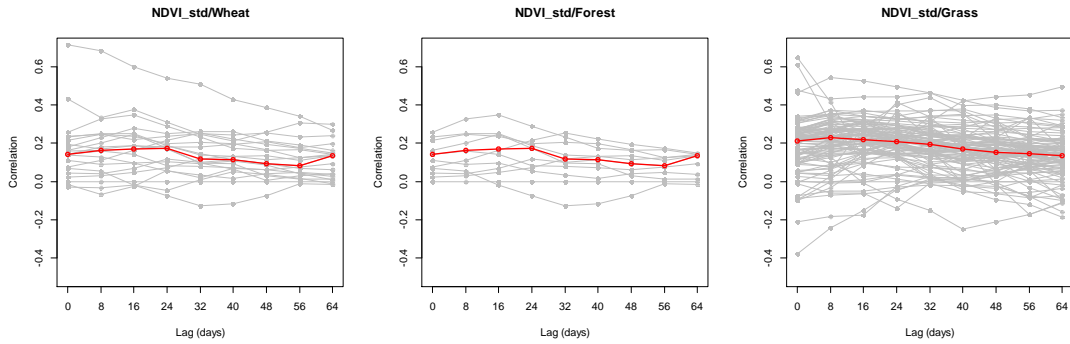


Figure 3-5: Response of Drought Indicator to Soil Moisture at Different Time Lags for Major Land Cover Types

Notes: Each row indicates the results for indicators derived from the same variable, respectively LST, ET and NDVI from the 1st to 3rd row. Each column represents the results for different land cover types, respectively wheat, forest and grass from the left to right. The gray lines indicate the results for different stations and the red line is the median for all stations.

As seen from Figure 3-5, three land cover types follow similar trends, of which grass has the largest variation across stations. A further comparison shows that for LST and ET derived indicators, the average correlations with soil moisture are a little bit higher for NDVI derived indicators.

3.5.4 Response of Remotely Sensed Indicators to Drought during Winter Wheat Main Growing Season

To investigate the performance of remotely sensed indicators to agricultural drought, for each 8-day period during main winter wheat growing season (March-June from DOY57 to DOY177), the correlation between the drought indicator and soil moisture was calculated at different time lags for each station. Based on the correlation profile at each 8-day period, the response time was identified for each station. Then, for each 8-day period of the main growing season, the number of winter wheat stations with a given response time were identified and summed. Similar with Section 3.5.3, for simplicity, only the results for standardized indicators are displayed in Table 3-1.

Table 3-1: Count of Winter Wheat Stations at Different Response Time during Winter Wheat Main Growing Season

RT	57	65	73	81	89	97	105	113	121	129	137	145	153	161	169	177	
LST	0	10	15	9	7	10	13	10	7	10	14	16	11	14	19	10	17
	8	5	2	1	3	5	2	3	3	3	2	3	5	2	0	6	1
	16	4	2	1	5	1	0	2	4	3	2	0	2	3	0	3	1
	24	1	0	7	2	1	3	4	5	3	1	0	0	0	0	0	0
	32	0	1	1	1	2	0	0	0	0	0	0	1	0	0	0	0
	40	0	0	0	0	0	1	0	0	0	0	0	0	0	0	0	0
	48	0	0	0	1	0	0	0	0	0	0	0	0	0	0	0	0
	56	0	0	0	0	0	0	0	0	0	0	0	0	0	0	0	0
	64	0	0	0	0	0	0	0	0	0	0	0	0	0	0	0	0
	NA	1	1	2	2	2	2	2	2	2	2	2	2	2	2	2	2
ET	0	14	13	7	3	9	8	5	8	12	4	14	12	15	14	9	14
	8	3	3	1	11	1	3	5	1	3	2	1	4	0	3	5	3
	16	1	1	6	0	3	5	4	4	0	11	3	1	3	0	3	1
	24	0	1	1	1	3	1	1	3	2	2	1	1	1	1	2	1
	32	2	1	4	3	3	2	4	3	2	0	0	1	0	1	0	0
	40	0	1	0	1	0	0	0	0	0	0	0	0	0	0	0	0
	48	0	0	0	0	0	0	0	0	0	0	0	0	0	0	0	0
	56	0	0	0	0	0	0	0	0	0	0	0	0	0	0	0	0
	64	0	0	0	0	0	0	0	0	0	0	0	0	0	0	0	0
	NA	1	1	2	2	2	2	2	2	2	2	2	2	2	2	2	2
NDVI	0	3	1	1	3	3	7	0	5	7	1	2	5	3	2	2	1
	8	8	4	1	3	3	1	7	2	4	3	3	2	2	3	1	6
	16	1	4	0	3	2	1	1	2	3	5	6	6	3	3	8	6
	24	2	0	4	2	3	3	1	6	1	6	5	1	3	5	3	1
	32	2	3	5	4	4	3	4	2	4	3	2	1	4	3	2	2
	40	2	4	4	2	1	2	4	2	0	1	1	3	2	3	1	3
	48	0	2	3	2	2	1	2	0	0	0	0	1	2	0	1	0
	56	1	1	0	0	1	1	0	0	0	0	0	0	0	0	1	0
	64	0	0	1	0	0	0	0	0	0	0	0	0	0	0	0	0
	NA	2	2	2	2	2	2	2	2	2	2	2	2	2	2	2	2

Notes: In this table, RT indicates Response Time, LST/ET/NDVI respectively indicates the standardized LST/ET/NDVI indicators, and 57,...,177 (Julian Day) indicates different stages of the growing season.

As seen from Table 3-1, compared with general drought response time in Section 3.5.1, the results during the winter wheat growing season show more variations. A close comparison indicates that ET and LST based indicators are similar, which shows more consistent response time across space during the early and late main growing season. For NDVI drought indicators, the response time has higher spatial variability as

compared to ET/LST; but as the growing season progresses, they show a slightly increasing consistency.

In addition, the corresponding correlation at the response time for each wheat station is shown for different periods of the main growing season to indicate the effectiveness of these indicators for drought monitoring at different growing stages and the evolution of this effectiveness during the growing season. Similarly, only the results for standardized drought indicators are shown in Figure 3-6.

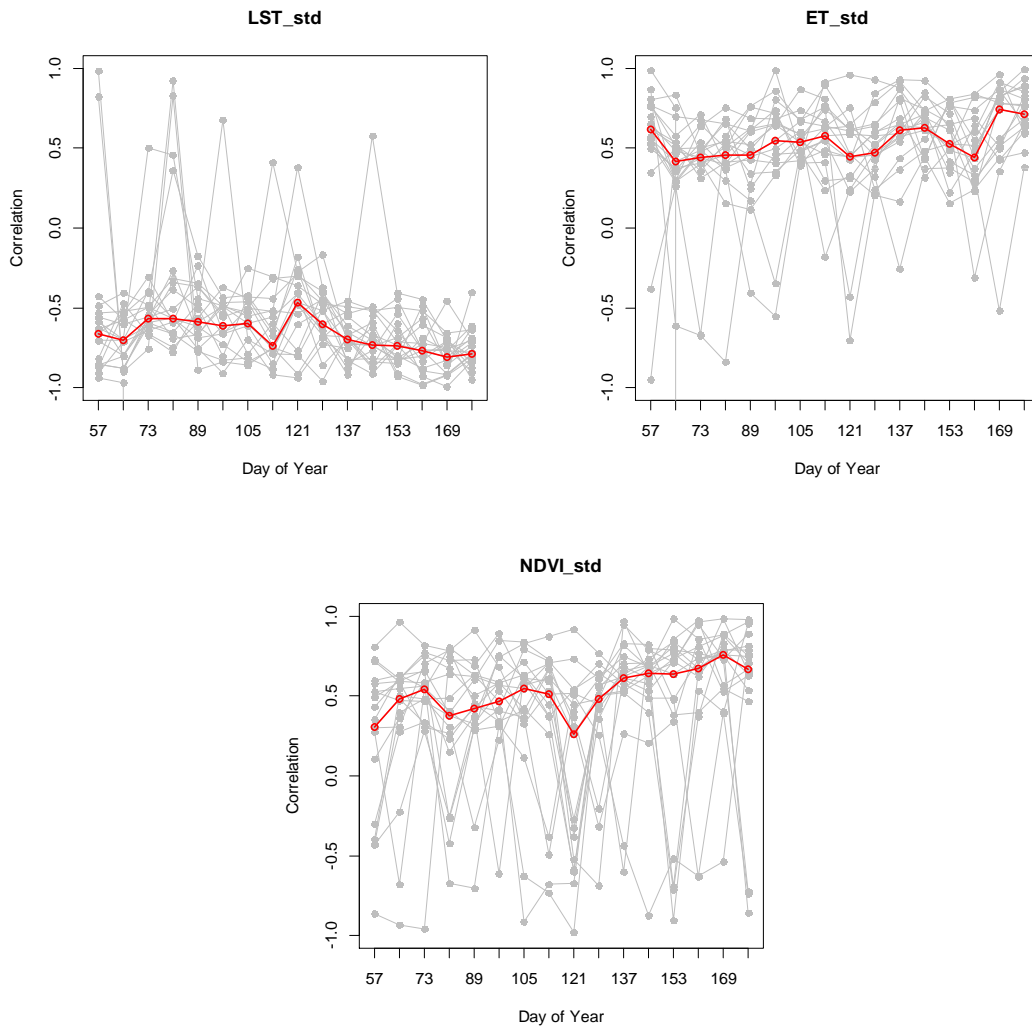


Figure 3-6: Time Series of Drought Indicator-Soil Moisture Correlation during the Winter Wheat Main Growing Season

As seen from Figure 3-6, ET and LST derived indicators are quite similar, which shows relatively stable and slightly better drought monitoring ability during the early and late winter wheat main growing season, but NDVI indicators show improving ability as the growing season progresses.

3.5.5 ASCAT Surface Soil Moisture Product for Agricultural Drought Monitoring in Southern U.S. Great Plains

The daily ascending and descending ASCAT SSM pixel values for each station were extracted for the entire time series from 2007-2012, and the in situ volumetric soil moisture (SM) was rescaled into relative soil moisture (RSM) between 0 and 1 using the maximum and minimum observed values from the existing valid NASMD data record from 2007-2012 for each station. Then, the performance of ASCAT SSM for characterizing drought across different stations, for different times of year, and for crop stations during the crop growing season, was explored. Also, comparisons were made between the effectiveness of ASCAT SSM for representing soil moisture at 5cm and 10cm, as well as between the ability of the ascending and descending SSM for drought monitoring.

- **Capability of ASCAT SSM for Characterizing Drought across Stations**

The general ability of ASCAT SSM for describing drought for each station was investigated by calculating the statistical correlation between ASCAT pixel values and in situ RSM using all available valid data record from 2007-2012 for both ascending and descending passes. The results show that almost all (164 of 165) stations have significant correlation between ASCAT SSM and in situ RSM (SSM-RSM) for both

ascending and descending passes ($p\text{-value} < 0.05$), of which 163 stations have a $p\text{-value}$ less than 0.01 for ascending pass and 164 for descending pass.

To further compare the performance of the ascending and descending ASCAT SSM for characterizing soil moisture and thus drought, the relationship between the ascending and descending SSM-RSM correlation was plotted for the 164 significantly correlated stations and shown in Figure 3-7. It can be seen from the regression line in Figure 3-7 that the descending correlation is generally higher than the ascending correlation possibly due to its overpass time in the morning, indicating the better ability of ASCAT descending SSM for capturing soil moisture and thus better drought characterizing in the study area.

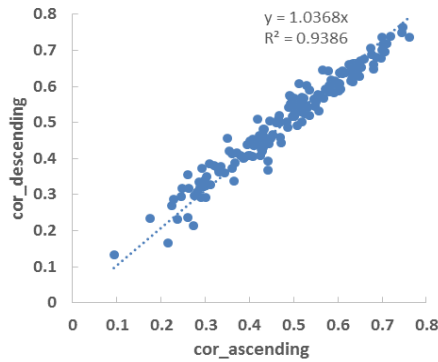


Figure 3-7: Relationship between ASCAT Ascending and Descending SSM-RSM Correlation

Figure 3-8 shows the distribution of the ASCAT descending SSM-RSM correlation for the 164 significantly correlated stations.

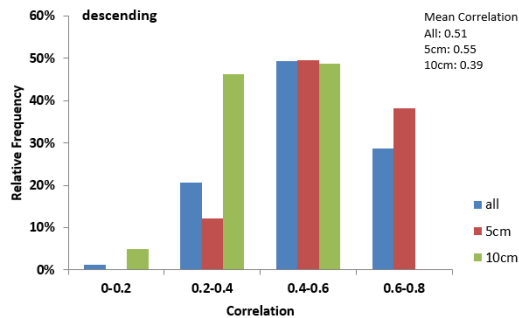


Figure 3-8: Histogram of ASCAT Descending SSM-RSM Correlation

As seen from Figure 3-8, almost all stations have a significant correlation between 0.2-0.8, with an average of about 0.5 and about half of the stations having a correlation between 0.4-0.6 at both 5cm and 10cm depths. Also, the higher average correlation for the 5cm stations demonstrates that ASCAT SSM can better capture the soil moisture at 5cm than 10cm.

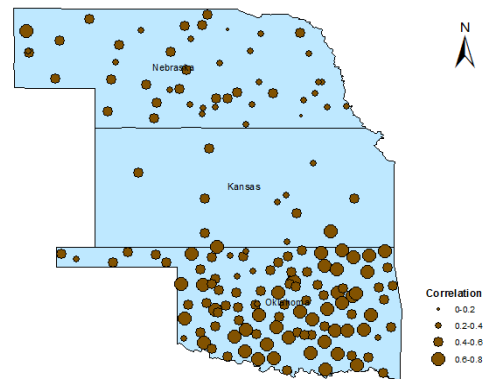


Figure 3-9: Spatial Pattern of Descending ASCAT SSM-RSM Correlation

Figure 3-9 shows the spatial pattern of ASCAT SSM-RSM correlation for the descending pass. As observed from Figure 3-9, higher correlation is generally concentrated in Oklahoma and Kansas, which corresponds to the surface soil measurements at 5cm depth and is consistent with Figure 3-8.

- **Seasonality of ASCAT SSM for Characterizing Drought**

To explore the seasonality of ASCAT SSM for describing drought, the daily correlation between ASCAT SSM and in situ RSM was calculated based on all valid data within 2007-2012 for each day of year from 1 to 365, using all, 5cm and 10cm stations for both ascending and descending passes. Despite the different correlation values among all, 5cm and 10cm stations, there is a generally similar trend within the time series of the entire year. For simplicity, only the results of all combined 5/10cm stations for both ascending and descending passes are displayed in Figure 3-10.

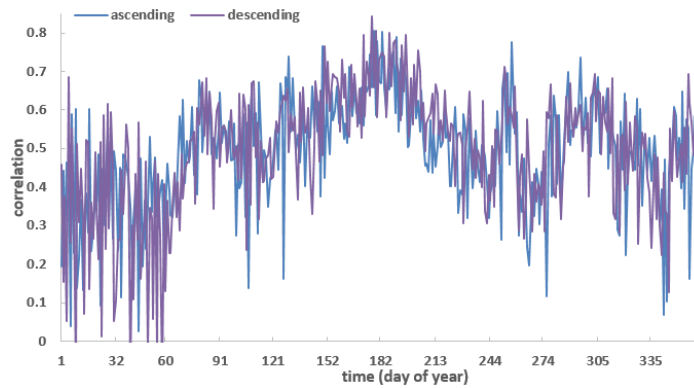


Figure 3-10: Time Series of ASCAT SSM-RSM Correlation

From Figure 3-10, it can be seen that despite a little higher average correlation for the descending pass during the time series, both ASCAT ascending and descending SSM show a consistent trend within the year. The fluctuating correlation across the year indicates the varying ability of ASCAT SSM for characterizing drought conditions. Consistently higher correlations above 0.5 are generally found around March-July and October-November, demonstrating the better performance of ASCAT SSM for monitoring soil moisture and thus agricultural drought conditions during this period. The relatively low correlation in winter (December-February) and fluctuation in summer (August-September) are possibly related to winter snow cover and summer precipitation, which thus impacts the accuracy of ASCAT SSM product during this period.

- **Performance of ASCAT SSM for Characterizing Agricultural Drought during Crop Growing Season**

The work above in Section 3.5.5 shows the general capability of ASCAT for characterizing drought across different stations and during different times of year. To test its ability specifically for agricultural drought during the growing season, soil moisture from March-June (the study area's dominant crop, i.e. winter wheat's main

growing season) for each of the 22 labeled crop stations were selected from all available records between 2007 and 2012. The SSM-RSM correlation for each crop station was calculated for both ascending and descending passes and the relationship between the ascending and descending correlation was plotted in Figure 3-11.

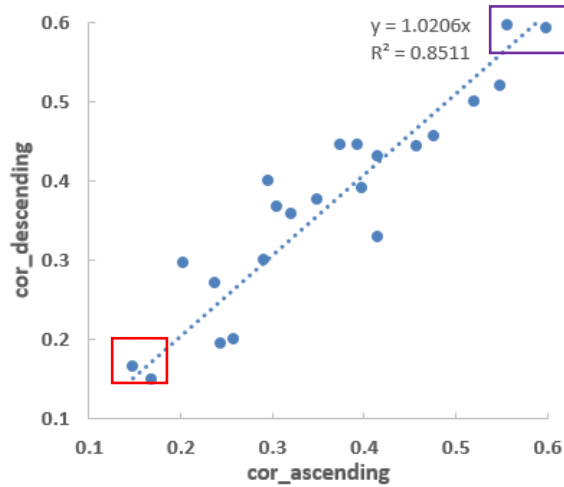


Figure 3-11: Relationship between ASCAT Ascending and Descending SSM-RSM Correlation for Crop Stations during Growing Season

The results shows that, despite relatively lower correlation as compared to all stations, all 22 crop stations show significant correlation between ASCAT SSM and in situ RSM for both ascending and descending passes. As indicated in Figure 3-11, except for 2 stations with low correlations at the bottom of the plot, the other 20 stations show highly significant correlation ($p\text{-value} < 0.01$). The two higher correlations at the top correspond to the 2 crop stations from Oklahoma with 5cm measurements, demonstrating the better ability of ASCAT SSM for depicting surface soil moisture at 5cm during crop growing season. Also, according to the regression line in Figure 3-11, the generally higher correlation of the descending SSM for crop stations also indicates its better ability for describing moisture status than the ascending SSM, which is consistent with the results for all stations based on the entire-year data.

3.5.6 Impacts of Drought on Agriculture in Southern U.S. Great Plains from Satellite Observations

- Case study in Kansas

Figure 3-12 and Figure 3-13 respectively show the 8-day NDVI anomaly and winter wheat yield for Kansas from 2000 through 2013.

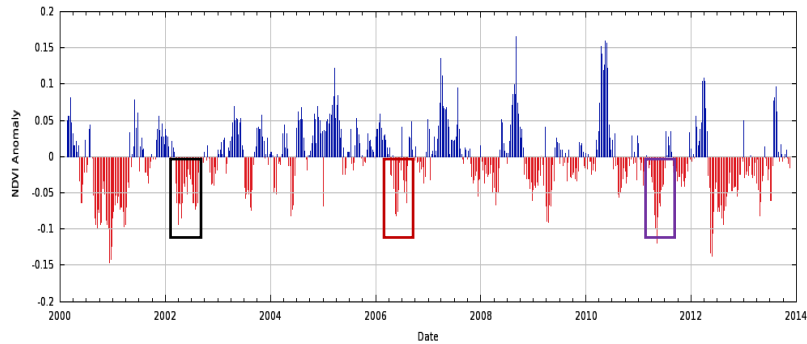


Figure 3-12: Time Series of NDVI Anomaly for Kansas Wheat Areas

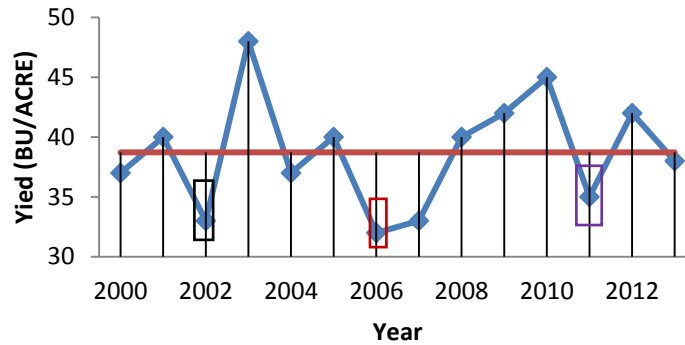


Figure 3-13: Winter Wheat Yield for Kansas

As indicated by the data, a fairly strong correlation between severe yield decline and NDVI anomaly during the growing season is seen (2002/2006/2011), except for 2007. In 2007, a late season frost led to a low yield. Since the crop had already reached its maximum vegetative stage at that time, the low yield was not captured by the NDVI anomaly. Thus, 2007 was excluded from the subsequent analysis. Meanwhile, it should

be noted that the magnitude of the yield anomaly is not exactly consistent with that of the NDVI anomaly during the growing season, due to different drought timing factors. As a creeping and accumulated process, the impacts of drought on crop production are also changing as the growing season progresses. Thus, it was important to investigate the impacts of drought on agricultural production within the entire growing season.

Traditional drought monitoring puts more emphasis on real-time monitoring. However, little work has been done to examine the evolution of drought impacts during the entire growing season using satellite data. In this section, the study period was set to winter wheat's main growing season (vegetative phase to pre-harvest) from March to June, and the impacts of drought on agricultural production were investigated by exploring the relationship between the Cumulative NDVI Anomaly (CANDVI) and yield for each period of the growing season. All combinations of CANDVI at different aggregated time scales during the main growing season were compared against winter wheat yield to show the impact of agricultural drought for that specific period. The results are displayed in Figure 3-14.

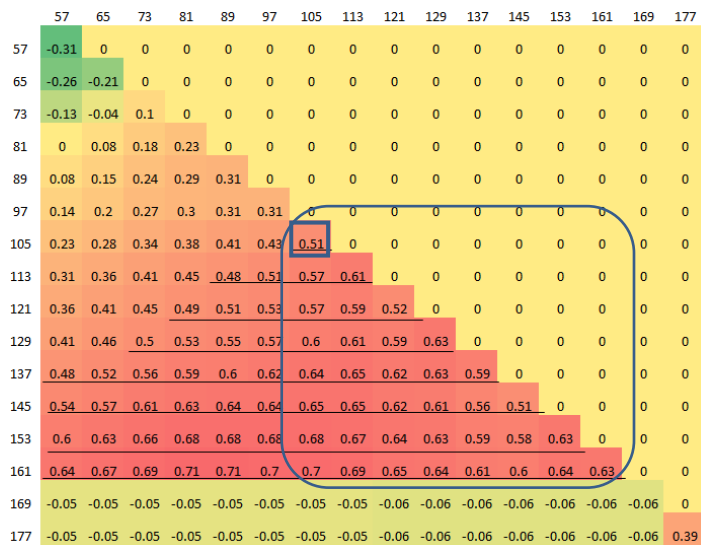


Figure 3-14: The Correlation Matrix between CANDVI and Winter Wheat Yield for Kansas

Notes: X-axis/Y-axis respectively indicate the start and end date (DOY), each cell value indicates the correlation between CANDVI (start at X-axis and end at Y-axis) and winter wheat yield using multi-year data (2000-2013 with 2007 excluded), and the values underlined indicate the correlation is significant at least at 0.1 level.

Figure 3-14 clearly shows the trajectory of drought impacts on final winter wheat yield during the main growing season, demonstrating varying impacts at different stages of crop development. It is evident that with the same start time, droughts of longer duration generally have a higher correlation with yield, which means prolonged droughts have higher impacts on crop yield. For droughts of similar duration, the agricultural impacts are closely related to its timing. As indicated by Figure 3-14, droughts occurring from Mid-April to Early-June (i.e. winter wheat’s late vegetative to ripening stages) tend to have more significant impacts; while at the early and late growth stages, the CANDVI and yield is not significantly correlated, indicating negligible drought impacts during these stages.

Based on the results from Figure 3-14, the continuous and significantly correlated region showing significant agricultural impacts was identified as the key period for effective agricultural drought alert (highlighted region in Figure 3-14). The drought impacts during this key alert period were analyzed in more detail, and the statistics of drought impacts during this period as well as the timing for drought impact emergence and maximum are summarized in Table 3-2.

Table 3-2: Drought Impacts on Winter Wheat Yield during Key Drought Alert Period

Key Alert	Correlation	Emergence	Max
Mid-April to Early-June	Max: 0.70	Mid-April (Jointing)	Mid-May (Filling)
	Min: 0.51		
	Mean: 0.61		

As seen from Table 3-2, drought begins to show significant crop impacts at the jointing stage around Mid-April, and the significant impacts continue through Early-

June. Thus, Mid-April to Early-June was identified as the key drought alert period for winter wheat monitoring. During this period, fairly high correlations between CANDVI and yield are observed with an average about 0.6, and the greatest drought impact is found during the grain filling stage around Mid-May. This is approximately 4-6 weeks ahead of harvest during the most drought sensitive period, which can be used to warn and prepare the agriculture community against the potential negative yield impacts.

- Case study in Oklahoma and Nebraska

Figure 3-15 shows the monthly PDSI time series from 2000 to 2015 for Oklahoma and Nebraska.

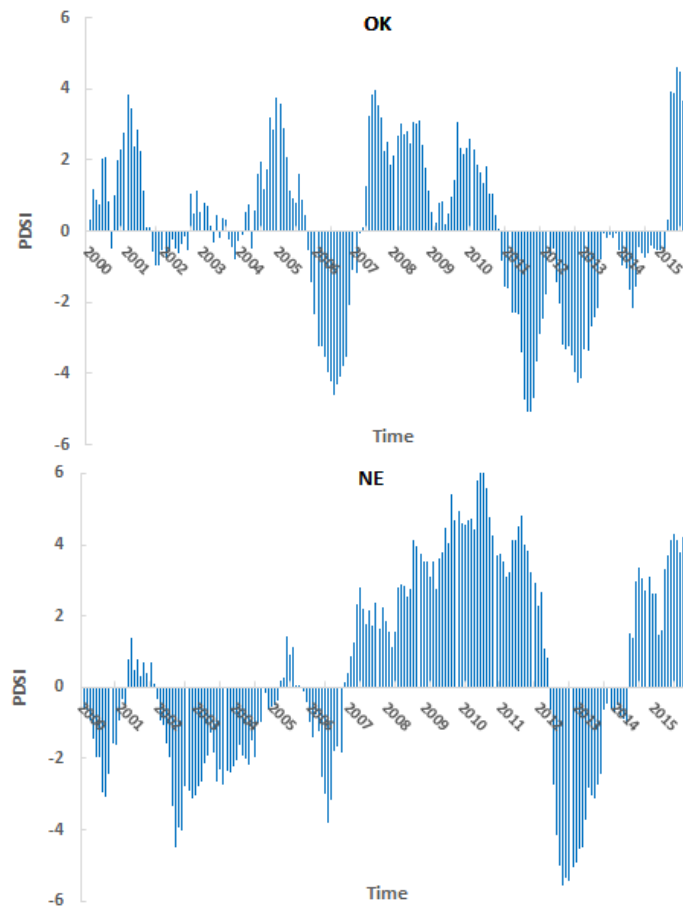


Figure 3-15: Monthly PDSI Time Series for Oklahoma (Top) and Nebraska (Bottom)

As observed from Figure 3-15, both Oklahoma and Nebraska have experienced frequent recent droughts ($PDSI \leq -1$). Of all the months from 2000 to 2015, Oklahoma underwent 5.2% mild drought ($-2 \leq PDSI < -1$), 6.3% moderate drought ($-3 \leq PDSI < -2$), 7.8% severe drought ($-4 \leq PDSI < -3$) and 5.2% extreme drought ($PDSI \leq -4$), with most occurring during 2006 and 2011-2014; Nebraska suffered from 11.5% mild drought, 10.9% moderate drought, 5.7% severe drought and 5.7% extreme drought, and most of these droughts occurred during 2000, 2002-2004, 2006 and 2012-2013. It's also noted that the drought occurrences during winter wheat main growing season, in 2014 for Oklahoma and in 2013 for Nebraska, also resulted in significant winter wheat loss.

The state winter wheat NDVI for both Oklahoma and Nebraska was aggregated from the 8-day MODIS NDVI data of winter wheat pixels, and used to describe the average winter wheat phenology in the state. It can be clearly seen from Figure 3-16 that, for both states, there was a significant decline in the state aggregated winter wheat NDVI during their respective drought years (Oklahoma: 2014 and Nebraska: 2013). Also, the NDVI in Oklahoma is much higher than that in Nebraska before both reaching the peak, indicating the higher winter wheat planting density in Oklahoma than in Nebraska. Both states show increasing NDVI trends, with vegetative peak observed around Mid-Late April in Oklahoma and around Mid-Late May in Nebraska, demonstrating a later winter wheat phenology in Nebraska.

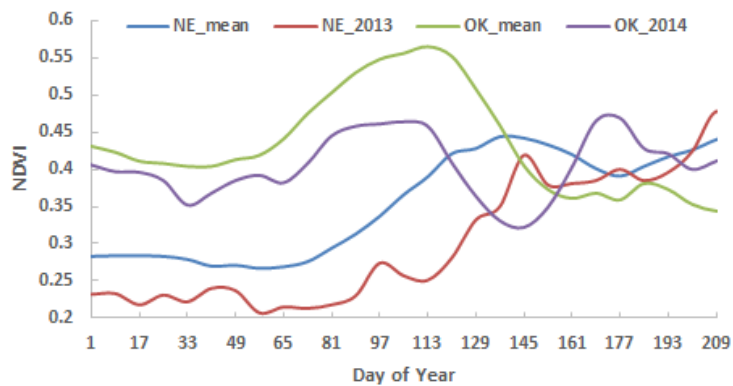


Figure 3-16: Time Series of State Aggregated NDVI over Winter Wheat Regions in Oklahoma and Nebraska

Notes: The green and blue line respectively represents the 2001-2011 mean for Oklahoma and Nebraska, the purple line indicates an agricultural drought year in Oklahoma in 2014, and the red line indicates an agricultural drought year in Nebraska in 2013.

Next, the agricultural drought indicator (ANDVI) was derived from the state aggregated winter wheat NDVI and the relationships between ANDVI and yield was explored to show the drought impacts at each 8-day of the main growing season (about March-June from DOY49-177) for both states and the result are shown in Figure 3-17.

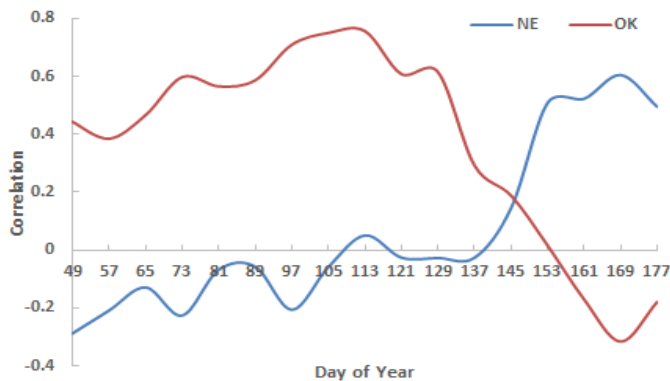


Figure 3-17: State-level 8-day Drought Impacts on Winter Wheat Yield during the Main Growing Season in Oklahoma and Nebraska

As seen from Figure 3-17, the correlations between the drought indicator and yield show an increasing trend before reaching the maximum for both states, indicating generally increasing drought impacts as the growing season progresses. However, the stable and higher correlation for Oklahoma indicates both more stable and more

significant drought impacts than Nebraska. In Nebraska, the winter wheat only makes up about 2% of the crops and the interferences from other crops as well as the soil background will impact the accuracy of remotely sensed indices for charactering drought conditions and thus the drought impact analysis. In Oklahoma, where the percentage of winter wheat is comparable with that of Kansas (both are more than 10%), the drought impacts show similar pattern with Kansas. However, due to the relatively earlier phenology (Figure 3-16) in Oklahoma, the drought impact patterns shift a bit, with the highest drought impact occurring around Mid-Late April in Oklahoma as compared to Mid-May in Kansas.

To explore the spatial variability, in addition to the drought impact comparisons at the state level, similar work was also carried out for each major winter wheat producing ASD as labeled in Figure 3-1. Figure 3-18 shows the time series of multi-year average winter wheat NDVI (2001-2011) for each of the 10 ASDs.

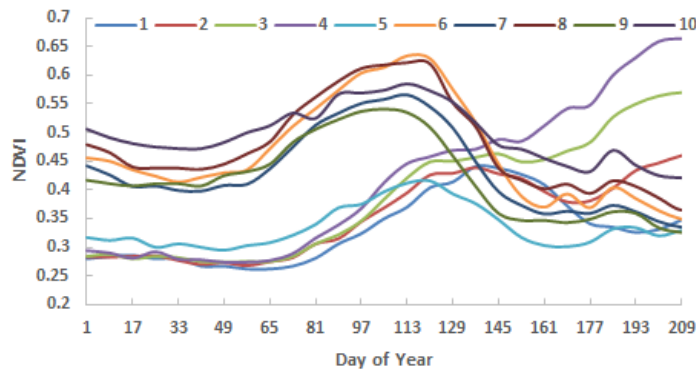


Figure 3-18: Time Series of ASD Aggregated NDVI over the Winter Wheat Regions for Oklahoma and Nebraska (2001-2011 Mean)

Note: The numbers from 1 to 10 indicate the number of primary winter wheat ASDs as indicated in Figure 3-1.

As observed from Figure 3-18, the 6 ASDs in Oklahoma follow a similar pattern, reaching the vegetative peak around Mid-Late April. However, the 4 ASDs in Nebraska follow another pattern, with the vegetative peak around Mid-Late May. This indicates

a later phenology in Nebraska than in Oklahoma, which is consistent with the state-level results. It is also noted that, except only one ASD in Oklahoma showing similar NDVI and thus similar planting density with the ASDs in Nebraska, all 5 other ASDs in Oklahoma have much higher NDVI than the 4 ASDs in Nebraska, indicating the much higher winter wheat planting density in Oklahoma.

Based on the ASD aggregated winter wheat NDVI, the drought indicator for each ASD was calculated and the 8-day drought impact on yield during main growing season (DOY49-177) for each ASD was also explored (Figure 3-19). As seen from Figure 3-19, among these 10 ASDs, 3 different drought-impact-pattern groups were found. The 6 ASDs in Oklahoma follow a similar pattern, showing a generally increasing drought impact during the main growing season, reaching the peak impact around Mid-Late April for 5 of the 6 ASDs, and declining quickly after that (the peak impact was observed in Early May for one ASD, followed by a slowly declining impact after that). For 2 ASDs in Nebraska with very small areas of winter wheat grown, no significant trends for drought impacts were observed during the growing season, possibly due to the stronger interference from background. For the other 2 ASDs in Nebraska, there is a fluctuating but also increasing drought impact, but a later peak impact around Mid-Late May was found. Those results are generally consistent with the results at the state level, and the highest drought impact typically occurs around the vegetative peak.

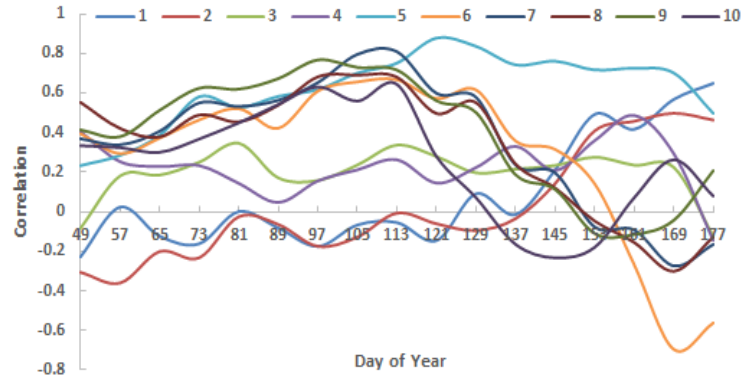


Figure 3-19: ASD-level 8-day Drought Impacts on Winter Wheat Yield during the Main Growing Season in Oklahoma and Nebraska

Note: The numbers from 1 to 10 indicate the number of primary winter wheat ASDs as indicated in Figure 3-1.

3.6 Conclusions and Discussions

Remote sensing provides great potential for drought monitoring and a lot of drought indicators have been developed since the 1980's. Most current satellite based drought indicators are generic and little work has been done to evaluate how these remotely sensed indicators perform for agricultural drought. Besides, there has been little prior work on performance comparison of different remotely sensed indicators for agricultural drought monitoring during the growing season. This chapter investigates the responses of remotely different sensed indicators to agricultural drought, revealing the responsiveness and effectiveness of each indicator to drought, and also evaluates the drought impact on agriculture production based on the vegetation condition derived drought indicators from remote sensing. The main conclusions are:

Within each type of drought indicators, the standardized (STI/SVI/SEI) and normalized (NTI/NVI/NEI) indicators show similar and slightly better performances than condition indicators (VCI/TCI/ECI). LST and ET based indicators show similar capabilities for drought monitoring in terms of both effectiveness and responsiveness.

LST and ET derived indicators are quite sensitive to drought, which shows immediate response after drought within 1 week; while for NDVI derived indicators, there is no consistent drought response time, generally varying from 1 to 5 weeks. During the winter wheat main growing season, LST and ET indicators show better performance (more consistent response time and better ability) across space during the early and late main growing season, while NDVI derived indicators show increasing performance as the growing season progresses possibly related to the increasing drought impact. This study is based on MODIS ET product, which doesn't show too much added-on values for agricultural drought monitoring as compared to MODIS LST product. More future work using other ET products, such as the ones developed based on Cammalleri et al. (2014) and Liang et al. (2013), is recommended for further verification.

The ASCAT SSM product is generally effective for characterizing drought conditions across different stations, with better representation of soil moisture at 5cm than 10cm depth. ASCAT SSM product shows varying capability for drought monitoring during the entire year. Better correlation is observed around March-July and October-November, indicating the effectiveness of ASCAT SSM for agricultural drought monitoring, and the relatively low and fluctuated correlation in December-February and summer August-September is related to winter snow cover and summer precipitation. Also, better drought monitoring capability is found for the ASCAT descending SSM related to its morning overpass time.

Drought has varying impacts during winter wheat main growing season, leading to different crop yield loss. Significant drought impacts emerge in Mid-April and last until Early-June, which is identified as the key alert period for agricultural drought

monitoring. Despite some variability, drought shows generally increasing impacts during winter wheat main growing season for all states, with the most severe drought effects during the grain filling stage around Mid-May in Kansas, Mid-Late April in Oklahoma and Mid-Late May in Nebraska during their corresponding vegetative peaks, generally 4-6 weeks prior to harvest. Also, more significant drought impacts are found in the states with higher planting density, such as Oklahoma as compared to Nebraska.

By demonstrating the merits and limitations of each indicator, this research can help inform an improved agricultural drought indicator consistently applicable at a large scale, which could be used to prototype an enhanced agricultural drought alert system. However, there remain some challenges in this study and much further work is needed. First, NASMD is an integrated database comprised of several regional networks, inevitably resulting in soil moisture measurement inconsistency due to different sensors, measurement depths and data qualities. Also, the CDL to identify station land covers is derived from remote sensing product, which might incur possible misclassification for certain stations limited by classification accuracy. Besides, there is a great spatial resolution mismatch between in situ measurements and satellite pixel values, as the in situ soil moisture measurements only represent a very small area (a few dm²) while the satellite data indicates an integrated condition for the pixel area (around km²). Finally, there exists large heterogeneity in the study area due to different climatology regimes and agricultural practices, which leads to the spatial variability of drought response as seen in this work and calls for continued future work to identify the potential factors contributing to this variability.

Although drought is the main driver for reduced crop productivity, it is difficult to distinguish drought from other confounding stresses in some cases, especially from satellite observations. More information, such as in situ drought record network and crop modelling, should be incorporated to help identify different agricultural stresses. Also, the remotely sensed drought indicator is often an anomaly-based metric calculated from long-term time series. The short data record from commonly used sensors, such as MODIS and ASCAT, influences the accuracy of the drought indicators and calls for further continuing monitoring as more satellite observations become available in the future. The study of remotely sensed drought indicators based on spatial domain in addition to the temporal domain will provide great potential for improved drought monitoring. Also, the drought characterization in this study is based on remotely sensed vegetation conditions. Considering the possible lagged response of vegetation growth to drought, using other more responsive information (e.g. LST/ET) for agricultural drought monitoring and the subsequent agricultural impacts assessment, would help improve the understanding of drought impacts.

Chapter 4: Assessing the Remotely Sensed Drought Severity Index for Agricultural Drought Monitoring and Impact Analysis in North China

4.1 Introduction

Drought is a common and recurring event for all climatic regimes, both dry and humid. Of all natural hazards, drought is the most complex and least understood, affecting large numbers of people and resulting in significant economic, social and environmental impacts (Wilhite, 2005). According to the International Disaster Database, the number of drought occurrences makes up only 5% of all natural disasters; however, drought results in 30% of the total people affected, ranking the top among all natural disasters (<http://www.emdat.be/>). With global warming and the frequent occurrence of extreme events, concerns about global drought and its impacts have become more pronounced in recent years (Dai, 2011), drawing increasing attention from governments, scientists and the public. Agriculture is the major sector to be affected by drought. Although the overall agricultural production has risen in recent years, agricultural drought constitutes the primary cause of crop failure, resulting in global food price instability and threatening global food security (World Bank, 2012). This calls for further study of agricultural drought and its impacts on crop production.

Most standard drought indices require precipitation data as a primary input (Wilhite, 2000), and many meteorological drought indicators have been developed, such as the Percentage of Normal Precipitation (NDMC, <http://www.drought.unl.edu/>), Percentage of Precipitation Anomaly (Zhang et al., 2009), Deciles Index (Gibbs &

Maher, 1967), Palmer Drought Severity Index (PDSI, Palmer, 1965) and Standardized Precipitation Index (SPI, McKee et al., 1993). While near real-time and high-quality precipitation data are available in some regions, many parts of the world lack sufficient rain-gauge networks, which influences the accuracy of drought indicators derived from meteorological data and presents significant challenges for global agricultural drought monitoring (Anderson et al., 2011). Drought can cause a decline in vegetation vigor which is detectable by remote sensing (Tucker, 1979). Satellite observations overcome some limitations of station-based meteorological observations, providing potential for cost-effective, spatially explicit and dynamic large-scale drought monitoring. The use of time-series satellite observations for drought monitoring began in the 1980's using AVHRR NDVI data (Tucker et al., 1986; Tucker & Choudhury, 1987; Tucker, 1989). Since then, many remotely sensed indicators have been developed based on vegetation conditions, surface temperature, combinations of vegetation conditions and surface temperature. Among those indicators, NDVI-based metrics are commonly used as indicators of vegetation stress and drought (Henricksen & Durkin, 1986; Tucker & Choudhury, 1987; Tucker, 1989; Gutman, 1990). Many drought indicators have been developed based on NDVI, such as Anomaly Vegetation Index (AVI) (Chen et al., 1994), Vegetation Condition Index (VCI) (Kogan, 1990, 1995a, 1995b; Liu & Kogan, 1996), Standardized Vegetation Index (SVI) (Peters et al., 2002), Monthly Vegetation Condition Index (MVCI) (McVicar & Jupp, 1998), and the Percent of Average Seasonal Greenness (PASG) (Brown et al., 2008). Also, land surface temperature (LST) data can provide vital information on evapotranspiration and vegetation water stress (Goward & Hope, 1989; Carlson et al., 1990; Nemani et al., 1993) and can be

used as an indicator of surface moisture status. To remove the effect of seasonal temperature variations, Mcvicar & Jupp (1998) developed the Normalized Difference Temperature Index (NDTI) and Kogan (1995a) developed the Temperature Condition Index (TCI) for drought monitoring based on LST. Several indicators based on combinations of vegetation indices and temperature have also been developed, such as the Vegetation Health Index (VHI) (Kogan, 1995a), Temperature Vegetation Index (TVI) (McVicar & Jupp, 1998), Vegetation Supply Water Index (VSWI) (McVicar & Jupp, 1998) and Temperature Vegetation Drought Index (TVDI) (Sandholt, 2002). While these indicators prove very useful for drought monitoring, they also have their limitations. Usually, there is a varying time lag between a drought event and vegetation response, which thus limits the responsiveness of vegetation condition derived indices for drought monitoring (Ji & Peter, 2003), and also NDVI alone can't fully represent the drought information (Saleska et al., 2007; Atkinson et al., 2011; Morton et al., 2014). In addition, missing data, for example in LST products due to cloud contamination (Williamson et al., 2013), can also impact their capability for continuously effective drought monitoring.

As a key component of the terrestrial water and energy cycle, evapotranspiration (ET) represents an important constraint on water availability, which thus is a more direct and effective parameter for describing ecosystem moisture status as compared to meteorological drought indices (Anderson et al., 2011), vegetation condition and LST derived indicators. Remote sensing has been recognized as the most feasible and cost-effective approach to provide spatially explicit ET information across terrestrial ecosystems (Jackson, 1984). In recent years, there has been an increasing trend of using

ET for drought monitoring (Anderson et al., 2007, 2011, 2013; Choi et al., 2013; Otkin et al., 2013). The Evaporative Stress Index (ESI) has been developed for drought monitoring by Anderson et al. (2007 & 2011), quantifying anomalies in the ratio of actual to potential ET (PET). Using inputs from the NASA Moderate Resolution Imaging Spectroradiometer (MODIS), Mu et al. (2007 & 2011) developed a model to estimate ET and PET, and produced the global MOD16 ET product at 8-day, monthly and annual intervals. Insufficient moisture limits the available water that vegetation can absorb and is frequently the leading cause of reduced photosynthetic capacity when large areas exhibit persistent vegetation stress. Utilizing surface ET information while taking into account vegetation response at the same time, a new remotely sensed drought index, Drought Severity Index (DSI), was recently proposed, integrating ET, PET and NDVI based on the MOD16 ET product (Mu et al., 2007 & 2011) and the MODIS13 NDVI (Huete et al., 2002) product. The DSI shows considerable potential for drought monitoring at the global scale (Mu et al., 2013a).

Agricultural production, especially in poor areas, remains highly dependent on weather conditions. The rapidly changing climate during the past decades has undoubtedly resulted in significant impacts on agricultural production. According to a global scale study on climate change and crop productivity, as of 2002, global warming since 1981 has led to a combined loss of roughly 40 Mt or \$5 billion for wheat, maize and barley per year (Lobell & Field, 2007). Another more recent study shows that global maize and wheat production respectively declined by 3.8% and 5.5%, as compared to the case without climate trends (Lobell et al., 2011b). In addition to global studies, there is a growing body of regional impact research. In Sub-Saharan Africa,

climate change has robust negative impacts on agriculture (Schlenker & Lobell, 2010). Lobell et al. (2011a) discovered that, with a 10C increase in temperature, about 65% of African maize growing regions would experience yield losses under well-irrigated conditions versus 100% under drought conditions. In Wisconsin, each additional degree higher than normal temperature in summer will decrease the corn and soybean yields by 13% and 16% respectively, while a modest increase in summer precipitation would boost the production by 5-10% (Kucharik & Serbin, 2008). In the central US, a drought impact study from 1995 to 2012 demonstrated that maize yields became more sensitive to drought associated with high vapor pressure deficiency (Lobell et al., 2014). With the exacerbated climate warming and irregularity of precipitation in the future, the drought issue and associated impacts will become even more pronounced. The agricultural areas suffering from high and very high agricultural drought hazard account for approximately 23.57% and 27.19% of the global agricultural areas, most of which are located within the major crop producing regions in China, Europe, Southeast Asia, U.S. and South America (Geng et al., 2015). Another recent study on global drought impacts on agriculture demonstrates that, despite the inconsistency between the magnitude of crop failure and that of drought severity, the historical severe droughts in 5 drought-prone countries (Brazil, Peru, Spain, Iran and China) have caused significant crop loss (Maize/Rice/Wheat/Soybean/Barley/Sorghum) (Wang et al., 2014). Also, at the regional scale, despite varying drought impacts across different regions, crop types and time periods, severe droughts are also found to be linked with significant crop yield reduction in the Czech Republic (Hlavinka et al., 2009), Midwest

U.S. (Mishra & Cherkauer, 2010), Ghana (Antwi-Agyei et al., 2012), Eastern Sahel (Elagib, 2014) and China (Hu et al., 2014; Qin et al., 2014; Ming et al., 2015).

The direct impacts of drought on agriculture involve the reduction in crop production and the drought impacts on crops are often investigated through crop simulation modelling. Crop growth models are eco-physiological models which simulate the plant behavior under different conditions and output the simulated crop production as well as various parameters (leaf area index, evapotranspiration, soil moisture and biomass) during crop growth (Huth et al., 2008; Huang et al., 2015a, 2015b). These models incorporate the impacts of changing weather conditions and improved technology & management practices on crop yields (Sivakumar et al., 2011), and thus can be used to simulate the response of crop yields to drought. Up to now, there has been some work on drought and its agricultural impacts based on crop growth models (Bryant et al., 1992; Song & Dong, 2006; Jia et al., 2011; Yu et al., 2014). Most existing crop models can be successfully used for simulating crop development process at the field scale; however, most of these models are complex and require a large number of input parameters that are not readily available at the regional scale. Remote sensing can provide temporally and spatially continuous information across the region, thus enabling the study on agricultural drought impacts over large areas at a finer spatial and temporal resolution (Vicente-Serrano, 2007).

North China is the most important agricultural areas for winter wheat in China and in recent years has suffered from frequent droughts, which highlights the importance of agricultural drought monitoring in this region. Using MODIS ET, PET and NDVI products, Mu et al. (2013a) generated the MODIS DSI dataset. Although the capability

of the DSI for drought monitoring has been demonstrated at the global scale, there has been little work to assess its utility for regional agricultural drought monitoring. Considering the distinct characteristics of agricultural land use in the North China region and varying accuracy of model input parameters across landscapes, an evaluation of the MODIS DSI for regional drought monitoring is warranted. Thus, the objective of this study in North China is (1) to examine the capability of MODIS DSI for describing regional moisture status against precipitation and soil moisture; (2) to evaluate the ability of the MODIS DSI for characterizing agricultural drought severity; (3) to explore the impacts of drought on crop production during the main winter wheat growing season.

4.2 Study Area

The important winter wheat producing region in North China was chosen as the study area, which extends from 31°23'N to 42°35'N in latitude and from 105°30'E to 122°42'E in longitude, and covers five provinces including Hebei, Henan, Shandong, Shanxi and Shaanxi (Figure 4-1). This region is mainly located in the semi-arid area of the mid-latitude zone and the semi-humid area of the warm temperate zone, and partly located in the arid area of the mid-latitude zone and the semi-arid area of the warm temperate zone. The main soil type in these regions is pedocals, the calcium soils from which the lime has not been leached. The annual precipitation is approximately 400-800 mm with large seasonal variability; only 30% of the precipitation occurs from October to May during the winter wheat growing season and about 70% occurs in late June to September during the maize growing season (Data Source: China Meteorological Administration, <http://cdc.cma.gov.cn/>). This region has both irrigated

and rainfed croplands, with the irrigated agriculture accounting for about 30% in Shanxi and Shaanxi, 36% in Henan and about half in Shandong and Hebei (Data Source: National Bureau of Statistics of China, <http://www.stats.gov.cn/>) and the prevailing planting pattern is dominated by an intensive dual-cropping system of winter wheat and summer maize. The major winter wheat variety planted in this region is the Hard White Winter Wheat. The production of winter wheat in these five provinces accounts for more than 70% of China's total output of winter wheat (Data Source: National Bureau of Statistics of China, <http://www.stats.gov.cn/>) and plays an important role in the Chinese domestic wheat market. Due to insufficient precipitation and high variability of precipitation in the growing season, this region is highly susceptible to spring and early summer droughts, and droughts have become the most dominant factor for wheat loss in this region (Song & Dong, 2006; Sun et al., 2008; Du et al., 2013). For the past years from 2000-2011, despite some changes in varieties and agricultural practices, this region has a relatively stable winter wheat sowing area and yields.

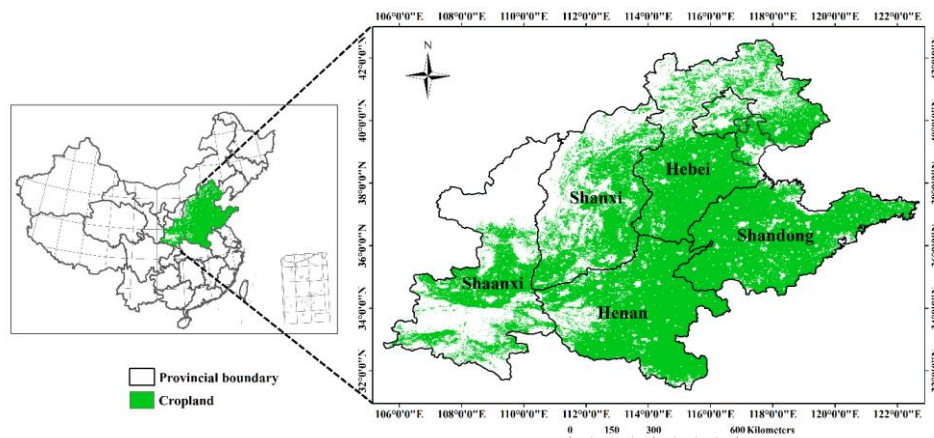


Figure 4-1: Chapter 4 Study Area Showing the MODIS Cropland Used in This Study

4.3 Data and Preprocessing

The data used in this study includes remote sensing data, gridded meteorological/soil moisture data, in situ meteorological data as well as agricultural statistical data. A detailed description of the dataset is listed as below.

4.3.1 Remote Sensing Data

The primary remote sensing data includes the 8-day MOD16 ET/PET and MOD13 NDVI products for 5 provinces at 1km resolution from 2000-2012, which are available from NTSG, University of Montana (<http://www.ntsg.umt.edu/project/mod16>) and the NASA Land Processes Distributed Active Archive Center (LP DAAC, <https://lpdaac.usgs.gov/>) respectively. The MOD16 algorithm is based on the Penman-Monteith equation using daily meteorological reanalysis data and 8-day MODIS derived vegetation dynamics as inputs. Four layers including ET, PET, Latent Heat (LE) and Potential Latent Heat (PLE), are generated in this product. For a detailed description of MOD16 ET algorithm and product, see Mu et al. (2007, 2011, 2013b). The MOD16 ET, PET data and MOD13 NDVI (Huete et al., 2002) data were used as the primary inputs for calculating the DSI. Also, the MOD12Q1 product using the University of Maryland (UMD) land cover classification scheme (available from LP DAAC, <https://lpdaac.usgs.gov/>, Friedl et al., 2002) was used to depict the cropland in the five provinces.

4.3.2 Gridded Meteorological/Soil Moisture data

To examine whether MODIS DSI can represent the moisture status, several gridded datasets were used in this study. Both daily and monthly gridded precipitation

at 0.5 degree from 2000-2012 were provided by China Meteorological Data Sharing Service System (<http://cdc.cma.gov.cn/>). The Climate Prediction Center soil moisture dataset, which contains monthly averaged soil moisture water height equivalents at 0.5 degree (CPC Soil Moisture data provided by the NOAA/OAR/ESRL PSD, Boulder, Colorado, USA, at <http://www.esrl.noaa.gov/psd/>), as well as the 0.5-degree PDSI dataset generated by Zhao & Running (2010) (ftp://ftp.ntsg.umt.edu/pub/NPP_Science_2010/PDSI/), were both used for the selected 5 provinces from 2000-2012.

4.3.3 In situ Station Data

Monthly precipitation data from more than 100 meteorological stations within the study region were used during 2000-2012, which was accessed from the China Meteorological Data Sharing Service System (<http://cdc.cma.gov.cn/>).

4.3.4 Agricultural Statistical Data

The drought affected agricultural areas represent the areas with a total grain yield reduction of more than 10%. For the 5 provinces, agricultural land areas and drought affected agricultural areas from 2000-2012 were accessed through the Crop and Disaster Databases of the Ministry of Agriculture of the People's Republic of China (<http://www.zzys.moa.gov.cn/>), which are sourced from China Statistical Yearbooks and China Agriculture Statistical Reports. Also, the province-level winter wheat yield data for 5 provinces from 2000-2011 were obtained from the National Bureau of Statistics of China (<http://data.stats.gov.cn/>) and the sub-province winter wheat yield data for Shaanxi Province from 2000-2012 were acquired through the Provincial

Bureau of Statistics. All those data were statistics based on the field surveys at different levels.

4.4 Methodology

4.4.1 Remotely Sensed Drought Severity Index

The Drought Severity Index (DSI), which integrates the drought diagnostic information from two sources (NDVI and ET/PET), was used as the primary remotely sensed drought indicator in this study. Due to the relatively greater noise in the non-growing season NDVI signal (Zhao & Running, 2010), Mu et al. (2013a) only used the MOD13 NDVI during the snow-free growing season labeled by the MODIS 8-day Climate Model Grid (CMG) 0.05° snow cover (MOD10C2; Hall and Riggs, 2007) in the MODIS DSI computation. For calculation of the DSI, the first step is to derive the standardized values of ET/PET ratio and NDVI (Equations 4-1 & 4-2).

$$Z_{ET/PET} = \frac{ET / PET - \overline{ET / PET}}{\sigma_{ET/PET}} \quad 4-1$$

$$Z_{NDVI} = \frac{NDVI - \overline{NDVI}}{\sigma_{NDVI}} \quad 4-2$$

After the ET/PET and NDVI are standardized, they are first added and then standardized again to derive the DSI (Equations 4-3 & 4-4).

$$Z = Z_{ET/PET} + Z_{NDVI} \quad 4-3$$

$$DSI = \frac{Z - \overline{Z}}{\sigma_Z} \quad 4-4$$

Where $\overline{ET / PET}$, \overline{NDVI} represent the long term (2000-2012) mean of ET/PET and NDVI respectively; $\sigma_{ET/PET}$, σ_{NDVI} , σ_Z represent the standardized deviation of

ET/PET, NDVI and Z respectively; $Z_{ET/PET}$, Z_{NDVI} represent the standardized value of ET/PET and NDVI respectively. A more detailed description of the DSI algorithm can be found in Mu et al. (2013a).

4.4.2 Meteorological/Hydrological/Agricultural Drought Indicators

Besides the remotely sensed drought indicator (DSI), other meteorological/hydrological indicators, such as Percentage of Precipitation Anomaly (PPA) and Relative Soil Moisture (RSW) (Equations 4-5 & 4-6), were used for comparison and evaluation with the DSI.

$$PPA = \frac{P - \bar{P}}{\bar{P}} * 100\% \quad 4-5$$

$$RSW = \frac{SM}{Max_{SM}} * 100\% \quad 4-6$$

Where P is precipitation, \bar{P} is the long term average for given period (2000-2012); SM is the soil moisture value provided by the CPC dataset, and Max_{SM} is the maximum of soil moisture from CPC, which is a constant value (760mm).

The agricultural drought severity (ADS) at the province level and the crop yield loss ratio (YLR) were also used, which are expressed as the percentage of agricultural areas affected by drought and the normalization of crop yield reduction relative to the multi-year average (Equations 4-7 & 4-8).

$$ADS = \frac{Drought\ Affected\ Ag\ Lands}{Ag\ Lands} * 100\% \quad 4-7$$

$$YLR = \frac{\overline{Yield} - Yield}{Yield} * 100\% \quad 4-8$$

4.4.3 Data Temporal Composite and Spatial Aggregation

MODIS ET/PET product has a spatial resolution of 1km and temporal resolutions of 8-day, monthly and annual. To evaluate MODIS DSI for drought monitoring, it was compared against precipitation, soil moisture and agricultural drought severity with different spatial and temporal scales. For consistent inter-comparisons, the 8-day/monthly/annual DSI at the 1-km spatial scale and the 8-day/annual DSI at the province scale were used in this study. For 8-day spatial DSI, it was calculated based on the 8-day NDVI, ET and PET inputs using Equations 4-1~4-4; for monthly/annual spatial DSI calculation, the MODIS NDVI data were first converted from 8-day into monthly/annual data using the time weighting method and then the monthly/annual spatial DSI was computed per pixel from the monthly/annual NDVI, ET and PET using Equations 4-1~4-4. For the 8-day and annual DSI at the province scale, the input NDVI/ET/PET data were first aggregated to the provincial level using the valid pixels within each province to match the precipitation, soil moisture data as well as agricultural statistics. Then, the computation of 8-day and annual provincial DSI followed the similar procedures with that of 8-day and annual spatial DSI described before, using the provincial aggregated values instead of the pixel values as inputs. Besides the DSI, both the temporal composite and spatial aggregation methods were also applied to other datasets, such as precipitation and soil moisture.

4.4.4 Evaluation Criteria

Regression models between the DSI and precipitation/soil moisture/agricultural drought severity were developed, and the determination coefficients (R^2) were used as the evaluation criteria of the DSI capability for effective drought monitoring. Also, the

Pearson's Correlation Coefficient (R, Equation 4-9) between DSI and crop yield at different time scales was also calculated to explore the impacts of drought occurring during different growth stages on the final yield and thus identify the key drought alert period.

$$R = \frac{\sum_{i=1}^n (x_i - \bar{x})(y_i - \bar{y})}{\sqrt{\sum_{i=1}^n (x_i - \bar{x})^2 \sum_{i=1}^n (y_i - \bar{y})^2}} \quad 4-9$$

Where x represents the DSI at different time scales, y represents yield or other related drought indicators, and n is the number of samples.

4.5 Results

4.5.1 Evaluation of Annual DSI for Drought Monitoring

The ET, PET and NDVI data from 2000-2012 were composited into annual values, aggregated to the province level, and then the annual DSI was computed per province for the same period using the annual aggregated value and Equations 4-1~4-4. After the annual DSI was derived, it was compared with both precipitation and soil moisture at the province level from 2000-2012 to examine its capability for characterizing moisture conditions.

- Comparison against precipitation

The 0.5-degree monthly gridded precipitation was first accumulated for each year to get the annual total. Then, the annual gridded precipitation was aggregated to the provincial annual precipitation from 2000-2012 and used to calculate the PPA at the province level using Equation 4-5. Finally, the regression models between the annual

MODIS DSI and PPA from 2000-2012 in 5 provinces were established and the results are shown as below.

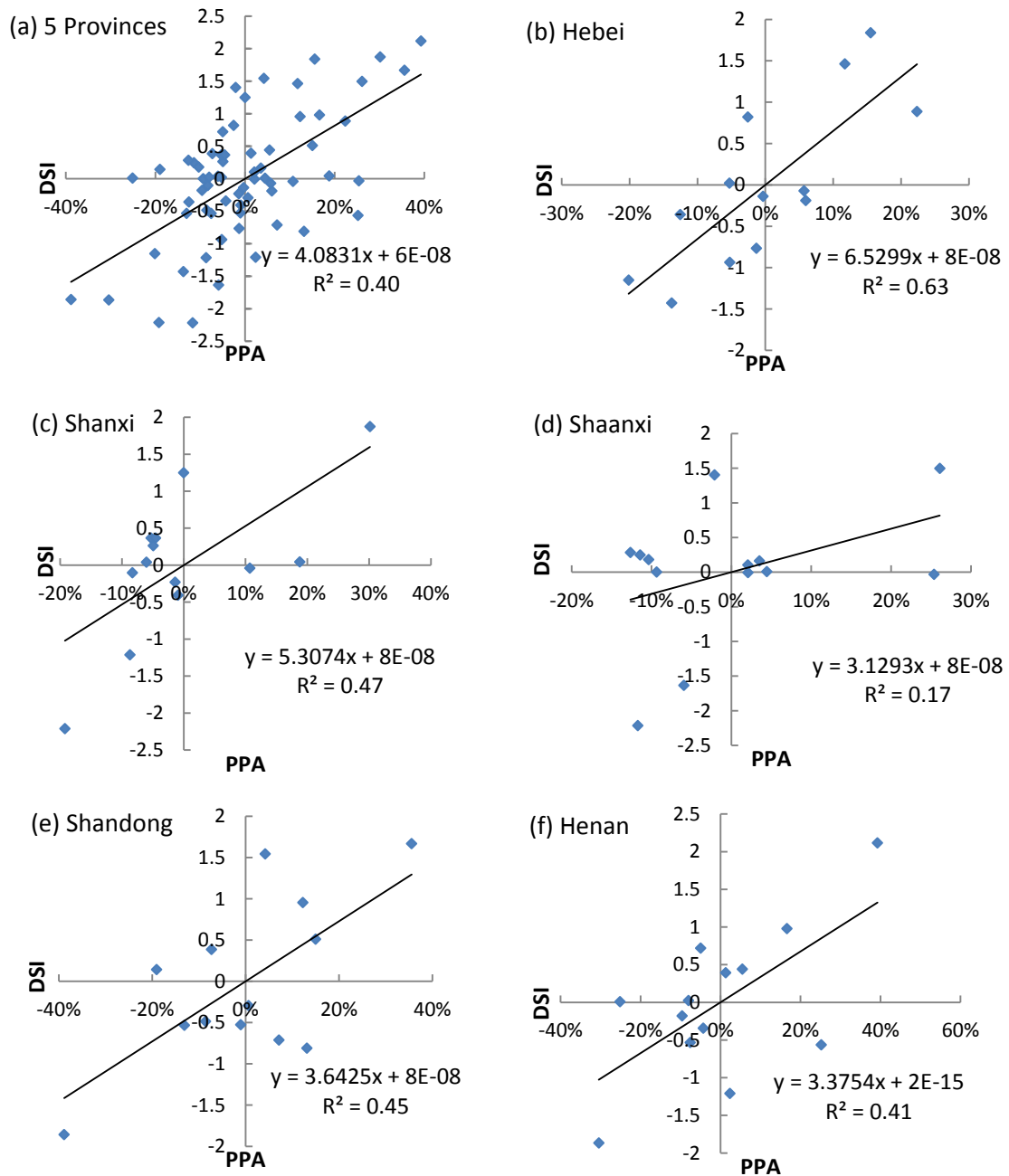


Figure 4-2: Relationships between Annual DSI and PPA in 5 Provinces (a) 5 Provinces (b) Hebei (c) Shanxi (d) Shaanxi (e) Shandong (f) Henan

As seen from Figure 4-2, the annual DSI shows a generally good relationship with the annual precipitation in 5 provinces. The R^2 of the regression model reaches almost

0.4 using all the data from 5 provinces together, which indicates the DSI has a good capability for drought monitoring at the yearly scale. The results also show that 4 out of the 5 provinces have stronger DSI-PPA statistical relationships, with Hebei having the best correlation, followed by Shanxi, Shandong, Henan, and finally Shaanxi. For each province, the precipitation is the average over the entire province due to its coarse resolution (0.5 degree), but the DSI is aggregated over the vegetated lands within the province. The mismatch between areas used for aggregating provincial precipitation and DSI can cause biases in the statistical relationships between them. Also, the gridded precipitation data is interpolated using observed data from the weather stations which are relatively sparsely distributed and may not represent the heterogeneous landscapes in the five provinces, and thus has substantial uncertainties (Data Source: China Meteorological Administration, <http://cdc.cma.gov.cn/>). The DSI is derived using ET/PET and NDVI, which has biases and uncertainties as well (Mu et al., 2007, 2011, 2013a; Philips et al., 2007; Saleska et al., 2007). All these uncertainties from either the precipitation or DSI data might also impact their statistical relationships.

Besides the comparison between provincial DSI and PPA, the relationships between DSI and precipitation at the station scale were also investigated. This study area covers more than 100 meteorological stations. The annual precipitation for each meteorological station was accumulated from the station monthly precipitation and then the PPA for each station was calculated. Also, the annual DSI for each station was extracted based on its location from the calculated annual DSI images. Then, the relationships between annual DSI and PPA were analyzed for each station and the results of the stations located within the arable areas are shown in Figure 4-3.

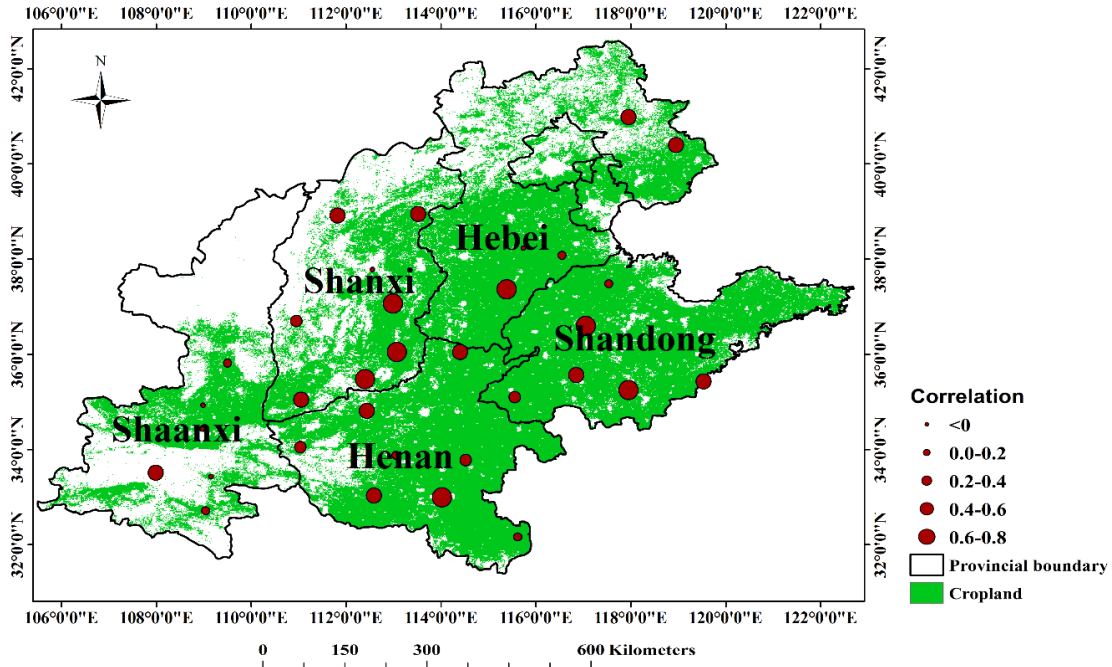


Figure 4-3: Spatial Pattern of the Correlation between Annual DSI and PPA
 Note: Only the stations located within the arable areas are displayed.

From Figure 4-3, despite varying correlations, most regions show consistently positive relationships between the DSI and PPA. It is also noticed that there is a mix of both high and low correlation for each province, of which the very low or even negative correlation may be related to local water management practices such as irrigation. The DSI is a comprehensive indicator of drought conditions for that region, integrating both water input from precipitation and irrigation and water discharge, and more irrigated regions tend to have poorer DSI-precipitation relationships as compared to rainfed regions due to the interference of irrigation.

- Comparison against soil moisture

Similarly, before exploring the relationships between the DSI and soil moisture, the monthly gridded soil moisture from CPC at 0.5-degree spatial resolution was averaged for each year and aggregated to the province level for the 5 provinces from 2000-2012. Then, the aggregated soil moisture at the province level was normalized

into relative soil water (RSW) using Equation 4-6. The relationships between DSI and RSW are displayed in Figure 4-4.

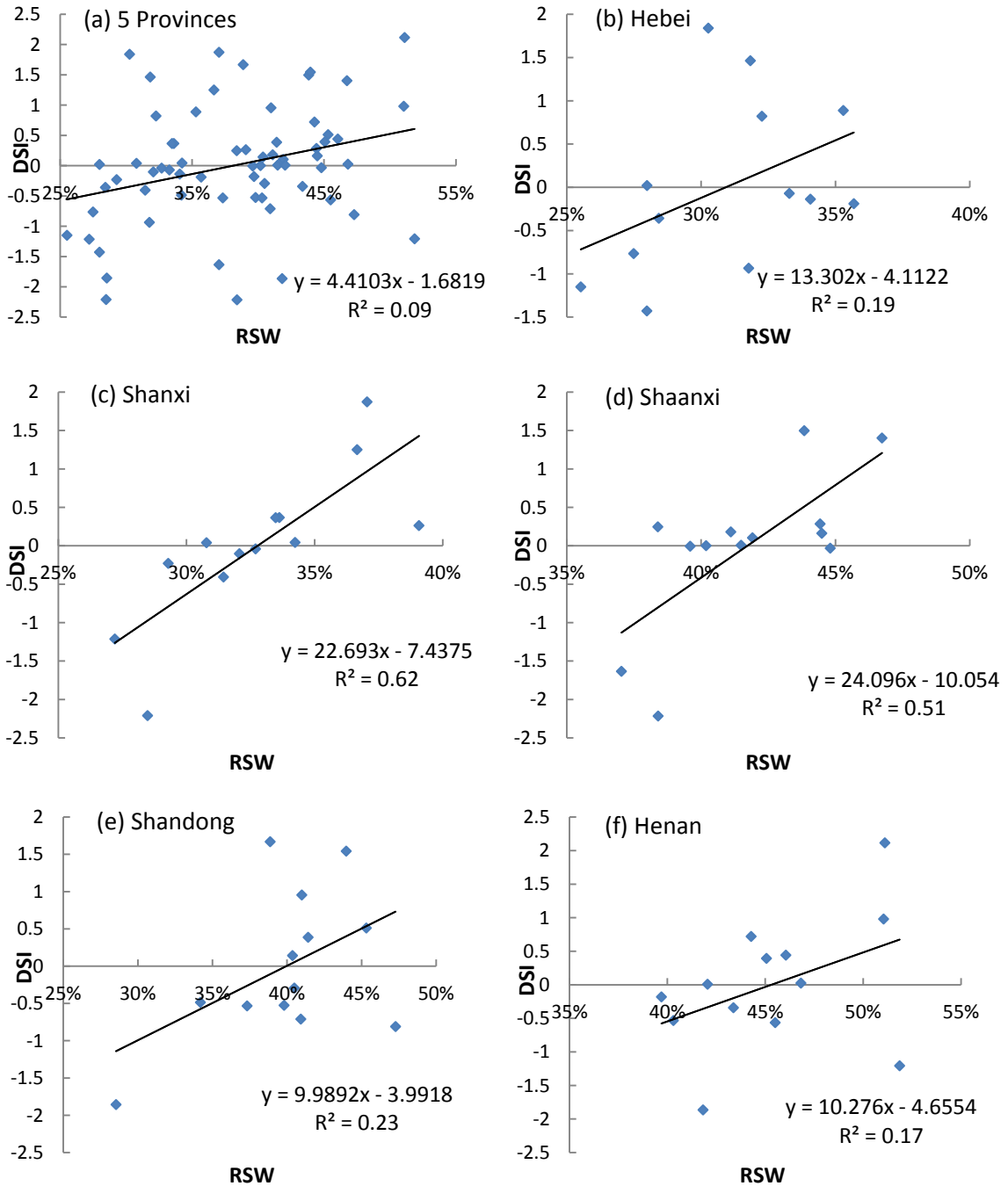


Figure 4-4: Relationships between Annual DSI and RSW in 5 Provinces (a) 5 Provinces (b) Hebei (c) Shanxi (d) Shaanxi (e) Shandong (f) Henan

According to Figure 4-4a, the relationship between the DSI and soil moisture in the 5 provinces is relatively poor despite that the DSI shows a generally consistent trend with the soil moisture conditions in 5 provinces. Better relationships between DSI and soil moisture were found in Shanxi and Shaanxi where agriculture is primarily rainfed. For the other 3 provinces where agriculture is heavily irrigated, the correlation between the DSI and soil moisture is relatively poor. The major reason for the poor relationships may come from the substantial uncertainties in the model-simulated CPC soil moisture data which uses precipitation and temperature as inputs (Huang et al., 1996; Dool et al., 2003; Fan et al., 2004). Using only precipitation and temperature without taking irrigation practices into account, the simulated soil moisture might be more reliable in the areas with no or little water management. The DSI derived from MODIS ET/PET and NDVI data is a comprehensive drought index which can reflect the irrigation information to some extent. This can partly explain the better relationships in the primarily rainfed agricultural provinces of Shanxi and Shaanxi and the poor correlation in the other 3 heavily irrigated provinces. All these uncertainties may explain the different performances between these two groups of provinces and the relative low correlation between soil moisture and DSI.

4.5.2 Evaluation of the DSI for Drought Monitoring during the Main Winter Wheat Growing Season

In addition to the evaluation of annual DSI, the capability of MODIS DSI for drought monitoring during the main winter wheat growing season (March-June) was also examined at 8-day intervals. First, the 8-day ET, PET and NDVI data were aggregated to the province level. Next, the provincial MODIS DSI was calculated using

Equations 4-1~4-4 during each growing season (March-June, DOY49-DOY177) over 2000-2012. To match the temporal resolution of 8-day MODIS DSI, the daily gridded precipitation was accumulated for the same 8-day time periods in March-June (DOY49-DOY177) for 2000-2012. Then, the accumulated 8-day total precipitation was aggregated to the province level and used for deriving PPA. Figure 4-5 shows the correlation between 8-day MODIS DSI and PPA during the main winter wheat growing season for each province.

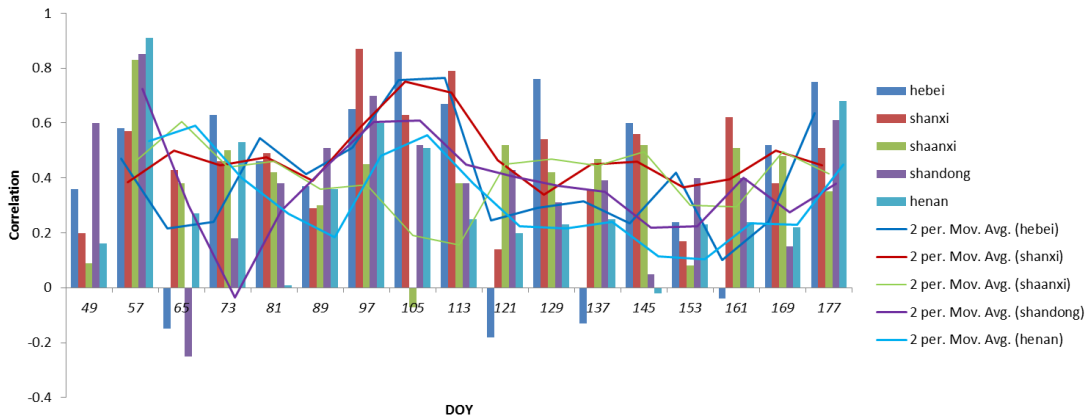


Figure 4-5: The Correlation between 8-day DSI and PPA in 5 Provinces during the Main Winter Wheat Growing Season

It can be seen from Figure 4-5 that there is an overall good relationship between 8-day MODIS DSI and PPA over the entire time series (more than 90%) of the winter wheat main growing season (at 8-day intervals). In general, MODIS DSI can effectively detect droughts caused by the total precipitation deficiency in each 8-day time period during the winter wheat main growing season. However, there also exist randomly low or negative correlations (less than 10%). As with the findings for comparison with precipitation in Section 4.5.1, one reason for the low or negative correlation between MODIS DSI and PPA might result from the large uncertainties in gridded precipitation (PPA) (Gao et al., 2010) and in the DSI. Also, each 8-day

moisture status is not only influenced by the accumulated 8-day precipitation but also possibly by water management such as irrigation and water discharge as well as the previous moisture status, and thus only precipitation itself cannot be used to identify specific drought impacts (McKee et al., 1993; Werick et al., 1994). The MODIS DSI integrates the current 8-day moisture status through ET/PET and accumulated antecedent moisture status using vegetation growth status through NDVI, all of which can partly explain the low or negative correlation with PPA. To smooth the outliers and thus show the general trend of 8-day DSI-PPA relationship over the time series, the second order moving average method was applied to the correlation. As seen from the smoothed results (lines in Figure 4-5), 4 of the 5 provinces (Hebei, Shanxi, Shandong, Henan) have a relatively consistent trend, reaching the highest correlation in April (winter wheat's jointing and booting stages), while Shaanxi has a relatively constant trend during the growing season. Also, the comparison between these provinces indicates that the DSI shows the best drought monitoring performance for Hebei, followed by Shanxi, Shandong, Henan, and Shaanxi, which is consistent with the annual results from Section 4.5.1.

To further demonstrate the DSI's capability for characterizing particular drought events, the monthly spatial MODIS DSI was compared with the monthly gridded PDSI. PDSI integrates precipitation, temperature and available water capacity, and is the most commonly used drought indicator (Palmer, 1965). In this study, the 0.5-degree monthly PDSI dataset generated by Zhao & Running (2010) was used. According to the record, 2009 was a typical drought year in North China. As a key period during the winter wheat main growing season, April (2009) was still impacted from the antecedent severe

drought in early 2009 and thus was selected to show the spatial patterns of monthly MODIS DSI and PDSI (Figure 4-6).

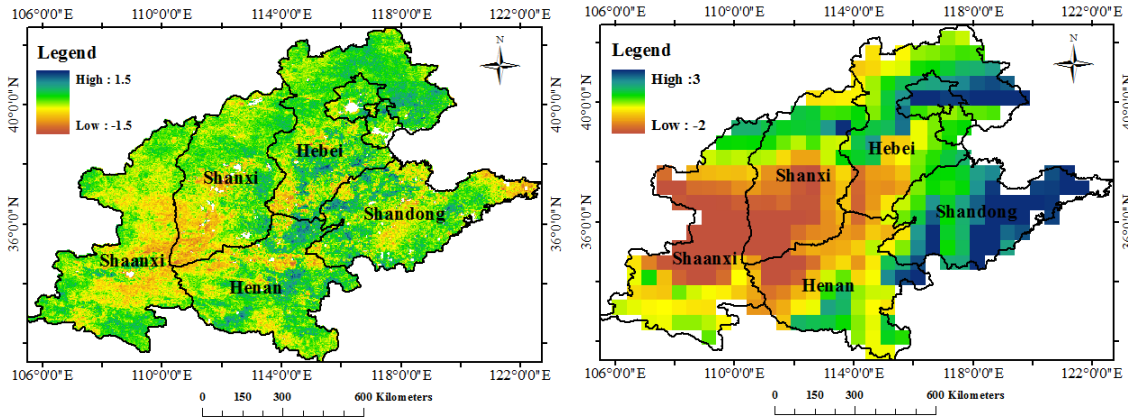


Figure 4-6: The Spatial Patterns of DSI (Left) and PDSI (Right) for April 2009

As seen from Figure 4-6, the DSI show a consistent but finer spatial pattern with the PDSI. Low DSI values correspond with low PDSI values in the region of South Hebei, North Henan, South Shanxi and Central Shaanxi, which are shown to be potential drought affected areas.

4.5.3 Evaluation of the DSI for Characterizing Agricultural Drought Severity

In addition to evaluation of the DSI for general drought monitoring (Sections 4.5.1 and 4.5.2), the DSI was compared with agricultural drought severity at the province level to investigate its capability for effective agricultural drought monitoring. Similarly to Section 4.5.1, the annual ET, PET and NDVI data were aggregated to the province level using the cropland pixels within the province (as indicated by the MODIS cropland mask). The annual cropland DSI was computed per province based on the annual aggregated ET, PET and NDVI using Equations 4-1~4-4. At the province level, the MODIS cropland DSI was compared with agricultural drought severity (ADS) calculated based on Equation 4-7. The results are shown in Figure 4-7.

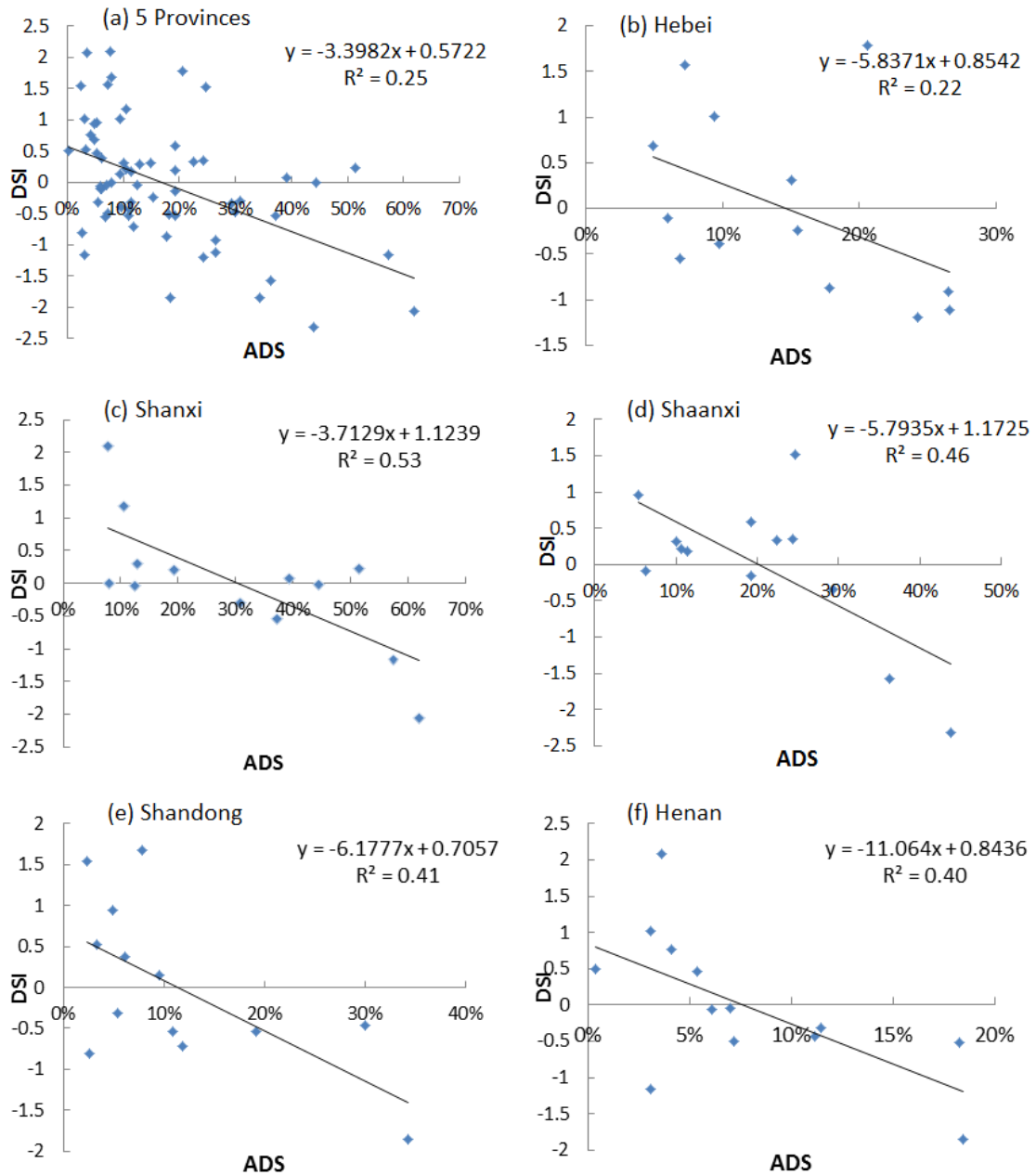


Figure 4-7: Relationships between Annual Cropland DSI and ADS in 5 Provinces (a) 5 Provinces (b) Hebei (c) Shanxi (d) Shaanxi (e) Shandong (f) Henan

It can be seen from Figure 4-7 that the DSI shows generally good capability for characterizing agricultural drought severity within the province. The determination coefficients (R^2) of statistical models for all provinces other than Hebei are about or above 0.4; and it is also noticed that the relatively low R in Hebei is seriously distorted

by the data point in 2003 probably due to the poor data quality of agricultural statistics for that year. The comparison between the results of 5 provinces indicates the DSI has better agricultural drought monitoring capability in Shanxi and Shaanxi which are relatively less irrigated, followed by Shandong, Henan and Hebei, and this result is consistent with the results of soil moisture in Section 4.5.1. Considering the possible uncertainties in the agricultural statistics, the DSI shows to be a good indicator for agricultural drought monitoring.

4.5.4 Exploring the Impacts of Agricultural Drought on Winter Wheat Yield during the Main Growing Season

In this section, the DSI was used as the primary indicator to investigate the drought impacts on winter wheat yield during the main growing season from March to June.

- The impacts of drought on winter wheat yield at 8-day intervals

Winter wheat is the dominant crop from March to June in North China, and thus the MODIS cropland mask can provide a general overview of the winter wheat regions. The 8-day ET, PET and NDVI data were aggregated to the province level using the MODIS cropland pixels within each province. Then, the 8-day winter wheat MODIS DSI was computed per province based on Equations 4-1~4-4 for March-June. For each province, the correlation between winter wheat MODIS DSI and winter wheat yield was examined for each 8-day time period from DOY49-DOY177 using the 12-year data (2000-2011). Figure 4-8 shows the correlation results for each 8-day time period during the main growing season in 5 provinces.

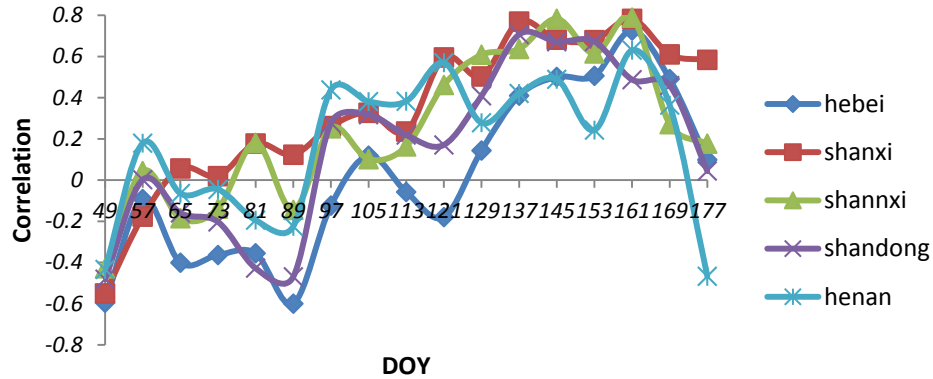


Figure 4-8: Correlation between 8-day Cropland DSI and Winter Wheat Yield during the Main Growing Season in 5 Provinces

The increasing correlation during the growing season in Figure 4-8 indicates increasing drought impacts on winter wheat yield during the main growing season (March-June). In March, winter wheat is at its green-up stage with relatively low plant cover. During this stage, since winter wheat is recovering from the long and cold winter, sufficient solar radiation and high temperature could boost photosynthetic capacity and play a larger role in crop growth. Thus, the very low or even negative correlation indicates that drought occurring during this stage has little impact or even positive impact on the final crop yield. The early season “drought” detected during this period is mainly driven by the temperature increase which is favorable for the crop growth, resulting in the occasionally positive agricultural impact. In April, winter wheat reaches its jointing and booting stages during which water becomes the dominant factor for limiting crop growth, and the correlation has turned positive and increased, which indicates effective drought impacts start to emerge and gradually increase during this period. The correlation continues to increase from April to May in Shanxi, Shaanxi, Shandong, and Hebei and reaches a steadily high level in May (winter wheat’s heading and grain-filling stages), which means drought occurring at winter wheat’s heading and

grain-filling stages tends to have the most significant impacts on the yearly winter wheat yield. However, for Henan, the correlation in May is similar to that of April, indicating similar agricultural impacts during heading/grain-filling stages and joint/booting stages. Besides, it is also noticed that droughts show significant fluctuations in terms of agricultural impacts in April during the winter wheat jointing/booting stages in Hebei, which may be related to regional irrigation, as well as fragmented land use and complex cropping patterns within the province. Although drought plays a dominant role in influencing the agricultural production, it should also be noted that drought is not the only factor impacting winter wheat yields. Other factors such as agricultural management (fertilizer and technology) as well as disturbance by insect outbreak can also significantly affect crop yields and influence this DSI-Yield relationship.

- The impacts of drought on winter wheat yield during different periods of the growing season

The first part of Section 4.5.4 investigated the time-series drought impacts for each 8-day of the main growing season. However, most of the time, we need to know the evolution of drought impacts on yield during the entire growing season, not just the drought impacts at each 8-day period. In this section, the impacts of drought occurring during any time period of the main winter wheat growing season (March-June from DOY 49 to DOY 177) were explored using the 8-day DSI data. First, the 8-day ET/PET and NDVI during the main growing season were composited into any time scale ($t=8*n$, $n=1, 2, 3, \dots$) and aggregated to the province using the MODIS cropland pixels within the province. Then, the cropland DSI for any time scale of the growing season between

2000 and 2011 was computed per province using Equations 4-1~4-4. For each province, the correlation analysis between cropland DSI and winter wheat yield from 2000-2011 was carried out at any time scale of the growing season. For simplicity, only the results for Shandong Province are displayed (Figure 4-9).

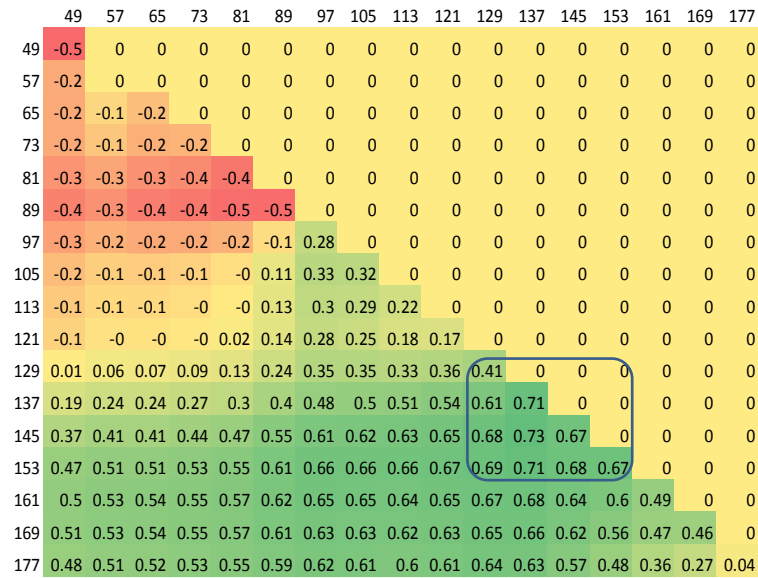


Figure 4-9: The Correlation Matrix between Cropland DSI and Winter Wheat Yield within the Main Growing Season in Shandong Province
 Notes: X-axis indicates the start date (DOY), Y-axis indicates the end date (DOY), and each cell value indicates the correlation between DSI (starting at X-axis and ending at the Y-axis) with yield using multi-year data (2000-2011).

Figure 4-9 clearly shows the trajectory of varying drought impacts on the yearly yield during different stages of the main growing season. Also, seen from Figure 4-9, with the same starting time, droughts of longer durations tend to have higher correlation with the yield, which means longer droughts have more impacts on crop yield; for droughts with similar duration, the impact is closely related to the timing. Based on the drought impact trajectory, the key period for effective agricultural drought alert was selected based on the following criteria: (1) the correlation between DSI and yield is significant; (2) the starting date provides a significant improvement in the correlation as compared to the previous date; (3) the significant correlation is continuous, ensuring

a stable period. From Figure 4-9, for Shandong, the correlation turns positive in early April (jointing stage), increases from April (jointing/booting stages) to May and reaches stably high values in May (heading/grain-filling stages), which indicates the drought starts to have emerging and growing agricultural impacts in April, with significant impacts in May and the most significant impact in mid-May. Similar analysis was also conducted for 4 other provinces, and the results are summarized in Table 4-1.

Table 4-1: Summaries of Agricultural Drought Impacts on Winter Wheat Yield in 5 Provinces

Province	Effective Agricultural Drought Monitoring				
	Start (DOY)	Key Period (DOY)	Mean Capability	Max Timing (DOY)	Max Capability
Hebei	137	137-161	0.57	161	0.73
Shanxi	121	121-161	0.71	137/161	0.77/0.78
Shaanxi	121	121-161	0.71	145/161	0.78/0.79
Shandong	129	129-153	0.66	137	0.71
Henan ¹	97	97-113	0.43	97	0.44
Henan ²	121	121-161	0.44	161	0.63

¹: “Mean Capability” indicates the mean DSI-yield correlation during the key alert period.

²: “Max Timing” indicates the time where the highest correlation is achieved (DOY).

³: “Max Capability” is the maximum correlation.

Consistent with Shandong Province, longer droughts have greater agricultural impacts and the impacts of droughts of similar duration are closely related to their timing for the 4 other provinces. As indicated in Table 1, similar patterns are found in Shanxi, Shaanxi and Shandong with a key agricultural drought alert period in May and the most significant drought impact in mid-May. Hebei and Henan show different patterns. In Hebei, there is an obvious lag regarding the start of key drought alert period, possibly caused by the delay of crop phenology as compared to other provinces; for Henan, two drought alert periods with similar agricultural drought impacts, in April and May respectively, can be identified. The results also reveal that drought tends to have weaker agricultural impacts in Henan, Hebei, Shandong as compared to Shanxi and Shaanxi, which is possibly due to the fact that Henan, Hebei and Shandong have

more sophisticated irrigation facilities and greater amounts of irrigation, and thus are less vulnerable to agricultural drought. Also, due to the lack of high-quality winter wheat mask, the MODIS cropland mask was used to depict the winter wheat regions in this study as mentioned before. However, as a result of the heterogeneity in terms of cropping systems, the winter wheat areas account for different proportions of the croplands across the 5 provinces, which leads to the different accuracies of using MODIS cropland for characterizing winter wheat in each province and thus might also contribute to the different results across the 5 provinces.

- Monitoring 2007 Shaanxi drought during winter wheat main growing season

According to meteorological records, Shaanxi Province suffered from severe drought in 2007, which caused significant agricultural losses with: drought affected areas (>10% crop loss) of 90.8 hm², drought impacted areas (>30% crop loss) of 54.8 hm² and crop failure areas (>70% crop loss) of 8.4 hm² (Data Source: <http://www.zzys.moa.gov.cn/>). Figures 4-10 and 4-11 show the winter wheat yield loss ratio (YLR) at sub-province level and the evolution of 8-day DSI for Shaanxi Province in 2007 respectively.

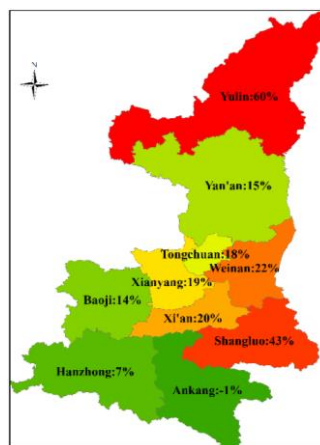


Figure 4-10: Winter Wheat Yield Loss at Sub-province Level in Shaanxi Province

It can be seen from Figure 4-10 that almost all the sub-province regions in Shaanxi Province show significant winter wheat loss except in Ankang. The most severe winter wheat loss areas are mainly concentrated in the Guangzhong Plain of Central Shaanxi, which covers Shangluo, Weinan, Xi'an, Xianyang and Tongchuan Regions, with a yield loss of about 20% or more.

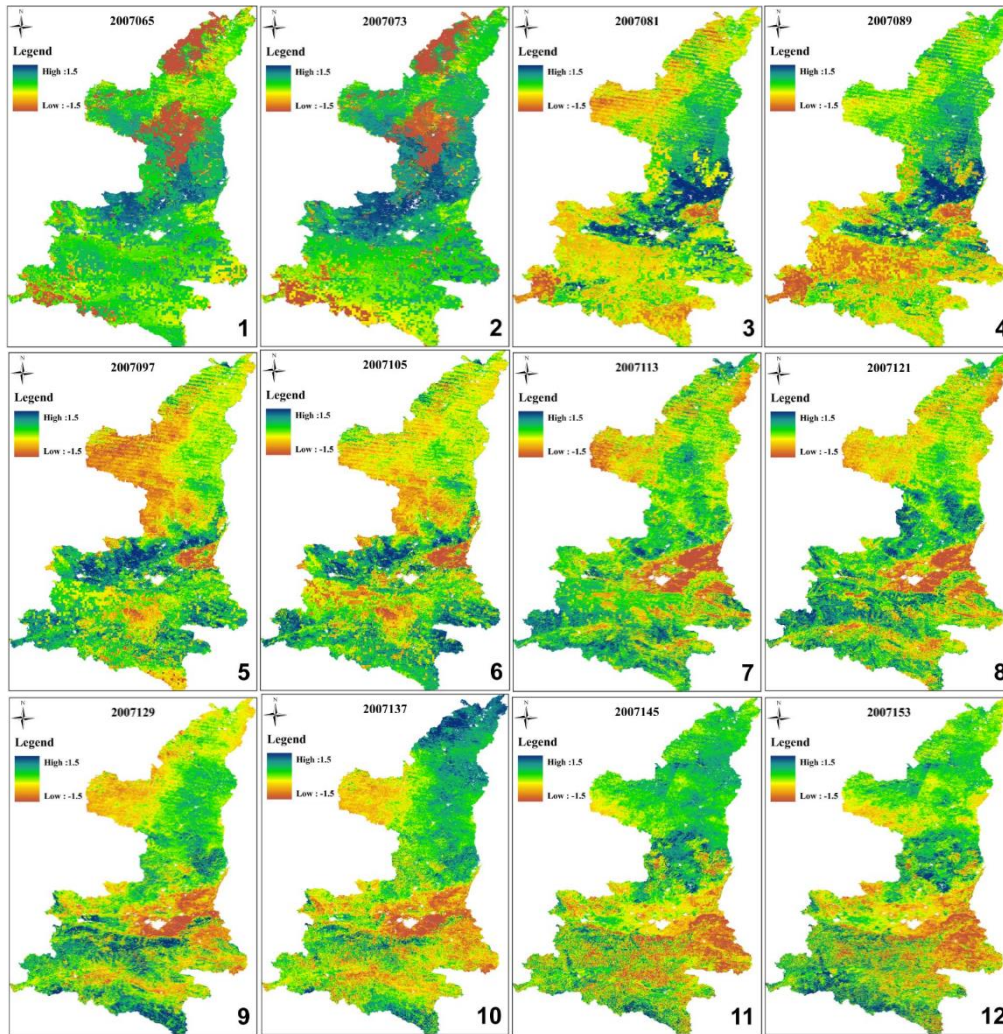


Figure 4-11: Spatial Patterns of 8-day DSI in Shaanxi Province during March-May, 2007

As depicted from the spatial DSI in Figure 4-11, consistent with the historical records, most of Shaanxi Province suffered from moderate to severe drought in March-May of 2007. In early March (DOY65-DOY73), drought showed up in part of Yulin

and Yan'an Regions of North Shaanxi (Figures 4-11.1 & 4-11.2). During winter wheat's green-up stage in mid-March (DOY81-DOY89), the drought impacted areas were mostly concentrated in South Shaanxi (Figures 4-11.3 & 4-11.4) and then moved to North Shaanxi during the jointing stage in early to mid-April (DOY97-DOY105, Figures 4-11.5 & 4-11.6). In Guanzhong Plain where the winter wheat is mostly planted, drought conditions began to emerge from mid-March in Weinan Region (DOY81-DOY89, Figures 4-11.3 & 4-11.4) and continued to expand and exacerbate until mid-May (Figures 4-11.5~4-11.9). By mid-May (DOY137-DOY145, Figures 4-11.10 & 4-11.11) during winter wheat heading and grain-filling stages, the drought conditions in Guanzhong Plain reached its maximum and at this stage the most drought impacted areas covered Shangluo, Weinan, Xi'an and Xianyang Regions, which are also the areas experiencing the largest crop loss, as indicated in Figure 4-10. This shows that winter wheat yield is more impacted by the drought conditions during its heading and grain-filling stages in May, which is also consistent with our results at the province level

4.6 Conclusions and Discussions

The DSI integrates information from vegetation condition and evapotranspiration, and shows considerable potential for drought monitoring at the global scale (Mu et al., 2013a). In this study, its regional utility for agricultural drought monitoring in the main winter wheat producing regions of North China was evaluated by exploring the capability of the DSI for describing regional moisture status, characterizing regional agricultural drought severity, as well as investigating drought impacts on crop yield

during the growing season. The main conclusions from the study are summarized below:

(1) Despite different performances in 5 provinces, the DSI is generally effective for quantifying moisture conditions at the province level. Generally, good relationships between DSI and precipitation are found at the yearly scale with varying ability for each month during the winter wheat main growing season (March-June). The best relationships are mostly found in April during the jointing and booting stages.

(2) The DSI shows a good capability for characterizing agricultural drought severity at the province level. Better relationships between DSI and agricultural drought severity are obtained for Shanxi and Shaanxi, which are less irrigated as compared to the other 3 provinces, indicating DSI is more suitable for drought monitoring in rainfed agricultural regions.

(3) Drought has varying impacts on crop yield during different stages of the growing season. Generally, drought shows increasing impacts on winter wheat during the growing season from March to June. Little impact is found in March (green-up stage), and drought starts to have agricultural impacts in April (jointing and booting stages) and reaches significant drought impacts in May (heading and grain-filling stages). Despite the varying drought impacts across 5 provinces and fluctuating drought impacts in certain provinces, the DSI shows relatively stable and high correlation with yield in May. Due to the phenology of winter wheat, drought information during the heading and grain-filling stages in May is essential for water management, and the DSI in this key alert period could therefore be used for effective agricultural drought monitoring in North China.

However, as a newly proposed indicator from the recently developed product, some issues still exist with the DSI and further work is needed. Firstly, as a remotely sensed data product, the MOD16 has its inherent uncertainties of 10-30% in ET measurements (Mu et al., 2011) varying across different land covers, elevations and climate zones (Velpuri et al., 2013), with an overall ET underestimation (Mu et al., 2011), especially for croplands (Liu et al., 2013; Velpuri et al., 2013; Hu et al., 2015). Also, for the dual-cropping system, the MOD16 ET product has its limitations, which shows only one peak and cannot reflect the variations in the typical dual-cropping systems (Liu et al., 2013). The MOD16 ET product was first generated at the global scale and integrates coarse resolution data into its calculation, such as the MERRA GMAO meteorological reanalysis data with an original resolution of about $0.5^{\circ} \times 0.6^{\circ}$. While this is feasible at the global scale, the product may be smoothed and have limited accuracy for regional use, thus influencing the accuracy of the derived drought indicator. Also, the coarse-resolution MERRA GMAO data cannot precisely reflect variations in local water management, such as irrigation. With many agricultural regions in the study area heavily irrigated, an improved ET product with finer-resolution regional meteorological data as input should benefit regional applications of the DSI. Secondly, in the DSI model, both vegetation condition and ET/PET are used. While the combined information from two sources may help improve drought monitoring, it should be noted that drought conditions as portrayed by these two sources are not synchronous. While an ET/PET based indicator tends to be quite responsive, there is usually a time lag between drought occurrences and the response of vegetation condition as shown by the NDVI (Ji & Peters, 2003). Thus, a study on

the time lag between ET/PET information and vegetation growth condition and how to effectively integrate this lagged relationship into the development of drought indicator, would be useful to help improve the DSI for drought monitoring. Thirdly, the drought impact analysis on winter wheat in this study was based on the DSI integration from MODIS labeled croplands, which are not exactly consistent with the winter wheat areas. The heterogeneity of these 5 provinces in terms of cropping system results in different accuracies of using MODIS cropland for characterizing winter wheat in each province, and the interfering co-existing crops other than winter wheat have undoubtedly impacted the DSI integration at the province level and the consequent drought impact analysis. With a more precise wheat mask becoming available in the future, the improved large-scale drought impact analysis could be expected. Besides, the regional DSI validation in this study focused mainly on the integrative evaluation at the province scale. For future work, more extensive validation at the sub-province, county as well as station scale is recommended to help test the performance of the DSI at different scales. Also, due to the diversity of crop phenology, planting patterns and agricultural management practices, the DSI shows different capacities across provinces. Further work is needed to help isolate possible impacting factors and therefore get an improved understanding of the DSI. Finally, due to its complexity, drought validation remains an issue. Determination of agricultural drought places more emphasis on its agricultural impacts. Given that crop growth is a continuous process and drought has varying agricultural impacts at different stages, it would be extremely important to develop a framework for effectively assessing the proposed indicator for use in agricultural drought monitoring.

Chapter 5: Exploring the Dynamics of Vegetation Growth and Surface Temperature Interactions for Improved Agricultural Drought Monitoring from Remote Sensing

5.1 Introduction

Drought can lead to a decline in vegetation greenness or an increase in vegetation surface temperature, which can both be observed from satellite. Since the 1980's, satellite-based indicators have been extensively used both in research and in operational systems for drought monitoring.

Of all those indices, the most commonly used one is the NDVI calculated from the NIR and red bands, which serves as a good indicator of vegetation growth conditions (Tucker, 1979). NDVI based metrics are commonly used for characterizing vegetation stress and drought, such as AVI (Chen et al, 1994, VCI (Kogan, 1990; Liu & Kogan, 1996), SVI (Peters et al., 2002). In a different approach from using NDVI, LST provides important information on vegetation water stress (Gutman, 1990) and thus moisture status. Many indicators have been developed for drought monitoring based on LST, such as NDTI (McVicar & Jupp, 1998) and TCI (Kogan et al., 1995a). To leverage the utilities of these two different data sources, several indicators have been developed based on the combination of NDVI and LST for improved drought monitoring, such as the VHI (Kogan, 1995a), TVI (McVicar & Jupp, 1998), VSWI (McVicar & Jupp, 1998), and TVDI (Sandholt, 2002), which have shown to be useful in many studies on drought monitoring.

Despite many existing studies to combine vegetation growth conditions and

surface temperature for drought monitoring, these works tend to assume that a strong negative relationship exists between LST and NDVI. However, the dynamics between NDVI and LST is not so straightforward, but vary across different seasons, regions and land cover/use types (Mukherjee et al., 2015; Karnieli et al., 2010; Raynolds et al., 2008; Karnieli et al., 2006; Weng et al., 2004). According to a study in North America, for vegetation growth, the LST-NDVI correlation is negative for low latitude and during the mid-growing season when water is the limiting factor; however, during the beginning and end of the growing season, a positive correlation is observed between LST and NDVI (Karnieli et al., 2010). Similar results were also found by Sun & Kafatos (2007), indicating the seasonality of the NDVI-LST relationships. For winter, the correlation between NDVI and LST is positive, while strong negative correlations are only found during the warm seasons. Thus, caution should be used while combining LST and NDVI for drought monitoring, and it should be restricted to the water-constrained conditions for vegetation growth (i.e., regions and time periods with a negative NDVI-LST relationship).

Besides the negative NDVI-LST relationship, the lagged NDVI-LST relationship is also commonly neglected in the development of drought indices. Currently synthetic drought indices, like VHI, VSWI and TVDI, are only simple mathematic combinations, assuming the simultaneous representation of drought conditions from different inputs. However, the sensitivity analysis of NDVI and LST derived indicators to soil moisture in Chapter 3 indicates the non-synchronous characterization of those indicators for agriculture drought. Based on Chapter 3, LST is a more responsive indicator for drought and shows immediate response when drought event occurs. However, NDVI

typically shows a lagged response, despite being a more useful indicator for characterizing drought impact on crop productivity during the growing season. Thus, the direct combination of these two data sources may confuse the drought signals from different time periods and impact the accuracy of drought monitoring. According to a study on time-lag effects of vegetation response to climate change at the global scale, the time-lag effects vary across the globe and as compared to the model without considering time-lag, climatic factors explained global vegetation growth better by integrating the time-lag effects (Wu et al., 2015). Thus, to more effectively and accurately integrate these two data sources, a simple mathematic combination is not sufficient. An exploration of the NDVI-LST dynamics and the integration of these dynamics provides considerable potential for prototyping an improved indicator.

Despite these prior efforts to investigate the relationships between NDVI and LST, these analyses were typically carried out on the monthly or bi-monthly basis, which is too coarse regarding the relatively shorter and faster changing crop phenology. Thus, a regional specific analysis in Kansas winter wheat areas at a much finer temporal resolution (8-day interval) is warranted. The goal of this work is to explore the NDVI-LST dynamics at 8-day interval during the main winter wheat growing season to get a better idea of NDVI-LST interactions, thus helping prototype an improved agricultural drought indicator.

5.2 Study Area

The pilot study area is chosen in Kansas, focusing on winter wheat during the main growing season from March to May. Kansas, often referred to as the Wheat State, is the biggest winter wheat producing state in the U.S., which produces about 20 percent

of the total domestic production and plays an important role in both global and domestic wheat markets. As indicated from USDA NASS CDL, Kansas has large areas of consecutive wheat fields, and the winter wheat is mainly concentrated in the western and central region of the state. Since the analysis will be carried out at 1km MODIS resolution, the winter wheat percentage for each 1km pixel was aggregated from the CDL to match the MODIS resolution, and the areas located within the MODIS h10v05 tile was used for the study in this chapter (Figure 5-1). As seen from the Figure 5-1, the most densely winter wheat planted areas are mainly concentrated in the middle of the state.

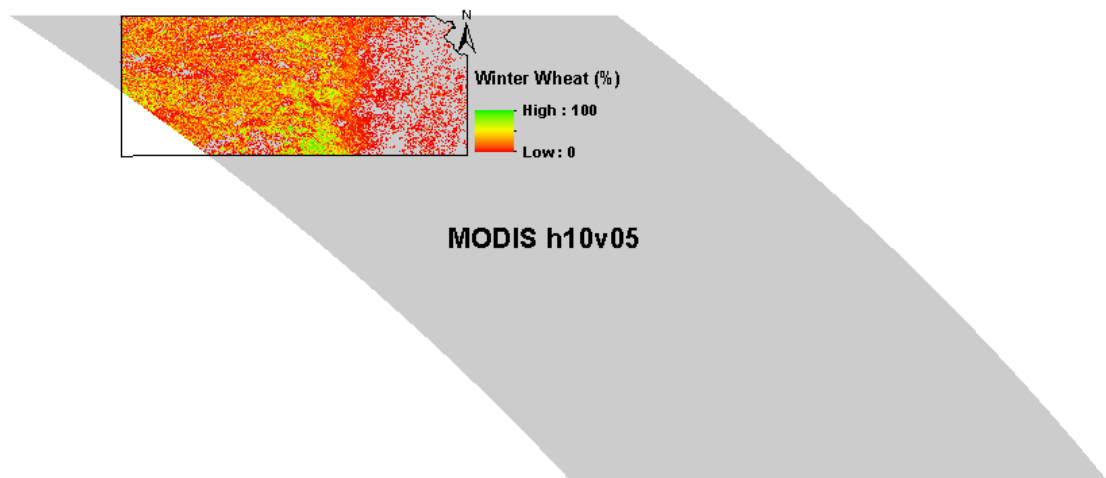


Figure 5-1: Chapter 5 Study Area Showing Winter Wheat Distribution at 1km Resolution

5.3 Data

The datasets used in this study were mainly remote sensing data, of which the 8-day MODIS products were used to better reflect the phenology of winter wheat. The details of the datasets are listed below:

5.3.1 MODIS Surface Reflectance

The 8-day MODIS surface reflectance product (MOD09A1) at 500m resolution which covers most of Kansas (tile number: h05v09) from 2000-2016 was used in this study and downloaded from NASA Land Processes Distributed Active Archive Center (LP DAAC, <https://lpdaac.usgs.gov/>). The reflectance product was converted into NDVI using Equation 3-11.

5.3.2 MODIS Surface Temperature

The 8-day MODIS land surface temperature/emissivity product (MOD11A2) at 1km resolution which covers most of Kansas (tile number: h05v09) from 2000-2016 was used in this study and also downloaded from LP DAAC.

5.3.3 Crop Mask

The 2011 CDL downloaded from the USDA NASS CropScape database (<http://nassgeodata.gmu.edu/CropScape/>) was used in this chapter. The winter wheat pixels were extracted from this multi-crop layer and then aggregated to 1km MODIS resolution to show its percentage.

5.4 Methodology

5.4.1 Spatial Aggregation

As mentioned in Section 5.3.1, the 500m MOD09A1 dataset was first converted into NDVI. Then, to match the resolution of MODIS surface temperature product (MOD11A2), the NDVI was aggregated into 1km resolution using the valid pixels within the 2*2 window.

5.4.2 Remotely Sensed Indicators

Based on the results from Chapter 3, ET based indicators show similar performances for drought monitoring with those derived from LST. Also, the performance of those indicators derived from the same data source are quite similar. For simplicity, in this study, we selected one NDVI derived indicator (Vegetation Condition Index, VCI) and one LST derived indicator (Temperature Condition Index, TCI) as an example to demonstrate the dynamics of NDVI and LST based drought indicators during the main winter wheat growing season (March-May). The LST and NDVI derived drought indicators (TCI & VCI) were calculated per pixel during the main winter wheat growing season (March-May) of 2000-2016 using Equations 3-3 & 3-6.

5.4.3 Lagged Statistical Analysis for Analyzing VCI-TCI Response

Similar to Chapter 3, the dynamics of VCI-TCI response were explored by analyzing the per-pixel statistical lagged relationships (up to 2 months) at different growing stages. The lagged relationship between VCI and TCI at different time lags was calculated for each pixel at each 8-day period of the main growing season using multi-year data. Then, the lag time for each pixel during the growing season was determined by searching for the optimal statistical relationship, and the spatial distribution of the time-lag effects was produced.

5.5 Results

Based on time-series NDVI and LST data at 1km resolution, the drought indicators (VCI and TCI) were calculated per pixel during winter wheat's main growing season

(March-May, also the drought sensitive season) from 2000 to 2016. Then, at each 8-day period of the main growing season, the (lagged) statistical relationship between VCI and TCI was explored per pixel with a time lag from 0 up to 64 days at the increase of 8 days, and the response time was determined. The spatial distribution of the response time, the corresponding correlation and the statistics of the results were displayed for each 8-day of the main growing season and divided into 4 stages: at the beginning of main growing season, before the vegetative peak, around the vegetative peak, and after the vegetative peak.

5.5.1 Dynamics of VCI-TCI Relationships at the Beginning of Main Growing Season

Figure 5-2 shows the VCI-TCI time lags and corresponding correlations at the beginning of main growing season (DOY65-DOY81), and the statistics of pixels at each time lag are also summarized in Table 5-1. As seen from Table 5-1 and Figure 5-2, at the beginning of main growing season, the majority of the region shows a negative VCI-TCI relationship without obvious time lag. This indicates a fast vegetation response to drought at this stage. Also, since winter wheat has just recovered from the long dormancy due to the long cold winter, temperature rather than water is the dominant factor for crop growth. As a result, an increase in temperature, which might lead to an early spring drought, is favorable for the crop growth. Consistent results were found across the wheat regions despite different growing densities.

Due to the availability of good data record, some differences in terms of the spatial pattern can be found. For DOY65, most valid pixels are concentrated in the Upper Left Corner of Kansas, with no time lag and a negative correlation. For DOY81, similar results were found as for DOY65. However, for DOY73, despite the consistent negative

correlation, the results are a little bit different, showing an increased time lag of 32 days. This might be related to the distribution of the valid winter wheat pixels. It can be seen that, for DOY73, most of those valid pixels are located in the southern part of the state. Due to a relatively earlier phenology as compared to the rest of the state, the crops in this area may have a better recovery from dormancy and thus be more resilient to the stress, leading to a lagged response.

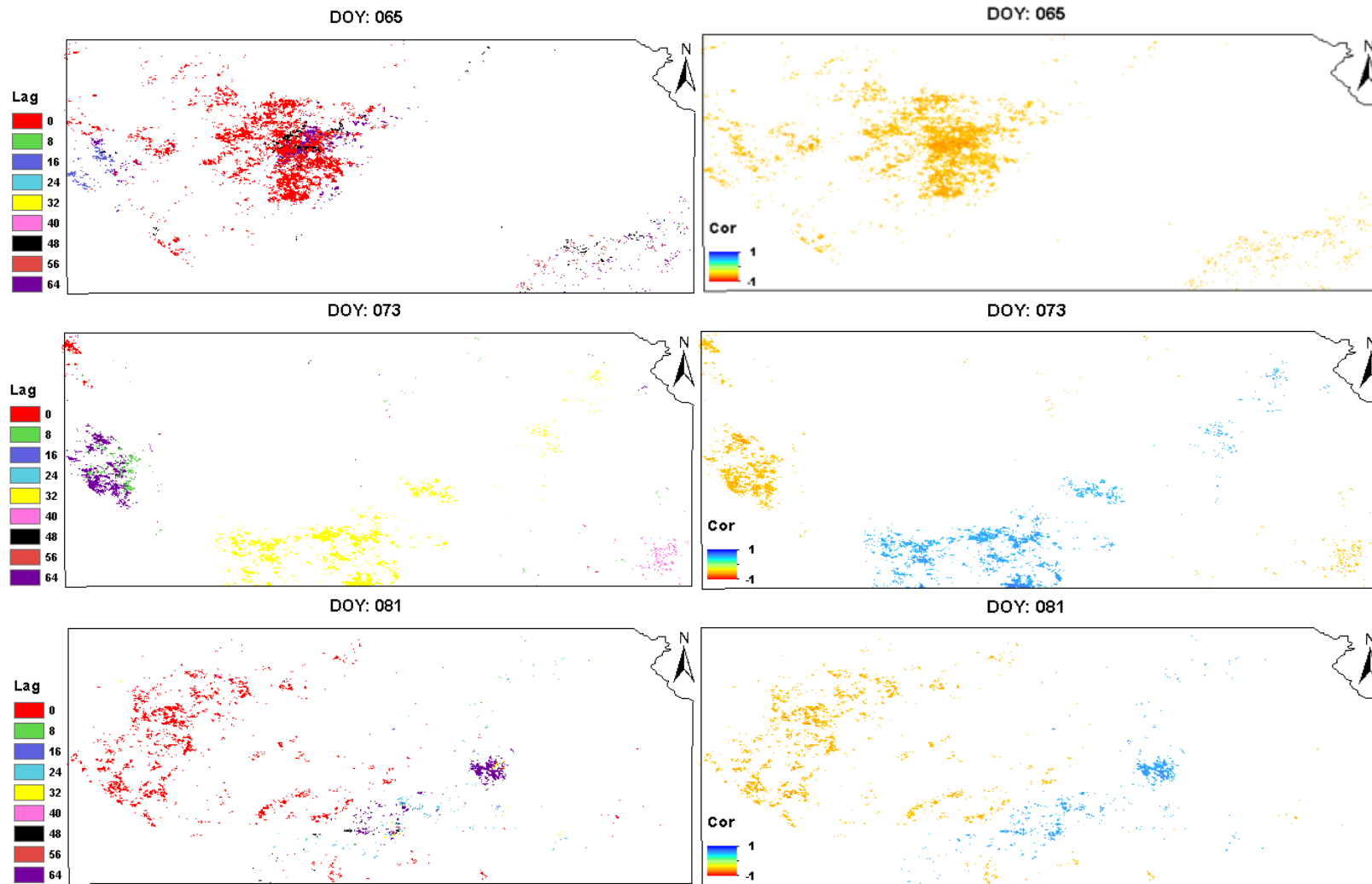


Figure 5-2: Spatial Distribution of VCI-TCI Response Time (Left) and Corresponding Correlation (Right) for DOY65-DOY81

Table 5-1: Count of Valid Winter Wheat Pixels at Different Response Times for Each Category (DOY65-DOY81)

	all	0-20%	20-40%	40-60%	60-80%	80-100%	
DOY65	0	7097	3838	1962	983	278	36
	8	32	27	3	2	0	0
	16	307	115	74	76	28	14
	24	12	11	1	0	0	0
	32	4	4	0	0	0	0
	40	0	0	0	0	0	0
	48	632	491	99	32	10	0
	56	665	454	146	52	12	1
	64	1282	721	319	184	51	7
DOY73	0	241	121	55	36	26	3
	8	589	249	148	119	53	20
	16	5	5	0	0	0	0
	24	4	0	2	1	0	1
	32	3806	1769	777	619	411	230
	40	282	277	3	2	0	0
	48	7	5	2	0	0	0
	56	14	7	3	2	2	0
	64	1420	541	346	321	158	54
DOY81	0	3949	2261	897	533	203	55
	8	39	23	12	3	1	0
	16	37	22	8	7	0	0
	24	410	240	85	51	22	12
	32	87	52	15	9	2	9
	40	20	12	2	6	0	0
	48	111	66	26	12	7	0
	56	31	20	7	4	0	0
	64	812	520	184	76	21	11

Notes: The x-axis indicates the winter wheat pixels at different percentage (all pixels, 0-20%, 20-40%, 40-60%, 60-80%, and 80-100%), and the y-axis indicates the response time from 0 to 64 days, and the each value inside the table indicates the number of valid winter wheat pixels at each response time lag for each category.

5.5.2 Dynamics of VCI-TCI Relationships before the Vegetative Peak

Figure 5-3 shows the VCI-TCI time lags and corresponding correlations before reaching the vegetative peak (DOY89-DOY105), and Table 5-2 also summarizes the statistics of pixels at each time lag. Similar to Section 5.5.1, a negative TCI-VCI relationship was observed across the majority of the region, with consistent results

across wheat regions of different growing percentages. At this stage, temperature is still the leading factor for crop growth, and an increase in the temperature (lower TCI) is favorable for the crop growth (higher VCI), demonstrating a negative VCI-TCI relationship. Compared to Section 5.5.1, as the crop growth progresses, an increased VCI-TCI response time was found. As indicated earlier, this is due to the fact that crops become more resilient to stress as they gradually recover from dormancy, resulting in a lagged vegetation response to drought.

From the time series at this stage, some differences were observed in terms of both spatial pattern and time lag. For DOY89, most valid pixels are concentrated in the Upper Left Corner of Kansas, with a time lag of 40 days. For DOY97, there is a relatively complete coverage of valid pixels across the state, with an even longer time lag of 64 days for the majority. For DOY105, most valid pixels were also concentrated in the Upper Left corner of Kansas, with a time lag of 64 days for the majority. We can also see that for DOY105, there is a small area near the southern border of the state showing a time lag of 16 days and a significant positive correlation. Possibly due to its earlier phenology in the south, this area has entered the stage where water is the limiting factor, and thus the drought induced by an increase in the temperature leads to the decline in crop growth, yielding a positive VCI-TCI relationship.

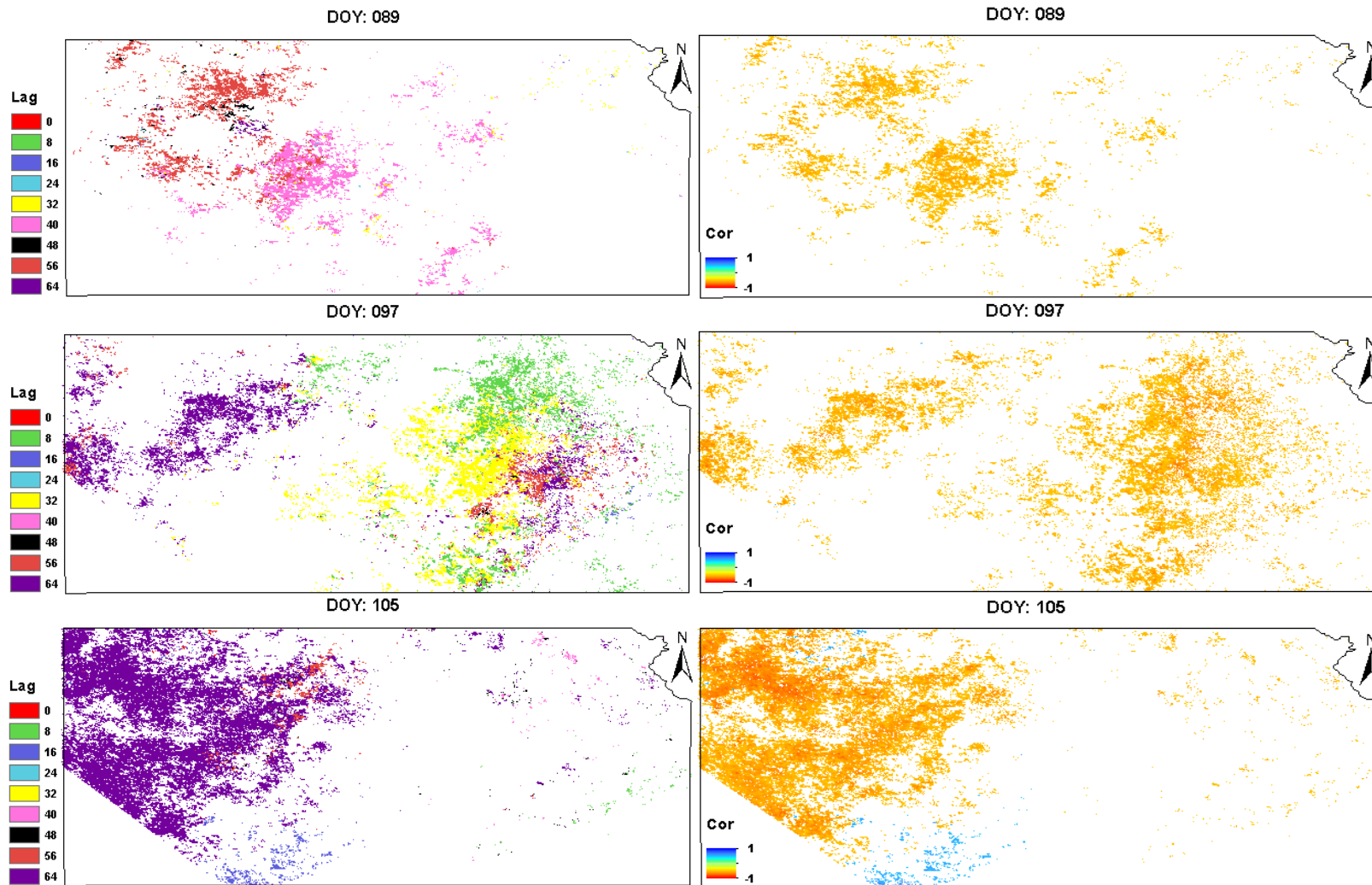


Figure 5-3: Spatial Distribution of VCI-TCI Response Time (Left) and Corresponding Correlation (Right) for DOY89-DOY105

Table 5-2: Count of Valid Winter Wheat Pixels at Different Response Times for Each Category (DOY89-DOY105)

	all	0-20%	20-40%	40-60%	60-80%	80-100%	
DOY89	0	16	8	4	2	2	0
	8	1	1	0	0	0	0
	16	50	41	4	1	4	0
	24	100	56	27	11	5	1
	32	450	326	76	30	14	4
	40	7275	3044	2256	1368	484	123
	48	562	323	141	64	31	3
	56	6780	3928	1688	824	294	46
	64	278	159	81	31	4	3
DOY97	0	34	14	5	9	4	2
	8	9323	7519	1156	420	180	48
	16	170	155	10	3	2	0
	24	3	3	0	0	0	0
	32	10899	7131	2013	1135	472	148
	40	11	4	4	1	2	0
	48	82	71	7	2	2	0
	56	3562	3117	247	140	49	9
	64	11722	7641	2302	1261	410	108
DOY105	0	90	58	21	11	0	0
	8	221	213	7	0	1	0
	16	1332	945	198	109	58	22
	24	3	0	2	1	0	0
	32	5	2		2	1	0
	40	359	338	18	2	1	0
	48	345	291	34	17	3	0
	56	1196	609	340	172	66	9
	64	39672	22941	9288	5066	1940	437

Notes: The x-axis indicates the winter wheat pixels at different percentage (all pixels, 0-20%, 20-40%, 40-60%, 60-80%, and 80-100%), and the y-axis indicates the response time from 0 to 64 days, and the each value inside the table indicates the number of valid winter wheat pixels at each response time lag for each category.

5.5.3 Dynamics of VCI-TCI Relationships around the Vegetative Peak

Figure 5-4 shows the VCI-TCI time lags and corresponding correlations around the vegetative peak (DOY113-DOY121), and Table 5-3 summarizes the statistics of pixels at each time lag. As seen from the Figure 5-4 and Table 5-3, the majority of the region shows no VCI-TCI time lag with a positive relationship. Again, this indicates a fast vegetation response to drought at this stage, as reflected by both temperature and

vegetation growth conditions. Also, at this stage, water has become the dominant factor for influencing crop growth, a lack of water will have an immediate impact on crop growth, and drought resulting from a temperature increase can cause immediate damage to the crops. Similarly, it can also be seen that consistent results were found across wheat regions with different growing density.

Due to the availability of the valid data record, the spatial patterns of response time and corresponding correlation are different. For DOY113, it has a sparsely dispersed distribution across the state. For DOY121, most valid winter wheat pixels are concentrated in the Upper Left Corner of the state, while for DOY129, a more complete coverage across the state (except the very southern border of the state) is found.

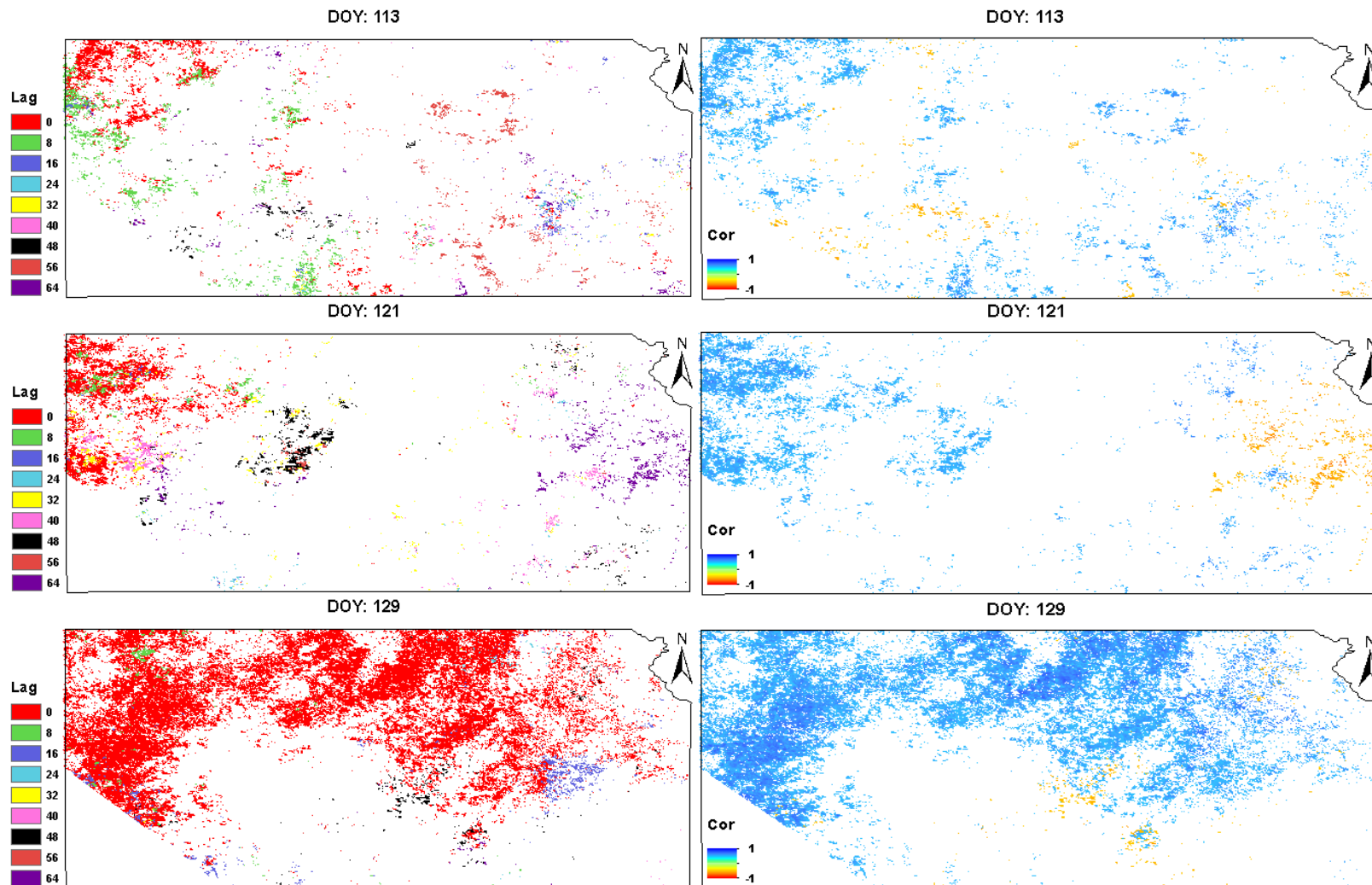


Figure 5-4: Spatial Distribution of VCI-TCI Response Time (Left) and Corresponding Correlation (Right) for DOY113-DOY129

Table 5-3: Count of Valid Winter Wheat Pixels at Different Response Times for Each Category (DOY113-DOY129)

	all	0-20%	20-40%	40-60%	60-80%	80-100%	
DOY113	0	5311	3281	1144	620	221	45
	8	3910	2430	830	433	171	46
	16	753	674	50	18	8	3
	24	156	127	10	13	5	1
	32	144	127	8	5	4	0
	40	230	162	36	23	8	1
	48	459	291	91	51	25	1
	56	1907	1490	283	89	39	6
	64	798	600	109	58	29	2
DOY121	0	7425	4153	1711	1047	415	99
	8	858	590	169	74	22	3
	16	181	107	41	16	12	5
	24	226	184	26	14	2	0
	32	1238	778	254	133	60	13
	40	1460	1055	210	149	38	8
	48	1724	1068	389	191	66	10
	56	354	230	86	32	5	1
	64	1976	1777	108	65	22	4
DOY129	0	57787	37376	12046	5852	2039	474
	8	738	427	154	85	48	24
	16	2072	1735	153	101	64	19
	24	239	188	39	10	2	0
	32	28	24	3	1	0	0
	40	48	46	2	0	0	0
	48	868	557	161	84	50	16
	56	23	15	4	3	1	0
	64	110	89	12	7	2	0

Notes: The x-axis indicates the winter wheat pixels at different percentage (all pixels, 0-20%, 20-40%, 40-60%, 60-80%, and 80-100%), and the y-axis indicates the response time from 0 to 64 days, and the each value inside the table indicates the number of valid winter wheat pixels at each response time lag for each category.

5.5.4 Dynamics of VCI-TCI Relationships after the Vegetative Peak

Figure 5-5 shows the VCI-TCI time lags and corresponding correlations after the vegetative peak (DOY129-DOY153), and the statistics of pixels at each time lag are also summarized in Table 5-4. After the crop vegetative peak, most regions generally have increased time lags with a dominant positive VCI-TCI relationship for the majority. At this stage, crop is not very water sensitive, and the occurrence of drought

due to a lack of water shows an immediate effect on temperature (TCI), but not on vegetation conditions (VCI), thus leading to a lagged response of VCI to TCI. However, as compared to temperature, water is still the dominant factor for crop growth at this stage, yielding a dominantly positive VCI-TCI relationship. Also, consistent results across the wheat regions with different growing percentage.

However, there still exist some differences in spatial pattern and response time. For DOY137, the valid winter wheat pixels are widely dispersed across the state, with a time lag of 24 days. For DOY145, the valid pixels are mostly distributed in the Upper Left Corner and middle of the state, also with a time lag of 24 days. For DOY153, the valid pixels are mostly concentrated in the Upper Left Corner and the south of Kansas, with a lag of 8 days for the majority. It was also noticed that, there is a small region on the Upper Left Corner showing negative VCI-TCI relationship for DOY145 and DOY153, implying a temperature increase is favorable for the crop growth. This might be related to the frosts occurring in this region after the vegetative peak (such as that in 2007), which lead to a decreased temperature and crop damage.

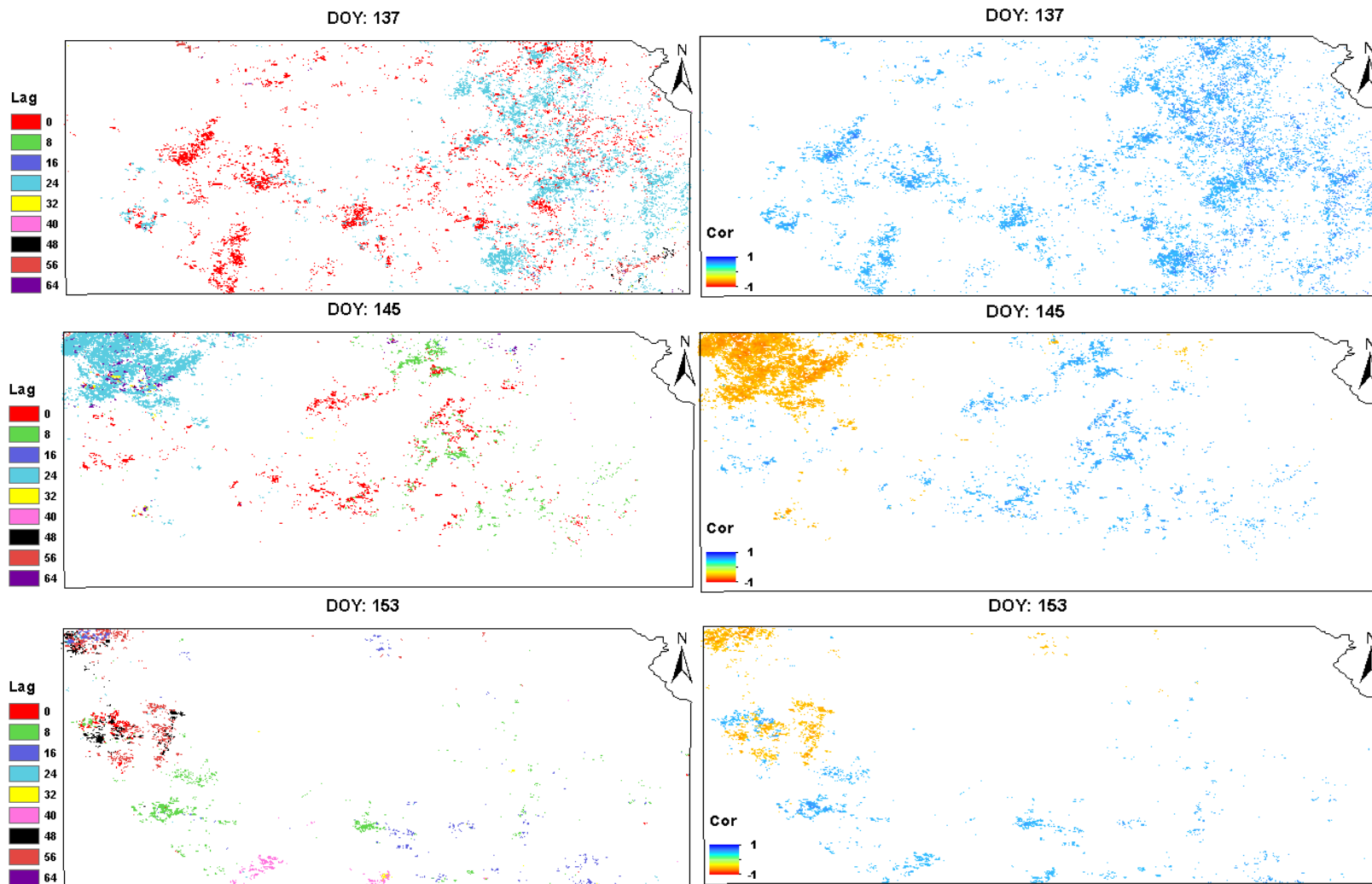


Figure 5-5: Spatial Distribution of VCI-TCI Response Time (Left) and Corresponding Correlation (Right) for DOY137-DOY153

Table 5-4: Count of Valid Winter Wheat Pixels at Different Response Times for Each Category (DOY137-DOY153)

	all	0-20%	20-40%	40-60%	60-80%	80-100%	
DOY137	0	8596	6201	1363	715	256	61
	8	1	1	0	0	0	0
	16	67	62	4	1	0	0
	24	9883	8899	686	228	55	15
	32	34	34	0	0	0	0
	40	37	36	1	0	0	0
	48	143	140	2	1	0	0
	56	367	327	28	9	3	0
64	40	37	3	0	0	0	
DOY145	0	2601	1643	565	265	105	23
	8	1823	1243	361	157	50	12
	16	41	27	12	2	0	0
	24	7864	4223	1933	1130	470	108
	32	166	100	39	21	6	0
	40	3	3	0	0	0	0
	48	10	0	5	3	2	0
	56	158	103	42	10	3	0
64	583	373	121	57	27	5	
DOY153	0	404	319	54	19	9	3
	8	1561	1118	259	130	49	5
	16	807	585	126	60	29	7
	24	101	62	20	13	5	1
	32	65	52	7	1	2	3
	40	476	293	72	60	33	18
	48	837	507	178	98	42	12
	56	1468	854	339	185	79	11
64	0	0	0	0	0	0	

Notes: The x-axis indicates the winter wheat pixels at different percentage (all pixels, 0-20%, 20-40%, 40-60%, 60-80%, and 80-100%), and the y-axis indicates the response time from 0 to 64 days, and the each value inside the table indicates the number of valid winter wheat pixels at each response time lag for each category.

5.6 Conclusions and Discussions

NDVI and LST provide great potential for drought monitoring. In this chapter, to more effectively integrate these information for improved drought monitoring, the dynamics of NDVI and LST derived indicators were explored both spatially across Kansas and temporally during the main winter wheat growing season. The relationships

between LST and NDVI derived drought indicators are a changing function in both spatial and temporal domains. Despite different growing densities across the wheat regions, consistent results are found.

(1) At the beginning of the main growing season, temperature is the dominant factor for crop growth and an increase in the temperature is favorable for crop growth, resulting in a fast VCI-TCI response and a negative relationship in most wheat regions.

(2) Before reaching the vegetative peak, although temperature is still the dominant factor for crop growth, crops become more resilient to stress as the growing season gradually progresses, leading to a mostly negative VCI-TCI relationship and an increased VCI-TCI response time generally ranging from 6 to 8 weeks.

(3) Around the vegetative peak, water becomes the dominant factor for crop growth. Crops are very sensitive to drought and the drought induced by a temperature increase causes damage to crop growth, yielding a fast TCI-VCI response and a positive relationship.

(4) After the vegetative peak, although water is still the dominant factor in most regions as compared to temperature, crops are no longer highly water-demanding, generating an increased response time ranging from 1 to 3 weeks with a dominant positive relationship.

The dynamics of VCI-TCI response have considerable implications for agricultural applications. As shown earlier in this chapter, before reaching the vegetative peak, a negative VCI-TCI relationship demonstrates that vegetation growth and temperature conditions represent different drought information, making the direct combination of NDVI and LST metrics for drought monitoring inappropriate. Thus, the integration of

VCI-TCI dynamics, including both the negative and lagged relationships, could be used to help develop an improved drought indicator. The VCI-TCI relationships with significant time lags, especially those before reaching the vegetative peak (Section 5.5.2), could also be used for prediction of vegetation conditions, which can provide useful inputs for agricultural applications such as yield forecasting.

However, some issues still exist and further work is needed. First, due to the missing LST and NDVI data from cloud contamination, there is a limited valid and cloud-free data record at certain growing stages for some regions. The data gaps in some regions make it difficult for the inter-comparison of spatial patterns during the growing season and the relatively short data record from 2000 also limit the accuracy of the results. Thus, the use of harmonized NDVI and LST products from a combination of different sensors, which can potentially provide a more consistent and complete long data record, is needed to help improve the study. With current/ongoing efforts on generating long term NDVI data record, such as the NASA LTDR project, it would be highly recommended to have a similar data product for LST, which can provide consistent, high-quality, and cloud-free LST data cover a long period (e.g. a 30-year period) at 250m (or finer) resolution at 8-day (or finer) interval. This long-term LST product itself can provide good basis for better describing the drought trajectory during the past decades, and also when combined with NDVI LTDR, it can help better unravel the interactions between vegetation growth condition and surface temperature while using a longer data record. Besides, the current response time is identified from the optimal statistical relationship, which is determined by locating the maximum absolute VCI-TCI correlation. Being a pure statistical method, this method is easily disturbed

by small changes in the input data, especially considering the short data record only available since 2000, and thus a more robust response time determination method is warranted.

Chapter 6: Conclusions

With the growing need for food and increasing demand for biofuels, the frequent occurrence of extreme weather events has resulted in unprecedented grain prices and severe market instability, threatening global food security. Although food insecurity is a complex issue, agricultural drought remains the primary cause for reduced production at the global scale and the recent “Global Food Crisis” in 2008, 2011 and 2012 has put global drought and its impact on crop production at the forefront, highlighting the need for effective agricultural drought monitoring. Earth observations, especially satellite observations, provide a practical, cost-effective, and timely means to obtain information related to crop condition and have long been recognized for their tremendous value in large scale drought monitoring. Research in this field has been active for several decades, however, due to the intrinsic complexity of drought and agriculture, there have been limited agricultural drought specific studies. To address this knowledge gap in the field of agricultural drought, this dissertation characterizes global agricultural drought risk, evaluates the different remotely sensed indicators for agricultural drought monitoring, investigates the drought impacts on agricultural production from satellite observations, and explores the dynamics of vegetation growth and temperature interaction to help prototype an improved agricultural drought monitoring system.

6.1 Summary Findings

The major findings of this dissertation are summarized as below:

Chapter 2 of this dissertation provided a unique overview of agriculture specific

drought risk consistent at the global scale by developing an agriculture-oriented global agricultural drought risk index (GADRI). The main conclusions of Chapter 2 are as follows: (1) Agricultural lands exhibit different drought regimes before and after the inclusion of agricultural growing season data, and more severe drought regimes are mostly found during the agricultural growing season. This demonstrates the importance of including consistent growing season data for accurate agricultural drought characterization. (2) At the global scale, the U.S. Corn Belt, Spain & Eastern Europe, Central Russia, India, North China and Australia have high agricultural drought risk and are shown to be hotspots of agricultural drought risk. It is worth noting that these are the main agricultural production regions including the major breadbaskets of the World, which has direct implications for international markets and food prices. (3) For the last three decades, different agricultural drought risk change patterns are found in different regions. Despite the increasing occurrence of drought events during the past three decades, there is a relatively stable and slight declining drought risk overall for the globe, while Australia exhibits a continuous increase and Brazil exhibits a continuing decrease, calling for future work to help characterize these trends with a longer data record.

Chapter 3 of this dissertation investigated the capabilities of remotely sensed indicators (vegetation condition, LST, ET and soil moisture based indicators) for agricultural drought monitoring in Southern U.S. Great Plains as well as evaluated the drought impact on agricultural production from remote sensing. The main conclusions are: (1) Standardized (SVI/STI/SEI) and normalized (NVI/NTI/NEI) indicators show similar and slightly better performances than condition indicators (VCI/TCI/ECI). (2)

LST and ET based indicators show similar capability for drought monitoring and exhibit an immediate response after drought; while for NDVI derived indicators, there is a lagged and no consistent drought response time, generally varying from 1 to 5 weeks. (3) During the main winter wheat main growing season, LST and ET derived indicators are similar and show better performances across space (more consistent response time and better ability) during the early and late main growing season, while the NDVI derived indicators show increasing performance as the main growing season progresses. (4) The ASCAT SSM product is generally effective for characterizing agricultural drought monitoring, with a better representation of drought conditions during winter wheat's growing season around March-July and October-November, and the ASCAT descending SSM is proved to be better than the ascending SSM for drought monitoring due to its overpass morning timing. (5) In terms of impacts, drought has time-varying impacts during the growing season. Despite some variability, drought shows generally increasing impacts during the winter wheat main growing season for all states. Significant impacts were observed between Mid-April and Early-June, with the most severe drought effects during the grain filling stage around Mid-May in Kansas, Mid-Late April in Oklahoma and Mid-Late May in Nebraska during their corresponding vegetative peaks. Also, more significant drought impacts are found in the states with higher planting density.

Chapter 4 of this dissertation assessed the capability of the remotely sensed Drought Severity Index (DSI) for agricultural drought monitoring and assessed drought impacts on winter wheat yield for five provinces in North China. Overall, the MODIS DSI is generally effective for characterizing moisture conditions at the province level,

with varying ability during the main winter wheat growing season and the best relationship observed for April during the jointing and booting stages. The MODIS DSI agrees well with agricultural drought severity at the province level, with better performance in rainfed-dominated than irrigation-dominated regions. Drought shows varying impacts on winter wheat yield at different stages of the main growing season, with the most significant impacts found during the heading and grain-filling stages, which could be used as the key alert period for effective agricultural drought monitoring.

Chapter 5 of the dissertation explored the dynamics of NDVI and LST derived indicators both spatially across Kansas and temporally during the main growing season of winter wheat. Consistent results were found across wheat regions of different crop densities. The relationships between LST and NDVI derived drought indicators change as a function of both spatial and temporal domains. The main conclusions are as follows: (1) At the beginning of the main growing season, temperature is the dominant factor for crop growth and an increase in the temperature is favorable for crop growth, resulting in a negative and fast VCI-TCI response in most wheat regions. (2) Before reaching the vegetative peak, although temperature is still the dominant factor for crop growth, crops become more resilient to the stress as the main growing season gradually progresses, leading to a mostly negative and lagged VCI-TCI response. (3) Around the vegetative peak, water becomes the dominant factor for crop growth. Crops are very sensitive to drought and the drought induced by a temperature increase causes immediate damage to crop growth, generally yielding a fast and positive VCI-TCI response. (4) After the vegetative peak, even though water is still the dominant factor

in most regions as compared to temperature, crops are not highly water-demanding any more, generating a dominantly positive and lagged VCI-TCI response. These results provide useful guidelines on the effective integration of different data sources for developing a synthetic index and also calls for new data integration algorithms instead of direct mathematical transformations.

6.2 Significance of the Research and Implications

Chapter 2 proposed a new agricultural specific drought risk index through integrating a consistent satellite-derived crop calendar as well as an agricultural productivity index, which provides a more accurate and consistent depiction of agricultural drought risk at the global scale. This research highlights drought prone regions and periods, thus helping alert crop analysts concerned with production forecasting and offering tools for analyzing crop outlooks.

By investigating the performance of different drought indicators in Chapters 3 & 4 and the dynamics of NDVI-LST interactions during the main growing season in Chapter 5, this research demonstrates the contribution (merits and limitations) of each indicator for drought monitoring, which can provide useful guidances on effective integration of different data sources for drought monitoring, inform an improved agricultural drought monitoring indicator consistently applicable at a large scale, and help prototype an integrated agricultural drought alert system. This proposed platform would include 3 modules (Figure 6-1): (1) recursive global agricultural drought risk analysis updated with newly added data, showing the regions that are more likely to suffer from agricultural drought (2) entire growing season real-time agricultural drought monitoring base layer from LST derived indicators (due to fast responsiveness),

showing the regions that are currently experiencing agricultural drought (3) main growing season agricultural drought monitoring focused on impact assessment from NDVI or combined NDVI/LST derived indicators during the vegetative peaks (due to fast drought response and most significant drought impact at this period), showing the regions that are potentially having negative crop impacts. This proposed integrated system can provide updated information on drought prone areas/alert periods, offer tools for assessing drought conditions and impact on agriculture, and provide reliable and timely information for drought management, thus contributing to effective drought mitigation, preparedness, response and recovery.

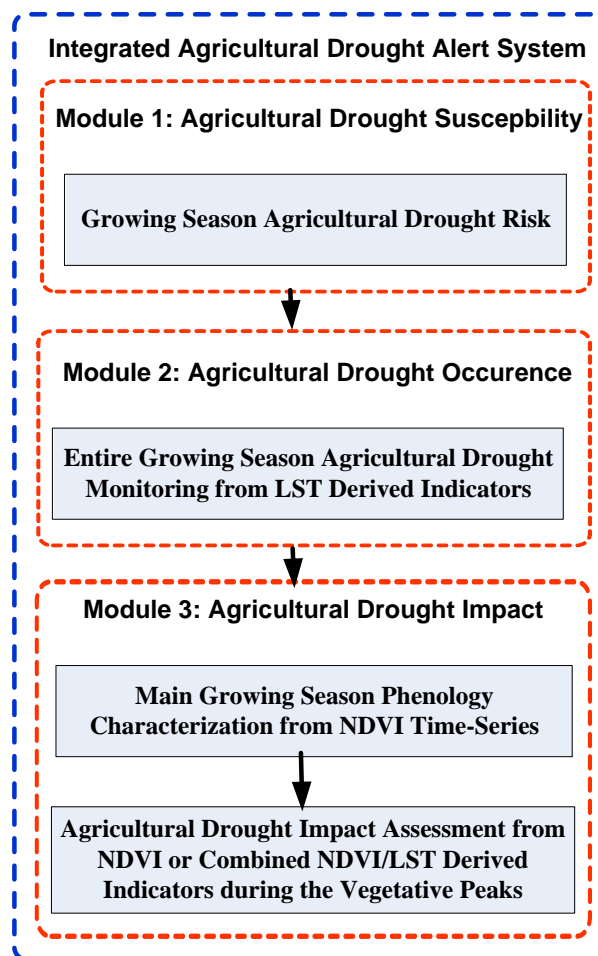


Figure 6-1: Conceptual Diagram of the Integrated Agricultural Drought Alert System

In addition, the dynamics of NDVI-LST interactions in Chapter 5, especially those lagged relationships before reaching the vegetative peak, could be used for forecasting vegetation growth conditions, which can provide useful inputs for agricultural applications such as yield forecasting. Also, the drought impact analysis from a remote sensing perspective presented in Chapters 3 & 4 provides a more precise drought assessment at a much finer spatial and temporal resolution, and thus more direct inputs for further developing an impact-oriented agricultural drought indicator from satellite observations.

Climate change, together with population growth and economic development, is putting an increasing pressure on the food system and threatening the food security. With a continuous changing climate, drought will play an increasingly important role in impacting agriculture through increasing crop water demand, reducing water availability for crop irrigation and decreasing crop productivity. However, several studies have produced different or even contradictory results regarding how drought is changing under climate change, depending on the indicators or algorithm selected for the analysis. Focusing on agriculture sector, this research enhances our understanding of agricultural drought, its impacts on crop production and the linkage of drought phenomenon to impacts, through which we can get a better understanding of agricultural drought causes/drivers, improve the accuracy of real-time agricultural drought monitoring, and provide useful inputs for better prediction of future agricultural drought conditions.

6.3 Future Research

This research has highlighted several important directions for future research to

better understand agricultural drought.

Due to its complexity, the validation of agricultural drought indicators remains an issue due to a lack of consensus in drought ground truth. Determination of agricultural drought places more emphasis on soil moisture or its agricultural impacts. Given that crop growth is a continuous process during the growing season and drought has varying agricultural impacts at different growing stages, it would be extremely important to develop a framework for effectively assessing the indicator for use in agricultural drought monitoring.

In a climatological context, drought monitoring often adopts an anomaly based metric calculated from long-term time series, which is a limitation for current satellite observations. Current commonly used sensors for large-scale drought monitoring, such as MODIS and ASCAT, have a relatively short data record, which influences the effectiveness of drought monitoring and thus drought impact analysis. To address this issue, based on current available data, spatial variability analysis can help identify regions experiencing similar drought impacts, and the study of drought indicators based on the spatial domain (homogeneous drought impact regions) in addition to the temporal domain provides potential for improved drought monitoring. On the other hand, the current limited data record calls for continued drought monitoring to better understand the trends in drought risk. New sensor technologies, continued advancements in the quality, temporal and spatial resolution of earth observations and a longer data record becoming available from operational sensors, offer more opportunities for enhancement of global agricultural drought monitoring and thus helping identify the trends in drought occurrence in agricultural lands. For example,

the NASA LTDR available since 1981 will enable more precise long-term characterization of global agricultural drought regimes, agricultural drought impact and subsequently agricultural drought risk at a finer temporal and spatial resolution. Although drought is the main driver for reduced crop productivity, sometimes it is difficult to be distinguished from other stresses (e.g., heat waves, insect outbreak), especially from satellite observations. More information from network of in situ drought records or crop modelling should be incorporated to help identify different agricultural stresses.

In terms of agricultural drought risk, considering the varying drought impacts on different crops, a crop-specific drought risk analysis is highly recommended, which integrates updated crop masks, crop calendars, irrigation distribution and water storage (both underground and surface), as well as other relevant social/economic factors (e.g., farmer's accessibility to drought resistant crop varieties and local food trade policies). In terms of drought impact analysis, the drought characterization in this work is based on remotely sensed indicators involving vegetation growth conditions, such as ANDVI and DSI. Considering the lagged response of vegetation conditions to drought, the utilization of other more responsive information (e.g. LST/ET) for characterizing agricultural drought as well as the subsequent agricultural impacts, would contribute to a better understanding of drought impacts. As for the DSI in Chapter 4, an improved ET product with finer-resolution regional meteorological inputs as well as taking into account local hydrological conditions (e.g. irrigation) will increase the accuracy of ET product and benefit regional applications for agricultural drought monitoring. In terms of the NDVI-LST dynamics, the missing LST and NDVI data from cloud

contamination limits the availability of a valid cloud-free record. Thus, the use of harmonized long-term NDVI and LST products from a combination of different sensors, which can possibly provide a more consistent and complete data record, is worth investigating. Current response time for both drought indicator and vegetation-temperature interactions is identified from optimal statistical relationship (i.e., locating the maximum absolute correlation), which is easily disturbed by small changes in the input data, especially considering the short data record used in this study (since 2000). A more robust response time determination method is warranted.

Future efforts should also focus on determining effective data integration methods to develop an improved agricultural drought monitoring indicator, which takes into consideration each drought indicator's contribution as well as the dynamics between them. Also, an impacted-oriented agricultural drought indicator can be informed by combining the improved agricultural drought monitoring indicator with the inputs of varying agricultural drought impacts during the growing season.

Bibliography

1. Anderson, M.C., Hain, C., Otkin, J., Zhan, X.W., Mo, K., Svoboda, M., Wardlow, B., Pimstein, A., 2013. An intercomparison of drought indicators based on thermal remote sensing and NLDAS-2 simulations with US drought monitor classifications. *Journal of Hydrometeorology*, 14(4), 1035-1056.
2. Anderson, M.C., Hain, C., Wardlow, B., Pimstein, A., Mecikalski, J.R., Kustas, W.P., 2011. Evaluation of drought indices based on thermal remote sensing of evapotranspiration over the continental United States. *Journal of Climate*, 24(8), 2025-2044.
3. Anderson, M.C., Norman, J.M., Mecikalski, J.R., Otkin, J.A., Kustas, W.P., 2007. A climatological study of evapotranspiration and moisture stress across the continental U.S. based on thermal remote sensing: 2. surface moisture climatology. *Journal of Geophysical Research*, 112(D11), DOI: 10.1029/2006JD007507.
4. Antwi-Agyei, P., Fraser, E.D.G., Dougill, A.J., Stringer, L.C., Simelton, E., 2012. Mapping the vulnerability of crop production to drought in Ghana using rainfall, yield and socioeconomic data. *Applied Geography*, 32 (2), 324-334.
5. Atkinson, P.M., Dash, J., Jeganathan, C., 2011. Amazon vegetation greenness as measured by satellite sensors over the last decade. *Geophysical Research Letters*, 38 (19), DOI: 10.1029/2011GL049118.
6. Biradar, C.M., Thenkabail, P.S., Noojipady, P., Li, Y., Dheeravath, V., Turrall, H., Velpuri, M., Gumma, M.K., Gangalakunta, O.R., Cai, X.L., Xiao, X., 2009. A global map of rainfed cropland areas (GMRCA) at the end of last millennium using remote sensing. *International Journal of Applied Earth Observation and Geoinformation*, 11(2), 114-129.
7. Blanc, É., 2012. The impact of climate change on crop yields in Sub-Saharan Africa. *American Journal of Climate Change*, 1(1), 1-13.
8. Blauhut, V., Gudmundsson, L., Stahl, K., 2015. Towards pan-European drought risk maps: quantifying the link between drought indices and reported drought impacts. *Environmental Research Letters*, 10(1), 014008.
9. Brown, J.F., Wardlow, B.D., Tadesse, T., Hayes, M.J., Reed, B.C., 2008. The Vegetation Drought Response Index (VegDRI): A new integrated approach for monitoring drought stress in vegetation. *GIScience & Remote Sensing*, 45(1), 16-46.

10. Bryant, K.J., Benson, V.W., Kiniry, J.R., Williams, J.R., Lacewell, R.D., 1992. Simulating corn yield response to irrigation timings: validation of the EPIC model. *Journal of Production Agriculture*, 5(2), 237-242.
11. Burke, E.J., Brown, S.J., 2008. Evaluating uncertainties in the projection of future drought. *Journal of Hydrometeorology*, 9(2), 292-299.
12. Burke, E. J., Brown, S. J., Christidis, N., 2006. Modeling the recent evolution of global drought and projections for the twenty-first century with the Hadley Centre climate model. *Journal of Hydrometeorology*, 7(5), 1113-1125.
13. Cammalleri, C., Anderson, M.C., Gao, F., Hain, C.R. and Kustas, W.P., 2014. Mapping daily evapotranspiration at field scales over rainfed and irrigated agricultural areas using remote sensing data fusion. *Agricultural and Forest Meteorology*, 186, 1-11.
14. Carlson, T.N., Perry, E.M., Schmugge, T.J., 1990. Remote estimation of soil moisture availability and fractional vegetation cover for agricultural fields. *Agricultural and Forest Meteorology*, 52(1-2), 45-69.
15. Carrão, H., Naumann, G., Barbosa, P., 2016. Mapping global patterns of drought risk: An empirical framework based on sub-national estimates of hazard, exposure and vulnerability. *Global Environmental Change*, 39, 108-124.
16. Chen, D., Huang, J., Jackson, T.J., 2005. Vegetation water content estimation for corn and soybeans using spectral indices derived from MODIS near- and short-wave infrared bands. *Remote Sensing of Environment*, 98(2-3), 225-236.
17. Chen, W.Y., Xiao, Q.G., Sheng, Y.W, 1994. Application of the anomaly vegetation index to monitor heavy drought in 1992. *Remote Sensing of Environment China*, 9(2), 106-112.
18. Choi, M., Jacobs, J.M., Anderson, M.C., Bosch, D.D., 2013. Evaluation of drought indices via remotely sensed data with hydrological variables. *Journal of Hydrology*, 476, 265-273.
19. Dai, A., 2013. Increasing drought under global warming in observations and models. *Nature Climate Change*, 3(1), 52-58.
20. Dai, A., 2011a. Drought under global warming: a review. *Wiley Interdisciplinary Reviews: Climate Change*, 2(1), 45-65.
21. Dai, A, 2011b. Characteristics and trends in various forms of the Palmer Drought Severity Index during 1900-2008. *Journal of Geophysical Research: Atmospheres*, 116(D12), DOI: 10.1029/2010JD015541.
22. Dai, A., Trenberth, K. E., Karl, T. R., 1998. Global variations in droughts and wet spells: 1900-1995. *Geophysical Research Letters*, 25(17), 3367-3370.

23. Dai, A., Trenberth, K. E., Qian, T., 2004. A global dataset of Palmer Drought Severity Index for 1870-2002: Relationship with soil moisture and effects of surface warming. *Journal of Hydrometeorology*, 5(6), 1117-1130.
24. Du, L., Tian, Q., Yu, T., Meng, Q., Jancso, T., Udvardy, P., Huang, Y., 2013. A comprehensive drought monitoring method integrating MODIS and TRMM data. *International Journal of Applied Earth Observation and Geoinformation*, 23, 245-253.
25. Elagib, N.A., 2014. Development and application of a drought risk index for food crop yield in Eastern Sahel. *Ecological Indicators*, 43, 114-125.
26. Fan, Y., van den Dool, H., 2004. Climate Prediction Center global monthly soil moisture data set at 0.5 degree resolution for 1948 to present. *Journal of Geophysical Research*, 109(D10), DOI: 10.1029/2003JD004345.
27. Fensholt, R., Sandholt, I., 2003. Derivation of a shortwave infrared water stress index from MODIS near- and shortwave infrared data in a semiarid environment. *Remote Sensing of Environment*, 87(1), 111-121.
28. Fischer, G., Tubiello, F.N., Van Velthuisen, H. and Wiberg, D.A., 2007. Climate change impacts on irrigation water requirements: effects of mitigation, 1990-2080. *Technological Forecasting and Social Change*, 74(7), 1083-1107.
29. Friedl, M.A., McIver, D.K., Hodges, J.C.F, Zhang, X.Y., Muchoney, D., Strahler, A.H., Woodcock, C.E., Gopal, S., Schneider, A., Cooper, A., Baccini, A., Gao, F., Schaaf, C., 2002. Global land cover mapping from MODIS: algorithms and early results. *Remote Sensing of Environment*, 83(1), 287-302.
30. Fritz, S., See, L., McCallum, I., You, L., Bun, A., Moltchanova, E., Duerauer M, Albrecht, F., Schill, C., Perger, C., Havlik, P., et al., 2015. Mapping global cropland and field size. *Global Change Biology*, 21(5), 1980-1992.
31. Gao, B.C., 1996. NDWI-A normalized difference water index for remote sensing of vegetation liquid water from space. *Remote Sensing of Environment*, 58(3): 257-266.
32. Gao, H., Tang, Q., Ferguson, C. R., Wood, E. F., Lettenmaier, D. P., 2010. Estimating the water budget of major U.S. river basins via remote sensing. *International Journal of Remote Sensing*, 31(14), 3955-3978.
33. Geng, G., Wu, J., Wang, Q., Lei, T., He, B., Li, X., Mo, X., Luo, H., Zhou, H., Liu, D., 2015. Agricultural drought hazard analysis during 1980-2008: a global perspective. *International Journal of Climatology*, 36(1), 389-399.
34. Gibbs, W.J., Maher, J.V., 1967. Rainfall deciles as drought indicators. *Australian Bureau of Meteorology Bulletin*, 48.

35. Goward, S.N., Hope, A.S., 1989. Evapotranspiration from combined reflected solar and emitted terrestrial radiation: Preliminary FIFE results from AVHRR data. *Advances in Space Research*, 9(7), 239-249.
36. Gutman, G.G., 1990. Towards monitoring droughts from space. *Journal of Climate*, 3(2), 282-295.
37. Gu, Y., Brown, J.F., Verdin, J.P., Wardlow, B., 2007. A five-year analysis of MODIS NDVI and NDWI for grassland drought assessment over the central Great Plains of the United States. *Geophysical Research Letters*, 34(6), DOI: 10.1029/2006GL029127.
38. Hall, D.K., Riggs, G.A., 2007. Accuracy assessment of the MODIS snow products. *Hydrological Processes*, 21(12), 1534-1547.
39. Hao, L., Zhang, X., Liu, S., 2012. Risk assessment to China's agricultural drought disaster in county unit. *Natural Hazards*, 61(2), 785-801.
40. Hayes, M.J., Wilhelmi, O.V., Knutson, C.L., 2004. Reducing drought risk: bridging theory and practice. *Natural Hazards Review*, 5(2), 106-113.
41. He, B., Wu, J., Lü, A., Cui, X., Zhou, L., Liu, M., Zhao, L., 2013. Quantitative assessment and spatial characteristic analysis of agricultural drought risk in China. *Natural Hazards*, 66(2), 155-166.
42. Heim, R.R., Brewer, M.J., 2010. The development of an international drought clearinghouse and summary of results of the April 2010 Global Drought Assessment Workshop. 2nd International Conference: Climate, Sustainability and Development in Semi-arid Regions, August 16-20, 2010, Fortaleza-Ceará, Brazil.
43. Henricksen, B.L., Durkin, J.W., 1986. Growing period and drought early warning in Africa using satellite data. *International Journal of Remote Sensing*, 7(11), 1583-1608.
44. Hlavinka, P., Trnka, M., Semerádová, D., Dubrovský, M., Žalud, Z., Možný, M., 2009. Effect of drought on yield variability of key crops in Czech Republic. *Agricultural and Forest Meteorology*, 149(3), 431-442.
45. Huang, J., Ma, H., Su, W., Zhang, X., Huang, Y., Fan, J., Wu, W., 2015b. Jointly assimilating MODIS LAI and ET products into the SWAP model for winter wheat yield estimation. *IEEE Journal of Selected Topics in Applied Earth Observations and Remote Sensing*, 8(8), 4060-4071.
46. Huang, J., Tian, L., Liang, S., Ma, H., Becker-Reshef, I., Huang, Y., Su, W., Zhang, X., Zhu, D., Wu, W., 2015a. Improving winter wheat yield estimation by

- assimilation of the leaf area index from Landsat TM and MODIS data into the WOFOST model. *Agricultural and Forest Meteorology*, 204, 106-121.
47. Huang, J., Van den Dool, H., Georgakakos, K.P., 1996. Analysis of model-calculated soil moisture over the United States (1931-93) and application to long-range temperature forecasts. *Journal of Climate*, 9(6), 1350-1362.
 48. Huete, A., Didan, K., Miura, T., Rodriguez, E.P., Gao, X., Ferreira, L.G., 2002. Overview of the radiometric and biophysical performance of the MODIS vegetation indices. *Remote Sensing of Environment*, 83(1), 195-213.
 49. Hu, G., Jia, L., Menenti, M., 2015. Comparison of MOD16 and LSA-SAF MSG evapotranspiration products over Europe for 2011. *Remote Sensing of Environment*, 156, 510-526.
 50. Huth, N.I., Carberry, P.S., Cocks, B., Graham, S., McGinness, H.M., O'Connell, D.A., 2008. Managing drought risk in eucalypt seedling establishment: an analysis using experiment and model. *Forest Ecology and Management*, 255(8), 3307-3317.
 51. Hu, Y., Liu, Y., Tang, H., Xu, Y., Pan, J., 2014. Contribution of drought to potential crop yield reduction in a wheat-maize rotation region in the North China Plain. *Journal of Integrative Agriculture*, 13(7), 1509-1519.
 52. IPCC. *Climate Change 2001: impacts, adaptation and vulnerability. Working group II report.* 2001, Cambridge University Press, London.
 53. IPCC. *Climate Change 2007: impacts, adaptation and vulnerability. Working Group II report.* 2007, Cambridge University Press, London.
 54. Jackson, R.D., 1982. Canopy temperature and crop water stress. *Advances in Irrigation*, 1, 43-85.
 55. Jackson, R.D., 1984. Total reflected solar radiation calculated from multi-band sensor data. *Agricultural and Forest Meteorology*, 33(2), 163-175.
 56. Janetos, A., Justice, C., Jahn, M., Obersteiner, M., Glauber, J., Mulhern, W., 2017. The risks of multiple breadbasket failures in the 21st century: a science research agenda. Boston University Pardee Center Research Report.
 57. Jia, H., Wang, J., Pan, D., Cao, C., 2011. Maize drought disaster risk assessment based on EPIC model: a case study of maize region in northern China. *Acta Geographica Sinica*, 66(5), 643-652.
 58. Ji, L., Peters, A.J., 2003. Assessing vegetation response to drought in the northern Great Plains using vegetation and drought indices. *Remote Sensing of Environment*, 87(1), 85-98.

59. Justice, C.O., Townshend, J.R.G., Holben, B.N., Tucker C.J., 1985. Analysis of the phenology of global vegetation using meteorological satellite data. *International Journal of Remote Sensing*, 6(8), 1272-1318.
60. Karnieli, A., Bayasgalan, M., Bayarjargal, Y., Agam, N., Khudulmur, S. and Tucker, C.J., 2006. Comments on the use of the vegetation health index over Mongolia. *International Journal of Remote Sensing*, 27(10), 2017-2024.
61. Karnieli, A., Agam, N., Pinker, R.T., Anderson, M., Imhoff, M.L., Gutman, G.G., Panov, N. and Goldberg, A., 2010. Use of NDVI and land surface temperature for drought assessment: merits and limitations. *Journal of climate*, 23(3), 618-633.
62. Kerr, Y.H., Waldteufel, P., Wigneron, J.P., Delwart, S., Cabot, F., Boutin, J., Escorihuela, M.J., Font, J., Reul, N., Gruhier, C., Juglea, S.E., 2010. The SMOS mission: new tool for monitoring key elements of the global water cycle. *Proceedings of the IEEE*, 98(5), 666-687.
63. Knutson, C., Hayes, M., Phillips, T., 1998. How to reduce drought risk. Wisconsin, Nebraska: Western Drought Coordination Council.
64. Kogan, F.N., 1990. Remote sensing of weather impacts on vegetation in non-homogeneous areas. *International Journal of Remote Sensing*, 11(8), 1405-1419.
65. Kogan, F.N., 1995a. Application of vegetation index and brightness temperature for drought detection. *Advances in Space Research*, 15(11), 91-100.
66. Kogan, F.N., 1995b. Droughts of the late 1980s in the United States as derived from NOAA polar-orbiting satellite data. *Bulletin of the American Meteorological Society*, 76(5), 655-668.
67. Kucharik, C. J., Serbin, S. P., 2008. Impacts of recent climate change on Wisconsin corn and soybean yield trends. *Environmental Research Letters*, 3(3), 034003.
68. Liang, S., Zhang, X., Xiao, Z., Cheng, J., Liu, Q. and Zhao, X., 2013. *Global LAnd Surface Satellite (GLASS) products: algorithms, validation and analysis*. Springer Science & Business Media.
69. Liu, S., Xu, Z., Zhu, Z., Jia, Z., Zhu, M., 2013. Measurements of evapotranspiration from eddy-covariance systems and large aperture scintillometers in the Hai River Basin, China. *Journal of Hydrology*, 487, 24-38.
70. Liu, W., Kogan, F.N., 1996. Monitoring regional drought using the Vegetation Condition Index. *International Journal of Remote Sensing*, 17(14), 2761-2782.
71. Liu, Y., Yang, Z., 2001. *Principles and algorithms of MODIS information processing*. Science Press, Beijing.

72. Li, Y., Ye, W., Wang, M., Yan, X., 2009. Climate change and drought: a risk assessment of crop-yield impacts. *Climate Research*, 39(1), 31-46.
73. Lobell, D.B., Baenziger, M., Magorokosho, C., Vivek, B., 2011a. Nonlinear heat effects on African maize as evidenced by historical yield trials. *Nature Climate Change*, 1(1), 42-45.
74. Lobell, D.B., Field, C.B., 2007. Global scale climate-crop yield relationships and the impacts of recent warming. *Environmental Research Letters*, 2(1), 014002.
75. Lobell, D.B., Roberts, M.J., Schlenker, W., Braun, N., Little, B.B., Rejesus, R.M., Hammer, G.L., 2014. Greater sensitivity to drought accompanies maize yield increase in the US Midwest. *Science*, 344 (6183), 516-519.
76. Lobell, D.B., Schlenker, W.S., Costa-Roberts, J., 2011b. Climate trends and global crop production since 1980. *Science*, 333(6042), 616-620.
77. Maliva, R., Missimer, T., 2012. Aridity and drought. In *Arid lands water evaluation and management*. Springer Berlin Heidelberg.
78. McKee, T.B., Doesken, N.J., Kleist, J., 1993. The relationship of drought frequency and duration to time scales. In *Eighth Conference on Applied Climatology*. Anaheim, California, America: Meteorological Society, 179-184.
79. McVicar, T., Jupp, D.L.B., 1998. The current and potential uses of remote sensing to aid decisions on drought exceptional circumstances in Australia: A review. *Agricultural Systems*, 57(3), 399-468.
80. Ming, B., Guo, Y.Q., Tao, H.B, Liu, G.Z., Li, S.k., Wang, P., 2015. SPEI_{PM}-based research on drought impact on maize yield in North China Plain. *Journal of Integrative Agriculture*, 14(4), 660-669.
81. Mishra, V., Cherkauer, K.A., 2010. Retrospective droughts in the crop growing season: Implications to corn and soybean yield in the Midwestern United States. *Agricultural and Forest Meteorology*, 150(7), 1030-1045.
82. Mishra, A. K., Singh, V.P., 2010. A review of drought concepts. *Journal of Hydrology*, 391(1), 202-216.
83. Morton, D.C., Nagol, J., Carabajal, C.C., Rosette, J., Palace, M., Cook, B.D., Vermote, E.F., Harding, D.J., North, P.R.J., 2014. Amazon forests maintain consistent canopy structure and greenness during the dry season. *Nature*, 506(7487), 221-224.
84. Mukherjee, S., Joshi, P.K. and Garg, R.D., 2015. Evaluation of LST downscaling algorithms on seasonal thermal data in humid subtropical regions of India. *International Journal of Remote Sensing*, 36(10), 2503-2523.

85. Mu, Q., Heinsch, F.A., Zhao, M., Running, S.W., 2007. Development of a global evapotranspiration algorithm based on MODIS and global meteorology data. *Remote Sensing of Environment*, 111(4), 519-536.
86. Mu, Q., Zhao, M., Running, S.W., 2011. Improvements to a MODIS global terrestrial evapotranspiration algorithm. *Remote Sensing of Environment*, 115(8), 1781-1800.
87. Mu, Q., Zhao, M., Kimball, J.S., McDowell, N.G., Running, S.W., 2013a. A remotely sensed global terrestrial drought severity index. *Bulletin of the American Meteorological Society*, 94(1), 83-98.
88. Mu, Q., Zhao, M., Running, S.W., 2013b. MODIS global terrestrial evapotranspiration (ET) product (NASA MOD16A2/A3) Collection 5. NASA Headquarters, 11/2013, Missoula.
89. Naeimi, V., Scipal, K., Bartalis, Z., Hasenauer, S., Wagner, W., 2009. An improved soil moisture retrieval algorithm for ERS and METOP scatterometer observations. *IEEE Transactions on Geoscience and Remote Sensing*, 47(7), 1999-2013.
90. Nemani, R., Pierce, L., Running, S., Goward, S., 1993. Developing satellite-derived estimates of surface moisture status. *Journal of Applied Meteorology*, 32(3), 548-557.
91. Njoku, E.G., Jackson, T.J., Lakshmi, V., Chan, T.K., Nghiem, S.V., 2003. Soil moisture retrieval from AMSR-E. *IEEE Transactions on Geoscience and Remote Sensing*, 41(2), 215-229.
92. Otkin, J.A., Anderson, M.C., Hain, C., Mladenova, I.E., Basara, J.B., Svoboda, M., 2013. Examining rapid onset drought development using the thermal infrared-based Evaporative Stress Index. *Journal of Hydrometeorology*, 14(4), 1057-1074.
93. Palmer, W.C. 1965. Meteorological drought. Research Paper No. 45. US Weather Bureau.
94. Pedelty, J., Devadiga, S., Masuoka, E., Brown, M., Pinzon J., Tucker C., Vermote, E., Prince S., Nagol J., Justice C., Roy D., 2007. Generating a long-term land data record from the AVHRR and MODIS instruments. In 2007 IEEE International Geoscience and Remote Sensing Symposium, 1021-1025.
95. Peters, A.J., Walter-Shea, E.A., Ji, L., Vina, A., Hayes, M., Svoboda, M.D., 2002. Drought monitoring with NDVI-based standardized vegetation index. *Photogrammetric Engineering and Remote Sensing*, 68(1), 71-75.

96. Phillips, O. L., Aragão, L.E.O.C., Lewis, S.L., 2009. Drought sensitivity of the Amazon rainforest. *Science*, 323(5919), 1344-1347.
97. Pittman, K., Hansen, M.C., Becker-Reshef, I., Potapov, P.V., Justice, C.O., 2010. Estimating global cropland extent with multi-year MODIS data. *Remote Sensing*, 2(7), 1844-1863.
98. Potopová, V., Štěpánek, P., Možný, M., Türkott, L., Soukup, J., 2015. Performance of the standardised precipitation evapotranspiration index at various lags for agricultural drought risk assessment in the Czech Republic. *Agricultural and Forest Meteorology*, 202, 26-38.
99. Qiao, P., Zhang, J., Yan, Q., Zhang, L., 2003. A study of soil water contents monitoring using TM6. *Bulletin of Surveying and Mapping*, 7(5), 14-18.
100. Qin, Z., Tang, H., Li, W., Zhang, H., Zhao, S., Wang, Q., 2014. Modelling impact of agro-drought on grain production in China. *International Journal of Disaster Risk Reduction*, 7, 109-121.
101. Ramankutty, N., Evan, A. T., Monfreda, C., Foley, J. A., 2008. Farming the planet: 1. Geographic distribution of global agricultural lands in the year 2000. *Global Biogeochemical Cycles*, 22(1), DOI: 10.1029/2007GB002952.
102. Raynolds, M.K., Comiso, J.C., Walker, D.A. and Verbyla, D., 2008. Relationship between satellite-derived land surface temperatures, arctic vegetation types, and NDVI. *Remote Sensing of Environment*, 112(4), 1884-1894.
103. Rossi, S., Weissteiner, C., Laguardia, G., Kurnik, B., Robustelli, M., Niemeyer, S., Gobron, N., 2008. Potential of MERIS fAPAR for drought detection. In *Proceedings of the Second MERIS/ (A) ATER User Workshop*, Sep 22-26, 2008, Frascati, Italy.
104. Saleska, S.R., Didan, K., Huete, A.R., da Rocha, H.R., 2007. Amazon forests green-up during 2005 drought. *Science*, 318(5850), 612.
105. Sandholt, I., Rasmussen, K., Anderson, J., 2002. A simple interpretation of the surface temperature/vegetation index space for assessment of surface moisture status. *Remote Sensing of Environment*, 79(2), 213-224.
106. Schlenker, W., Lobell, D.B., 2010. Robust negative impacts of climate change on African agriculture. *Environmental Research Letters*, 5(1), 014010.
107. Schrier, G., Barichivich, J., Briffa, K. R., Jones, P.D., 2013. A scPDSI-based global data set of dry and wet spells for 1901-2009. *Journal of Geophysical Research: Atmospheres*, 118(10), 4025-4048.
108. Shahid, S., Behrawan, H., 2008. Drought risk assessment in the western part of Bangladesh. *Natural Hazards*, 46(3), 391-413.

109. Siebert, S., Henrich, V., Frenken, K., Burke, J., 2013. Global Map of Irrigation Areas version 5. Rheinische Friedrich-Wilhelms-University, Bonn, Germany/Food and Agriculture Organization of the United Nations, Rome, Italy.
110. Sivakumar, M.V.K, Raymond, P.M., Wilhite, D.A., Deborah, A.W., 2011. Agricultural drought indices. Proceedings of the WMO/UNISDR Expert Group Meeting on Agricultural Drought Indices, 2-4 June 2010, Murcia, Spain: Geneva, Switzerland: World Meteorological Organization.
111. Song, Y., Dong, W., 2006. Influence of drought on winter wheat yield in China during 1961-2000. *Journal of Natural Disasters*, 15(6), 227-231.
112. Spinoni, J., Naumann, G., Carrao, H., Barbosa, P., Vogt, J., 2014. World drought frequency, duration, and severity for 1951-2010. *International Journal of Climatology*, 34(8), 2792-2804.
113. Sun, D., Kafatos, M., 2007. Note on the NDVI-LST relationship and the use of temperature-related drought indices over North America. *Geophysical Research Letters*, 34(24), DOI: 10.1029/2007GL031485.
114. Sun, L., Mitchell, S.W., Davidson, A., 2012. Multiple drought indices for agricultural drought risk assessment on the Canadian prairies. *International Journal of Climatology*, 32(11), 1628-1639.
115. Sun, W., Wang, P.X., Zhang, S.Y., Zhu, D.H., Liu, J.M., Chen, J.H., Yang, H.S., 2008. Using the vegetation temperature condition index for time series drought occurrence monitoring in the Guanzhong Plain, PR China. *International Journal of Remote Sensing*, 29(17-18), 5133-5144.
116. Swenson, S.C., 2012. GRACE monthly land water mass grids NETCDF RELEASE 5.0. Physical Oceanography Distributed Active Archive Center (PO. DAAC), California, <http://dx.doi.org/10.5067/TELND-NC005>.
117. Tadesse, T., Brown, J.F., Hayes, M.J., 2005. A new approach for predicting drought-related vegetation stress: Integrating satellite, climate, and biophysical data over the U.S. central plains. *ISPRS Journal of Photogrammetry and Remote Sensing*, 59(4): 244-253.
118. Tannehill, I.R., 1947. Drought: its causes and effects. Princeton, NJ: Princeton University.
119. Teixeira, E. I., Fischer, G., van Velthuisen, H., Walter, C., Ewert, F., 2013. Global hot-spots of heat stress on agricultural crops due to climate change. *Agricultural and Forest Meteorology*, 170, 206-215.
120. Thenkabail, P.S., Biradar, C.M., Noojipady, P., Dheeravath, V., Li, Y., Velpuri, M., Gumma, M., Gangalakunta, O.R.P., Turrall, H., Cai, X., Vithanage, J., 2009.

- Global Irrigated Area Map (GIAM) derived from remote sensing for the end of the last millennium. *International Journal of Remote Sensing*, 30(14), 3679-3733.
121. Tucker, C.J., 1979. Red and photographic infrared linear combinations for monitoring vegetation. *Remote Sensing of Environment*, 8(2), 127-150.
 122. Tucker, C.J., 1989. Comparing SMMR and AVHRR data for drought monitoring. *International Journal of Remote Sensing*, 10(10), 1663-1672.
 123. Tucker, C.J., Choudhury, B.J., 1987. Satellite remote sensing of drought conditions. *Remote Sensing of Environment*, 23(2), 243-251.
 124. Tucker, C.J., Justice, C.O., Prince, S.D., 1986. Monitoring the grasslands of the Sahel 1984-1985. *International Journal of Remote Sensing*, 7(11), 1571-1583.
 125. Van der Schrier, G., Briffa, K. R., Jones, P. D., Osborn, T. J., 2006a. Summer moisture variability across Europe. *Journal of Climate*, 19(12), 2818-2834.
 126. Van der Schrier, G., Briffa, K.R., Osborn, T.J., Cook, E.R., 2006b. Summer moisture availability across North America. *Journal of Geophysical Research: Atmospheres*, 111(D11), DOI: 10.1029/2005JD006745.
 127. Velpuri, N. M., Senay, G. B., Singh, R. K., Bohms, S., Verdin, J. P., 2013. A comprehensive evaluation of two MODIS evapotranspiration products over the conterminous United States: using point and gridded FLUXNET and water balance ET. *Remote Sensing of Environment*, 139, 35-49.
 128. Vicente-Serrano, S.M., 2007. Evaluating the impact of drought using remote sensing in a Mediterranean, semi-arid region. *Natural Hazards*, 40(1), 173-208.
 129. Vicente-Serrano, S.M., Beguería, S., López-Moreno, J.I., 2010. A multiscalar drought index sensitive to global warming: the standardized precipitation evapotranspiration index. *Journal of climate*, 23(7), 1696-1718.
 130. Wang, L., Qu, J., 2007. NMDI: a normalized multi-band drought index for monitoring soil and vegetation moisture with satellite remote sensing. *Geophysical Research Letters*, 34(20), DOI: 10.1029/2007GL031021.
 131. Wang, Q., Wu, J., Lei, T., He, B., Wu, Z., Liu, M., Mo. X., Geng, G., Li, X., Zhou, H., Liu, D., 2014. Temporal-spatial characteristics of severe drought events and their impact on agriculture on a global scale. *Quaternary International*, 349, 10-21.
 132. Wagner, W., Lemoine, G., Rott, H., 1999. A method for estimating soil moisture from ERS scatterometer and soil data. *Remote sensing of environment*, 70(2), 191-207.

133. Wagner, W., Hahn, S., Kidd, R., Melzer, T., Bartalis, Z., Hasenauer, S., Figa-Saldaña, J., de Rosnay, P., Jann, A., Schneider, S., Komma, J., 2013. The ASCAT soil moisture product: A review of its specifications, validation results, and emerging applications. *Meteorologische Zeitschrift*, 22(1), 5-33.
134. Wells, N., Goddard, S., Hayes, M.J., 2004. A self-calibrating Palmer drought severity index. *Journal of Climate*, 17(12), 2335-2351.
135. Weng, Q., Lu, D. and Schubring, J., 2004. Estimation of land surface temperature-vegetation abundance relationship for urban heat island studies. *Remote sensing of Environment*, 89(4), 467-483.
136. Werick, W.J., Willeke, G.E., Guttman, N.B., Hosking, J.R.M., Wallis, J.R., 1994. National drought atlas developed. *Eos, Transactions American Geophysical Union*, 75(8), 89-90.
137. Whitcraft, A. K., Becker-Reshef, I., Justice, C.O., 2015. Agricultural growing season calendars derived from MODIS surface reflectance. *International Journal of Digital Earth*, 8(3), 173-197.
138. Wilhite, D.A., Glantz, M.H., 1985. Understanding the drought phenomenon: the role of definitions. *Water International*, 10(3), 111-120.
139. Wilhite, D.A., 1993. *Drought assessment, management, and planning: theory and case studies*. Kluwer Academic Publishers, Norwell.
140. Wilhite, D.A., 2000. *Drought: a global assessment*. Routledge Publishers, London.
141. Wilhite, D.A., 2005. *Drought and water crises: science, technology, and management issues*. CRC Press, Boca Raton.
142. Williams, A.P., Seager, R., Abatzoglou, J.T., Cook, B.I., Smerdon, J.E., Cook, E.R., 2015. Contribution of anthropogenic warming to California drought during 2012-2014. *Geophysical Research Letters*, 42(16), 6819-6828.
143. Williamson, S.N., Hik, D.S., Gamon, J.A., Kavanaugh, J.L., Koh, S., 2013. Evaluating cloud contamination in clear-sky MODIS Terra daytime land surface temperatures using ground-based meteorology station observations. *Journal of Climate*, 26(5), 1551-1560.
144. World Bank. *Food price watch, 2012*. Washington, DC.
145. Wu, D., Zhao, X., Liang, S., Zhou, T., Huang, K., Tang, B., Zhao, W., 2015. Time-lag effects of global vegetation responses to climate change. *Global Change Biology*, 21(9), 3520-3531.

146. Wu, H., Hubbard, K.G., Wilhite, D.A., 2004. An agricultural drought risk-assessment model for corn and soybeans. *International Journal of Climatology*, 24(6), 723-741.
147. Wu, H., Wilhite, D.A., 2004. An operational agricultural drought risk assessment model for Nebraska, USA. *Natural Hazards*, 33(1), 1-21.
148. Wu, J., Zhou, L., Liu, M., Zhang, J., Leng, S., Diao, C., 2013. Establishing and assessing the Integrated Surface Drought Index (ISDI) for agricultural drought monitoring in mid-eastern China. *International Journal of Applied Earth Observation and Geoinformation*, 23, 397-410.
149. Xu, X., Ge, Q., Zheng, J., Dai, E., Zhang, X., He, S., Liu, G., 2013. Agricultural drought risk analysis based on three main crops in prefecture-level cities in the monsoon region of east China. *Natural Hazards*, 66(2), 1257-1272.
150. Yu, C., Li, C., Xin, Q., Chen, H., Zhang, J., Zhang, F., Li, X., Clinton, N., Huang, X., Yue, Y., Gong, P., 2014. Dynamic assessment of the impact of drought on agricultural yield and scale-dependent return periods over large geographic regions. *Environmental Modelling & Software*, 62, 454-464.
151. Zhang, Q., Pan, G., Ma, Z., 2009. *Drought*. China Meteorological Press, Beijing.
152. Zhao, M., Running, S.W., 2010. Drought-induced reduction in global terrestrial net primary production from 2000 through 2009. *Science*, 329(5994), 940-943.